Declaration of Compliance

I, Sakib Mowdood, hereby declare that this is an independent work according to the exam regulations of Norwegian University of Science and Technology (NTNU).

Place and Time: Trondheim − Gløshaugen, September 2022.

Dedication

This thesis is dedicated to my parents. For their endless love, support and encouragement.

Acknowledgement

I would like to show my sincerest gratitude to my supervisor, Prof. Bjørn E. Christensen, at Department of Biotechnology and Food Science, NTNU, for the continuous support throughout the course of this thesis.

Secondly, I want to express my heartfelt gratitude to Prof. Dr. Sulalit Bandyopadhyay, at Department of Chemical Engineering, NTNU, for believing in me and encouraging me to the finish. His outstanding expertise and guiding abilities have proven to be extremely beneficial in both academic and practical work. This project would not have seen the light without of his insight.

Thirdly, I would like to thank Nesrine Bali, PhD scholar at Department of Chemical Engineering, NTNU for all her insightful advice and practical help provided while working in laboratories and theoretical works. A special mention was all the microscopy assistance throughout the course of the work using TEM and especially STEM which she characterized the particles.

The fellows of Particle Engineering Research Group have always actively helped me in improving my research capabilities with healthy discussions during the group meetings. They have always provided a friendly working environment. I would also like to thank Ahmad, Hammad and Christopher who gave me training in all the necessary instrument I needed in particle engineering labs for characterizing the particles.

I would also thank my parents especially my father who has always groomed and preached me as mentor and my mother for her ever-growing love and undying support.

Abstract

Nanomaterials are materials with at least one dimension in the billionth of a meter range (10^{-9} m). Significant research has been undertaken over the last two decades on the development and engineering of magnetic nanoparticles. Magnetic particles provide extremely efficient energy harvesting systems that have the potential to revolutionize current treatment and diagnostic procedures. The specific nature of the surface coating is crucial since it can impact important IONP features such as colloidal stability, toxicity, magnetism, and labeling efficiency. Polymers are commonly employed as IONP coatings because they can improve colloidal stability in hydrophilic circumstances and preserve the iron oxide core from degradation.

In this study, chitosan was used for coating IONPs using nanoprecipitation method. This project was divided into three phases. Bare chitosan NPs synthesis, IONPs synthesis and lastly chitosan coated IONPs synthesis. The size, surface charge, molecular structure analysis and magnetic properties (IONPs only) were characterized of those particles. Preliminary study was also done by synthesizing PLGA NPs and PLGA-IONPs.

The chitosan NPs were synthesized by nanoprecipitation method and the hydrodynamic sizes were measured by DLS and lumisizer. The diluted sample sizes were between 150-350 nm and concentrated sample sizes were between 500-1200 nm. The size distribution analysis observed smallest to largest size from 371 nm to 3920 nm and mean size was 1271. The zeta potentials of the samples ranged between (-18 to -40 mV and 25-35 mV depending on non-solvent removal technique). The study of different parameters like polymer concentration, molecular weight, stirring duration and flow rate that can influence the chitosan NP size was performed. FT-IR data was done to observe the functional bond peaks of the NPs and confirm the surfactant coating on the surface. STEM characterization observed polydisperse samples and largest particle was sized between 1-2 µm.

Then IONPs were synthesized by co-precipitation method. The hydrodynamic sizes and zeta potentials were 176 ± 4 nm and -32 ± 0.3 mV. The size distribution analysis observed smallest to largest hydrodynamic size from 24 nm to 39 nm and mean size was 39 nm. The TEM characteristics observed 10 ± 3 nm dried particle size. FT-IR data was done to observe the functional bond peaks of the IONPs and VSM data proved the superparamagnetism property.

Chitosan coated IONPs were synthesized by nanoprecipitation method. A comparison study was done to confirm nanoprecipitation method is better than mixing process by observing their hydrodynamic sizes and STEM characteristics. The hydrodynamic sizes were between 900-1500 nm and zeta potential were between 25-30 mV. The zeta potential could suggest the surface of the NPs were coated with chitosan. The size distribution analysis observed smallest to largest hydrodynamic size from 58 nm to 261 nm and mean size was 91 nm. Surface characterization was done by analyzing the isoelectric point and FT-IR data. The JMP design for study of different parameters (polymer concentration, IONPs concentration, flow rate and methanol volume) was performed using screening design. R^2 was 0.22 which indicated a poor fit for this data set. Some small size optimization was done later to narrow down the optimum parameters to synthesize small NP sizes for biomedical application.

Table of Contents

List of Figures

List of Tables

List of Abbreviations

IONPs	Iron Oxide Nanoparticles
NPs	Nanoparticles
CS	Chitosan
PLGA	Poly (lactide-co-glycolide) acid

1. Introduction

1.1 Polymers

A polymer is a substance or material that are made up of repeating units called monomers. From synthetic plastics like polystyrene to natural biopolymers like DNA and proteins that are essential to biological structure and function, polymers come in many shapes and sizes. They have unique physical features such as toughness, high elasticity, viscoelasticity, and a tendency to form amorphous and semicrystalline structures rather than crystals due to their subsequently huge molecular mass compared to small molecules [1].

There are mainly two types of polymers, synthetic polymer and natural polymer also known as biopolymer [1]. Some of the common biopolymers are collagen, chitosan, cellulose, starch etc. which are used in wide variety of applications [2].

Among all the applications, biopolymers are excellent choice of drug delivery carriers due to their biodegradable, biocompatibility and bioactivity [3]. They can bind and interact with metals and organic pollutants because of containing a number of repeating carboxyl, hydroxyl, and amino functional groups which help to design a positively or negatively charged carrier, inducing biological interaction with target organs, tissues and cells [2]. Due to its strong affinity for cell membrane, chitosan, which was initially positively charged, has been used in a variety of medicinal techniques via oral, nasal, intravenous, and ocular routes. This polymer has been used as a drug carrier by making NPs of chitosan and loading them with different drugs like rifampicin [4], chloramphenicol [5], tetracycline hydrochloride [6] etc. Drug delivery occurs after the deterioration and erosion of the polymeric shell caused by external stimuli like temperature and pH, [7] etc.

1.2 Chitosan

Chitosan is a polysaccharide which can be derives from chitin, a hard shell-like substance that can be found on the Crustaceans such as shrimps, crabs, lobster, krill and in certain fungi (Mucoraceae) [8]. Seven million tons of chitin are harvested annually which makes this biopolymer extremely cheap and readily available. Through chemical and enzymatic process called deacetylation, chitin can be converted into chitosan. Because of their unique structures, highly sophisticated

functionality and multi-dimensional properties, chitosan has become popular in medical, pharmaceutical, biomedical, chemical, food industries.

1.2.1 Physicochemical properties of Chitosan

Chitosan is a copolymer made up of d-glucosamine and N acetyl-d-glucosamine units that comes in a variety of grades based on the degree of acetylation [9]. It is a polycationic polymer having two hydroxyl groups, one amino group and in the repeating glycosidic residue [10]. The carbohydrate backbone consisting of (1→4)-linked d-glucosamine with varying degrees of N-acetylation and the acetylamino group substitutes the hydroxyl group on the C2 position (Fig 1) [11]. Chitosan has a strong crystalline structure after purification due to its intermolecular and intramolecular hydrogen bonding.

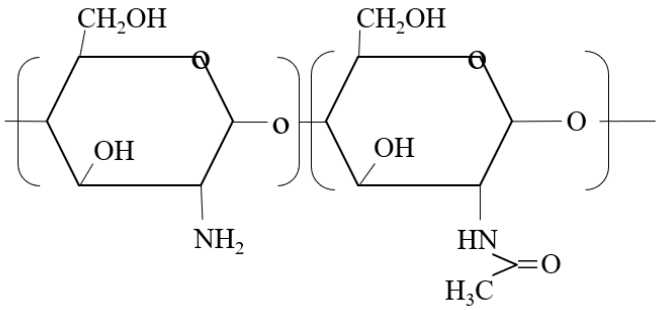

Figure 1: Chemical Structure of Chitosan

Chitosan is produced via the thermochemical deacetylation of chitin in the presence of alkali. Several alkaline techniques have been proposed, the majority of which include hydrolysis of the acetated position using sodium or potassium hydroxide solutions and a combination of anhydrous hydrazine and hydrazine sulfate [12]. Chitin is N-deacetylated when it is treated with an aqueous 40–45 percent (w/v) NaOH solution at 90–120 C for 4–5 hours. The polymer molecular weight and degree of deacetylation are determined by the deacetylation conditions. Main amino groups of the molecule give sites for a variety of side group attachments under moderate reaction conditions. The ability of chemical modification makes it a fantastic material for bioproduction [13]. Furthermore, the cationic, hemostatic, and insoluble at high pH qualities of chitosan may be reversed by sulfating the amine, which renders the molecule anionic and water-soluble, with the addition of anticoagulant properties [14]. Connected side of chitosan groups produce adaptable materials with unique functionality, alter biological qualities, and change physical properties.

The primary research interests in chitosan are its feature with various molecular weights and degree of deacetylation (DA) from chitin, the relationship between its solution characteristics and the DA, the preparation of derivatives, and applications.

The molecular weight of chitosan can vary from various range but most of the commercial chitosan have a range between 50-2000 kDa [15]. Based on molecular weight chitosan can be grouped into three groups such as low molecular weight (100 kDa), medium molecular weight (100–1000 kDa), and high molecular weight (>1000 kDa). Molecular weight has lots of effects on different characteristics of chitosan such as solubility, biodegradability, mucoadhesion etc. The mucoadhesion increases with the increase of molecular weight but the solubility and biodegradation increase with the decrease of the molecular weight of chitosan [16].

The DA is the most essential characteristic for chitosan characterization since it determines its properties and uses. The DA indicates the percentage of d-glucosamine units in the total number of units (N-acetyl-d-glucosamine + d-glucosamine) [17]. The DA of chitosan is typically between 60% -98 %. It is a water-soluble cationic polyelectrolyte composed of amines with different pH values. These amines get protonated and positively charged at low pH but deprotonate at higher pH. Chitosan solubility is determined by the DA. It is soluble in weak acidic solutions with a pH less than 6.0. Because it contains primary amino groups with a pKa value of 6.3 and can be considered a strong base. The presence of amino groups implies that pH has a significant impact on charged state of chitosan and characteristics [18]. Hyunmin et al. and Rinaudo et al reported that the function of chitosan protonation in the presence of acetic acid and hydrochloric acid, the degree of ionization is dependent on the pH and pK of the acid [19].

Chitosan has several biological properties making it an attractive substance for use in medical applications. These properties include biodegradability, anti-microbial effects, mucoadhesiveness, less toxicity, immune system stimulation and wound healing acceleration [20]. Eight human chitinases have been discovered so far, three of which exhibit enzymatic activity on chitosan [21]. Chitosan biodegradation results in the creation of non-toxic, variable-length oligosaccharides. These oligosaccharides might be absorbed into metabolic pathways or excreted [22]. The degradation rate of chitosan is mostly related to its degree of deacetylation, but also to the distribution of N-acetyl D-glucosamine residues and molecular mass as well [12].

Due to protonation of amino groups, chitosan has positive charges in acidic medium and can bind with negative residues in mucin, improving mucoadhesive characteristics. The antimicrobial activity of chitosan can be explained by two different mechanisms. The first mechanism claimed that positive charges on chitosan could bind with negative charges on the bacterial cell surface, altering permeability and leaking solutes outside the cells. The second hypothesis was that it could bind to bacterial DNA cells, preventing RNA synthesis [23].

1.2.2 Various forms of Chitosan

Chitosan can be used in a variety of ways with various technology. Microspheres, fibers, hydrogels, membranes, and nanoparticles are several types of Chitosan depending on their uses. Seenuvasan et al, reported that solubility of Chitosan is very important parameter for changing the forms of Chitosan as it involves blending in liquid state [24]. Mitra and Dey, suggested that it is possible to obtain the Chitosan beads or microspheres by the solvent evaporation and emulsion methods [25]. The beads are usually formed by blending other components like xanthan, gelatin, alginate, and cellulose with Chitosan. Drug molecules could be cross-linked to the beads for effective medical applications. Chitosan hydrogels are formed by the cross-linkage facilitated by the organic solvents [26]. Another study suggests that compared to its bulk form, fibrous form of chitosan has better mechanical qualities. These are made using electrospinning methods [27]. Membranes or films of chitosan is produced via casting procedures. These flexible chitosan membranes have some barrier properties that make them helpful for a variety of cosmetic and contact lens applications. Cui et al, reported that porousness and elasticity of the membrane determines its characteristics [28]. With variations in the DA, membranes with various tensile strength, permeability, elongation and water absorption may be created.

1.2.3 Different synthesizing methods of chitosan nanoparticles

Chitosan nanoparticles were originally mentioned in 1994 when Ohya et al. suggested using them to administer the anticancer medication 5-fluorouracil intravenously [29]. These nanoparticles were created by emulsifying and cross-linking chitosan. Since then, these systems have undergone substantial research for drug delivery purposes, and the original formulation has either been changed by using other manufacturing techniques or employed for other applications such as protein carriers, gene delivery vector, or active ingredients in toothpastes. Furthermore, researchers have created new chitosan nanoparticle formulations with supplementary matrix-forming

components. Numerous techniques have been created, mostly involving emulsification, various coacervations, or even slight changes of these. More precisely, the techniques include desolvation, ionic gelation, reverse micellar method, emulsion droplet coalescence, and emulsion solvent diffusion [30].

1.2.3.1 Emulsification and cross-linking

This process, which involved creating a W/O emulsion before adding a cross-linking agent to harden the produced droplets, was the first to be utilized to create chitosan nanoparticles. Chitosan's reactive amino groups covalently cross-link with aldehyde groups of glutaraldehyde after the emulsion is formed, which results in the creation of nanoparticles (Figure 2). Chitosan nanoparticles, which were employed to transport 5-fluorouracil, were first created by Ohya et al [29]. Songjiang et al altered the oil phase composition of the approach to include liquid paraffin and petroleum ether for the same drug delivery objective [31]. It has been shown that the amount of cross-linking and the speed of stirring have a significant impact on the final particle size [30].

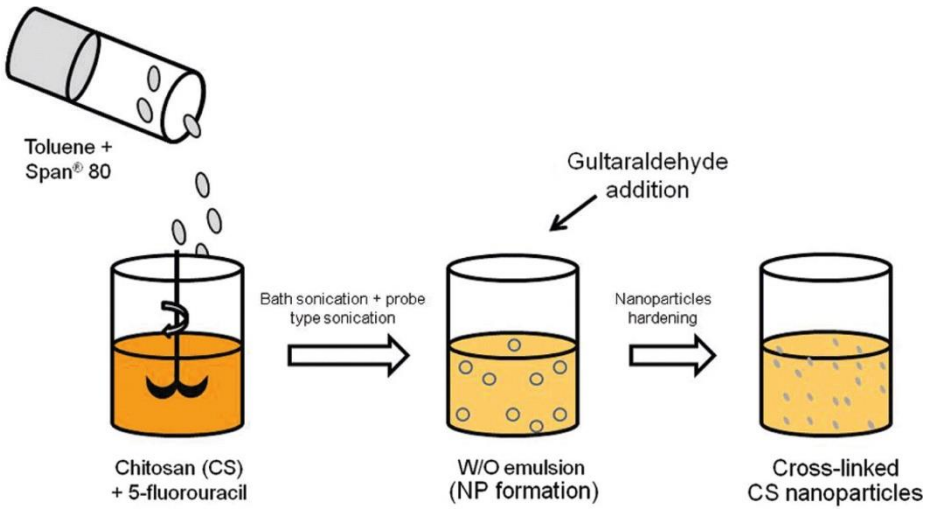

Figure 2: Graphical representation Emulsification and cross-linking [27]

1.2.3.2 Emulsion solvent diffusion

The process for making chitosan nanoparticles includes agitating an aqueous solution of chitosan and a stabilizer (such as poloxamer and lecithin) while adding an organic phase (such as methylene chloride and acetone) containing the hydrophobic medication. As a result, an O/W emulsion is created, which is then homogenized under high pressure. Then, at room temperature and reduced

pressure, methylene chloride is removed. As acetone diffuses into the aqueous phase at this point, chitosan's solubility decreases and nanoparticles start to form as the polymer precipitates. To allow for the full diffusion of acetone, more water is typically added. Centrifugation is the final step in the isolation of nanoparticles [27].

1.2.3.3 Reverse micellization

Mitra et al. was the first to describe the creation of chitosan nanoparticles from reverse micelles as a method for tumor-targeted administration. Reverse micelles form in a W/O system because they are W/O droplets, as opposed to ordinary micelles, which do so in an O/W setting [27]. In this process of reverse micellization, a lipophilic surfactant is dissolved in a suitable organic solvent, such as n-hexane, to create a W/O microemulsion. It has been used to clean surfaces using surfactants such sodium bis(ethylhexyl) sulfosuccinate, (AOT) or cetyl trimethylammonium bromide. The organic phase is then covered with an aqueous phase that contains chitosan, the medication, and glutaraldehyde while being continuously stirred. At this stage, reverse micelles are generated. After solvent evaporation, nanoparticles are then extracted.

1.2.3.4 Ionic gelation

Ionic gelation technique is based on the ionic interactions between the positively charged primary amino groups of chitosan and the negatively charged groups of polyanion such as TPP. TPP is non-toxic and multivalent, making it an ideal ion cross-linking agent. This physical cross-linking procedure prevents damage to medications, particularly biological medicines, by avoiding the use of chemical emulsifiers and cross-linking agents, which are often deadly to living organisms. As soon as a TPP solution is added to a chitosan solution at room temperature while being gently stirred, nanoparticle production occurs. The resulting slurry should be centrifuged to separate the nanoparticles from unreacted chitosan and TPP after stirring should be kept for about 10 minutes to facilitate particle stability. The resulting nanoparticle pellet is then redissolved in water [27].

1.2.3.5 Disolvation

The preparation of chitosan nanoparticles by this method is very simple and mild as it involves the dropwise addition of a competing agent of greater hydrophilicity. Substances such as sodium sulfate and non-solvents miscible with water, like acetone, have been proposed as precipitating agents. The use of desolvating agents was reported for the first time for the preparation of micron-sized carriers. As the salt enters in contact with the aqueous environment of chitosan solution, a

progressive elimination of solvation water surrounding it occurs. Eventually, this process leads to the polymer insolubilization and its consequent precipitation. This effect is observed because water–salt interactions are more favorable than those occurring between the water and the polymer. It is very frequent to include a stabilizer such as polysorbate 80 in the preparation medium, to stabilize the nanoparticle suspension. A subsequent process of cross-linking, for instance with glutaraldehyde, has been described in order to harden the nanoparticles. Factors such as chitosan molecular weight, concentration, amount of desolvating agent and stirring rate have been found to strongly affect the final characteristics of nanoparticles [27].

1.3 Iron Oxide Nanoparticles (IONPs)

Iron oxides are common naturally occurring substances that are also simple to synthesize in a laboratory. Including oxides, hydroxides, and oxide-hydroxides, there are 16 different types of iron oxide. These minerals are a result of aqueous reactions under various redox and pH conditions. They are fundamentally composed of Fe, O, and/or OH, but differ in the valency of iron and overall crystal structure. Some of the important iron oxides are goethite, akaganeite, magnetite, hematite and lepidocrocite [32].

Iron oxide nanoparticles (IONPs) consist of maghemite (γ-Fe2O3) and/or magnetite (Fe3O4) particles [33]. Due to their physiochemical characteristics, including as superparamagnetism, iron oxide nanoparticles (IONPs) have been used in a variety of applications, including targeted drug administration, catalysis, hyperthermia, and magnetic resonance imaging (MRI), among others. A form of magnetism seen in ferromagnetic or ferrimagnetic NPs is superparamagnetism. The temperature-dependent random direction-flipping magnetic domains of the NPs. The term "Neel relaxation time" refers to the period between two flips. The average value of NPs' magnetization is virtually zero if the measurement period for magnetization takes longer than Neel relaxation time in the absence of an external magnetic field. Superparamagnetic state is present in such NPs [34]. It is necessary for NPs to consist only of single magnetic domains, or for each atom in NPs to be a single magnetic domain, for them to be superparamagnetic. The NPs will develop a single strong magnetic moment during magnetization. NPs have a chance of becoming superparamagnetic if their diameter is less than 3–50 nm [34]. Numerous synthesis methods, including coprecipitation, hydrothermal synthesis, thermal decomposition, sol-gel synthesis, etc.,

can be used to create IONPs. IONPs are often produced in organic solvents using synthetic techniques such thermal decomposition, and they must then be phase-transferred into water for most of their uses, particularly in biomedicine. Additionally, IONP phase transfer enhances colloidal stability and prevents aggregation. The hydrophobic surface of IONPs is often modified with a polymer or ligand that is hydrophilic and increases the stability of IONPs in the aqueous phase. Through the ligand shell or polymer embedding, IONPs can be sterically stabilized [35]. Electrostatic stabilization of IONPs is achieved by adsorption of ions of stabilizers on the surface of IONPs. Kurlyandskaya et al reported that sodium citrate is a very good stabilizer, and the citrate anions are adsorbed on the surface of IONPs to provide electrostatic stability making IONPs colloidally stable [36]. Some other phase transfer ligands are citric acid, α-cyclodextrin, polyethylene glycol (PEG), Pluronic F127 and Chitosan, they change the hydrophobic nature of IONPs into hydrophilic nature preventing aggregation of IONPs [37].

The mono-dispersity of IONPs is crucial for biomedical and other applications because when IONPs aggregate, their magnetic characteristics vary, making it challenging to employ them for further applications. For instance, aggregation has a significant impact on the heating caused by an alternating magnetic field if they are employed to produce hyperthermia [38].

For applications like targeted drug delivery, IONPs need to be biocompatible inside living cells. So, surface modification is necessary for that i.e., surface coating or encapsulation of the IONPs. Nanoprecipitation, emulsion diffusion, salting-out, flash nanoprecipitation and solvent evaporation etc. are different techniques for surface coating or encapsulation by polymer. Coating of IONPs along with specific drugs is important to protect the NPs from aggregation and chemical degradation [38].

1.4 Synthesis of Polymeric nanoparticles

Polymeric nanoparticles can be synthesized by different types of method such as precipitation-based method including nanoprecipitation, salting out, rapid expansion of supercritical fluid into liquid and dialysis, direct composting method such as melting technique, microfluids and template-based technique, emulsion-based technique etc.

In this section, Chitosan NPs synthesis methods will be discussed briefly since Chitosan NPs have been used for coating of IONPs in this project.

1.4.1 Salting out

The physical, chemical, and mechanical properties of polymers that affect the kinetics of drug release as well as other processes including erosion, diffusion, and relaxation are primarily affected by salting-out agents. To link the relationship between the physicochemical and physicomechanical properties of polymer and release kinetics of the drug delivery systems, understanding and elucidating the mechanism underlying this phenomenon is crucial. According to Jitta et al, the 3D network of the polymer may be modified by salting out, which changes the morphology, glass-transition temperatures, robustness, and bond vibrations by using the variation in free energy to the salting-out agents [39]. Physical stiffness and swelling kinetics are controlled by electrolytic inclusions changing the environment and structure of matrix. The stability of water structures in aqueous polymeric solutions is caused by a reduction in the hydrogen bonding of the polymeric chain with water molecules during salting out. The polymeric chains become stiff due to the chemical bonds between the salts and monomers, which further alters the polymer characteristics and produces dimensionally stable polymers with increased structural integrity that are suitable for the ongoing release of medicines. The drug release kinetics are considerably changed by changes in the physiochemical characteristics. The choice of a salting-out agent is an important stage in the synthesis of polymeric nanoparticles since it plays a significant role in increasing encapsulation efficacy of the formulation. Some of the most often used salting-out agents are mineral salts like aluminum, magnesium, and sodium chlorides, non-electrolytes like sucrose, or metal sulfates, sulfites, carbonates, nitrates, or phosphates [39].

1.4.2 Super-critical Fluid

Super-critical fluid technology is effective at encapsulating different pharmaceuticals into polymer matrices. In this method, a polymer and medicine are dissolved using a supercritical fluid, such as carbon dioxide (CO_2). NPs are produced because of the fast growth of the mixture. The rapid expansion of supercritical solution (RESS) and the rapid expansion of supercritical solution into a liquid solvent are the two main processes involved in this method (RESOLV). The only application of RESS is for drugs with low drug concentrations and low molecular weight [40]. Duarte et al, reported that dexamethasone drug loaded with chitosan scaffolds was synthesized using supercritical fluid technology. Various parameters in this study were observed such as effect of pressure, temperature and contact time to evaluate the best operating conditions for impregnation process. The loading capacity of the scaffolds as well as the release profiles of the drug out of the

delivery device were also evaluated. Although this method makes it easier to create NPs with the fewest contaminants and residuals, the costs associated with running these operations are relatively significant. Additionally, the process is complicated by the need for cosolvents and surfactants to dissolve strong polar solvents into CO_2 [41].

1.4.3 Spray Drying

Spray drying is a fast, continuous process, that leads to the transformation of a liquid feed into dry particles. This process is completed in three steps, atomization, the mixing of fine droplets with gas stream and separating and gathering dry powder [42]. This method effectively encapsulates hydrophilic medications including ceftazidime, amoxicillin, and proteins such as insulin [43]. With this method, a polymer is first dissolved in a volatile organic solvent before being combined with an aqueous drug solution to create an emulsion. The NPs are created by spraying the emulsion via a regular nozzle into a hot nitrogen chamber, where they are then dried and cleaned before being used again. Nguyen et al reported that chitosan-amoxicillin complex was synthesized by spray drying method to investigate the antimicrobial activity against *Streptococcus pneumoniae* [44]. They used a Buchi Nano B90 as spray dryer. The size of the NPs and zeta potential were measured. The average size was between 160-1200 nm as they use three different molecular weights of chitosan. The zeta was between 55-35 mV. They also change the nozzle size of the spray dryer to see the effect of the size and zeta potential of the particles. Another study examined the entrapment efficiency and drug loading content of insulin-chitosan NPs, Guo et al. The quickest release of insulin and maximum rate of cellular uptake were achieved by spray drying the nanoparticles. The loading content was 25.2% and drug entrapment efficiency was 98.7% [43].

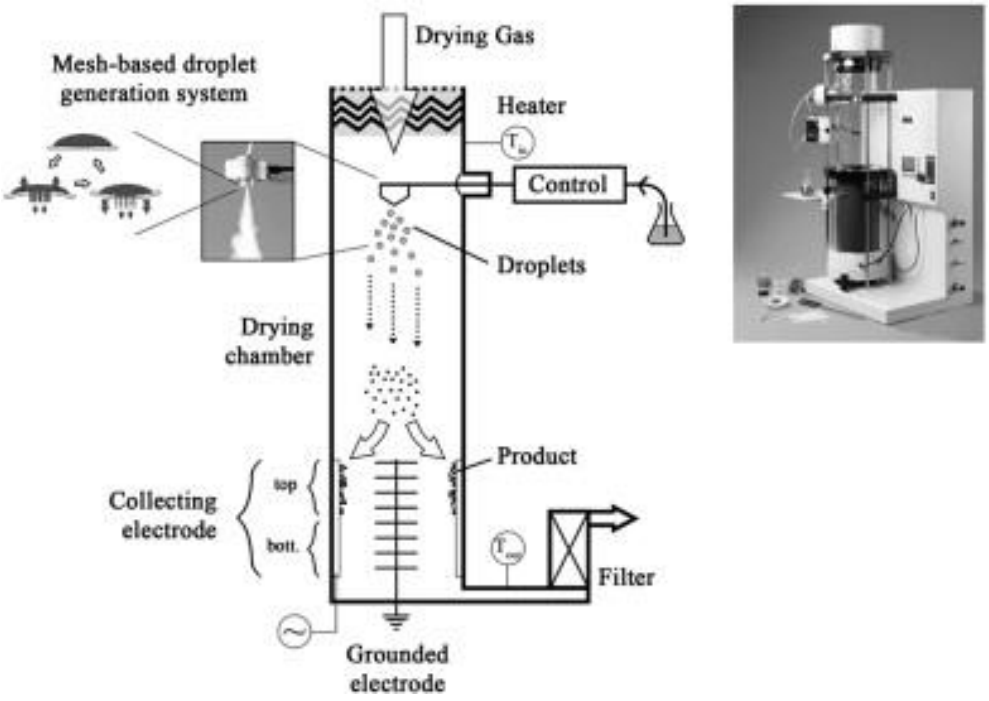

Figure 3: Schematic working principle of spray dryer B90 [44]

1.4.4 Microfluidics

At the nanoscale, nanoparticles have special characteristics because their surface area is quite big compared to their volume. Importantly, the size and form of nanoparticles affect their physiochemical characteristics. Nanoparticles must be synthesized with properly regulated size and shape to benefit from this phenomenon. Due to more exact control over size and form, resulting in a smaller size distribution of particles, microfluidic devices have demonstrated benefits over conventional batch synthesis procedures in the creation of nanoparticles [45].

According to Junping Ma et al, nanoparticles can be synthesized by two types of microfluidic system: single-phase continuous flow system and multiphase flow systems [46]. In a single-phase system, continuous laminar flow streams of single or multiple fluids flow through microchannels where nucleation and growth take place. The geometry of the microfluidic channel can be utilized to precisely control mixing and reaction times. Single-phase systems offer continuous modification in terms of allowing subsequent addition of reagents throughout the reaction [47].

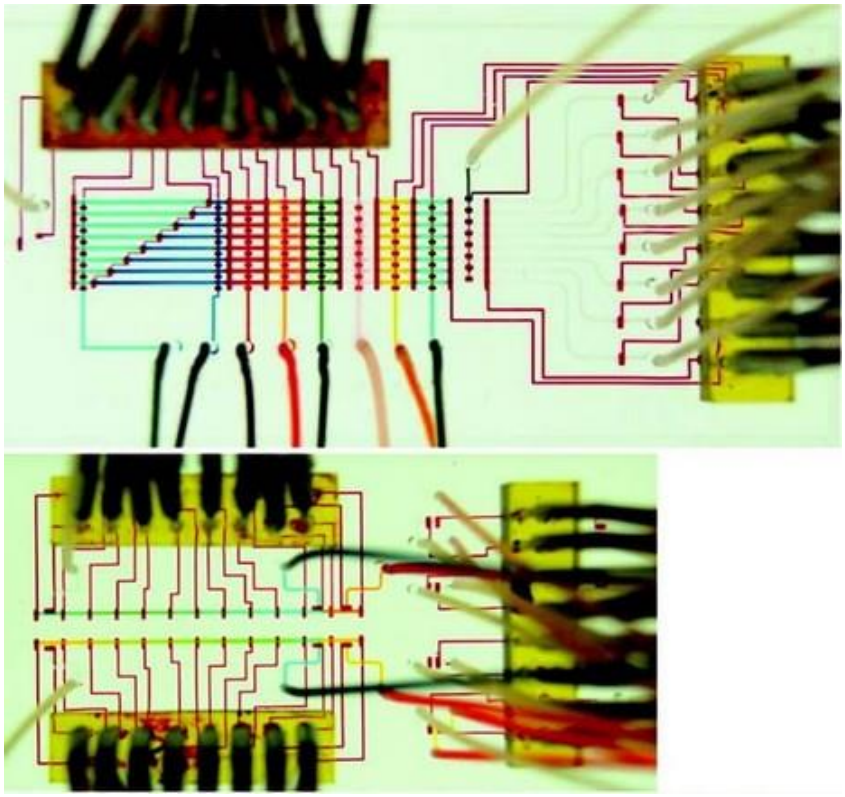

Figure 4: single-phase continuous flow system for nano-synthesis [48].

Microfluidic devices with multiphase flows comprise two or several immiscible fluids in segmented phases. The discrete segments act as small individual reaction chambers, where mixing is generated as each segment moves inside the channels. The very small volume of the droplet, typically on the picoliter scale, favours efficient thermal exchange and high reaction speed [49].

According to Mathew James et al, IONPs were synthesized by co-precipitation methods using microfluidic device. They suggested that coprecipitation synthesis of IONPs in microfluidic

devices provides a promising alternative to the classical technique of adding a base into a reservoir solution of iron salts. The chips allow precise control over the flow rates of the iron solution and base solution as they meet to begin nucleation and growth [50]. Farzad et al, synthesize alendronate-loaded chitosan nanoparticles by cross junction microfluidic device for introducing a suitable element for bone tissue engineering scaffolds [51]. Alendronate-loaded chitosan nanoparticles were created in six types with various physical characteristics by controlling the reaction condition in microfluidic device. The hydrodynamic diameter of synthesized particles was 102 to 215 nm.

1.5 Nanoprecipitation

Nanoprecipitation was developed by Fessi et al, often known as the solvent displacement process [52]. This process is one of the easiest ways to encapsulate organic or inorganic moieties into a polymer matrix. Polymeric nanoparticle synthesis is accomplished using nanoprecipitation. In this procedure, a solvent phase and a solid phase are mixed and a phase that is not solvent. The organic solvent makes up the solvent phase in which the non-solvent dissolves an organic/inorganic moiety phase includes a surfactant that inhibits the aggregation of an NPs and provides the NPs stability [53]. In this process, an organic solvent is often used to dissolve a polymer or other moieties such as drug or protein before being introduced dropwise to the non-solvent phase, which contains water and a surfactant. The employed organic solvent is miscible in water or another non-solvent, but the dissolved polymer or other moiety is insoluble in non-solvent, which causes them to precipitate and form a globule structure. These globule formations are stable because of the surfactant in the non-solvent phase. The generation of NPs in nanoprecipitation is explained by two different methods. The Gibbs-Marangoni effect, which asserts that the surface tension gradient causes the mass transfer between the fluids, is one of the processes that regulates the dissolution of the solvent phase into the non-solvent phase. Second is the explanation of NPs formation via Classical Nucleation Theory. Both mechanisms are discussed in detail in the following section.

1.5.1 Mechanism of Nanoprecipitation

Quintanar et al, suggested the mechanism for NP synthesis in nanoprecipitation by Gibbs-Marangoni effect or interfacial turbulence [54]. Surface tension fluctuations between the solvent and non-solvent phases provide the basis for this process. While the surface tension of the solvent phase is low, that of the non-solvent phase is high and exerts a larger draw on the surrounding liquid. Due to the difference in surface tension, there is turbulence at the solvent-non-solvent phase contact, which results in the development of counterflows at the interface of both phases. Increased mass transfer from one phase to another is the outcome of these flows. Because the solvent phase is miscible with the non-solvent phase, the solvent phase begins to break down into smaller and smaller droplets, culminating in solvent dissolution and polymer precipitation as NPs. The Marangoni Number (Ma) can be used to determine the interfacial tension gradient. Only when the value of Ma is bigger than the values of the solvent and non-solvent phases may the system become unstable. When the concentration gradient is responsible for the surface tension gradient, the Ma is given as:

$$Ma = \frac{\Delta\gamma \cdot \Delta C}{\eta \cdot DAB} \qquad (1)$$

Where ΔY is the interfacial tension gradient, ΔC is the concentration gradient, η is the organic phase viscosity, and D_{AB} is the organic phase diffusion coefficient in aqueous phase. This schematic of this mechanism is presented below [54].

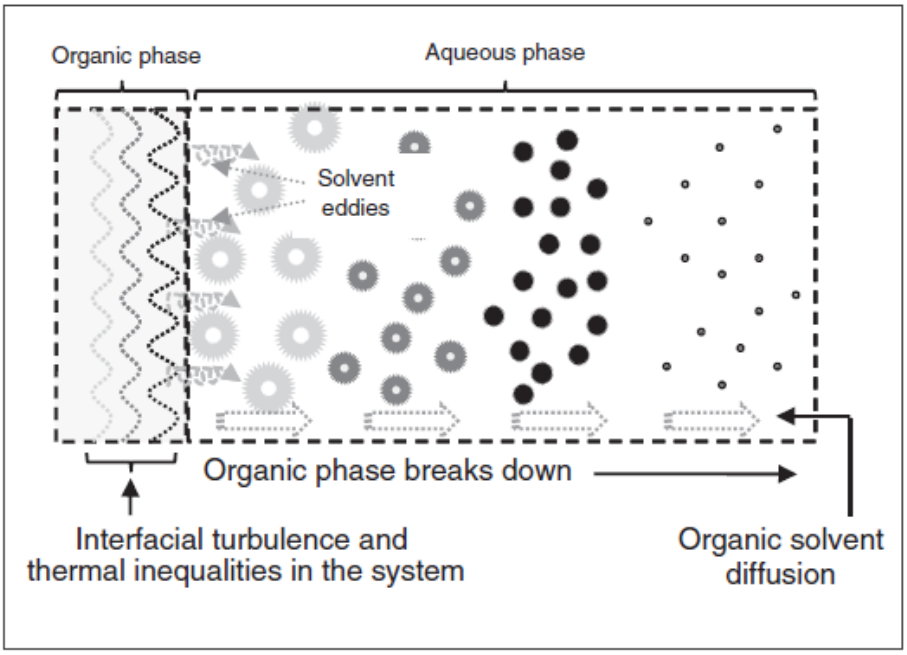

Figure 5: Schematic of mechanism of nanoprecipitation explained by Gibbs-Marangoni effect [54].

Ostrovsky et al, demonstrated that increasing the concentration of organic solvent in water causes a drop in ΔY. As a result, the Marangoni effect reduces, and hence mass transfer from one phase to another reduces. They suggested in this work that natural convection and forced mixing impact mixing intensity, which is reliant on mixture density [55].

Joye et al explained that particle formation in the nanoprecipitation process involves four steps: supersaturation, nucleation, growth, and coagulation [56]. This explanation was based on the theory of Sugimoto regarding polymer precipitation [57]. Supersaturation, defined as the ratio of polymer concentration to solubility in the solvent combination, is the driving force behind these events. As demonstrated in Figure 5, adding solvent to non-solvent reduces the ability of solvent to dissolve polymer, resulting in supersaturation and polymer precipitation. Following that, polymer particles combine and form primary nuclei to achieve thermodynamic stability; this

process is known as nucleation. The generated nuclei grow due to the interaction of solute molecules until they reach a critical dimension that is resistant to dissolution [56]. Fluid dynamics and phase mixing play a crucial role. They impact supersaturation and, due to the speed with which particles form, they also govern the nucleation rate. As a result, poor mixing yields few large nanoparticles (low nucleation rate), whereas good mixing yields a high nucleation rate and a greater population of tiny particles [58].

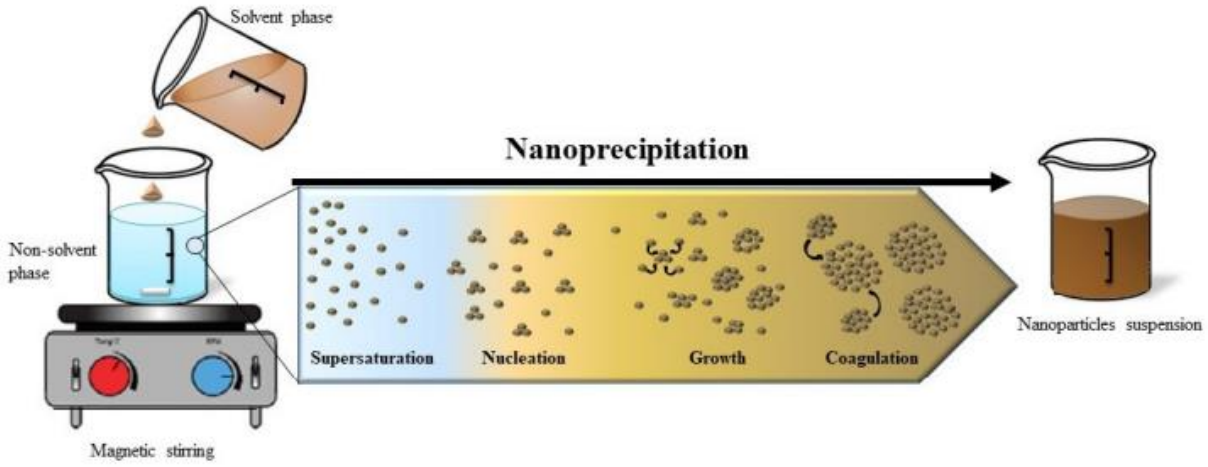

Figure 6: Four phases of Nanoprecipitation [59].

Nuclei development for condensation or coagulation occurs when the solute concentration falls below the critical supersaturation concentration. Condensation is the process by which single molecules are added to the surface of a particle. This phase terminates when the solute concentration falls below the equilibrium saturation concentration. Another key driving mechanism for particle development is coagulation. It is the adherence of particles to one another that occurs when attractive forces (Van Der Waals, hydrophobic contacts, etc.) outnumber repulsive forces (steric or electrostatic repulsion). The particles within the aggregate can be freed by using mechanical forces such as stirring, homogenization, or ultrasound. Nanoparticles, on the other hand, may consolidate through the aggregation process, resulting in the production of stable particles. The coagulation stage is determined by the frequency and efficiency of collisions. Collision frequency is defined as the number of collisions per unit time per unit volume and varies with particle concentration, particle size, and particle velocity. The collision efficiency, on the other hand, shows the number of collisions that result in coagulation and is determined by the

balance of attracting and repulsive forces between the particles. Stabilizing agents might be introduced during the procedure to protect particles from coagulation [60].

1.5.2 Factors affecting particle size in Nanoprecipitation

In nanoprecipitation, a variety of variables can affect the size and shape of NPs. Most researchers have focused their study on the following variables: polymer concentration, organic/aqueous phase ratio, organic phase addition rate, solvent type, and polymer molecular weight. The literature will be used to support detailed discussion of each of these factors.

1.5.2.1 Effect of polymer concentration

The polymer concentration has been observed to have a significant effect on the size of NPs in most research studies. Luque-Alcaraz et al, observed the increase of chitosan NPs on concentration. They used 0.5 and 2 mg/ml chitosan solution and the hydrodynamic sizes were range from 600-1900 nm [58]. According to Classical Nucleation Theory, a rise in super-saturation will occur due to an increase in polymer chains in the solvent phase. A greater number of nuclei will be formed, and the rate of NP growth will be rapid. As a result, raising the polymer concentration will increase the rate of NP growth, resulting in larger NPs. The second explanation is an increase in the viscosity of the organic phase produced by increased polymer concentration. Because the amount of polymer in the drop will grow significantly, the precipitation of polymer from the solvent will be impeded due to slower solvent diffusion into the nonsolvent phase, resulting in bigger NPs [61].

1.5.2.2 Effect of Temperature

Nanoprecipitation process is often stated to be performed at ambient or room temperature, there are just a few reports that study the influence of temperature on nanoprecipitation. Zhang et al, studied the influence of temperature (10, 20, 30, and 40 °C) on particle size generated by nanoprecipitation [60]. They noticed a drop in particle size from roughly 800 to 300 nm as the temperature was reduced from 40 to 10 °C. They hypothesized that smaller particles were caused by poor solubility, resulting in high supersaturation and a quicker nucleating rate at low temperatures. However, the reverse tendency was reported in another study [62]. They found that increasing the temperature by 10 ° C resulted in a 10 nm drop in particle size, with an overall decrease of roughly 100 nm when the temperature was raised from 0 to 80 ° C. They proposed that enhanced polymer solubility at higher temperatures limits precipitation [63].

1.5.2.3 Effect of solvent/non-solvent phase ratio

In several studies it was observed that by increasing the volume of non-solvent phase, the average mean size of the particles decreases. Luque-Alcaraz et al, observed in the chitosan NPs preparation that after increasing the non-solvent (methanol) volume from 10 to 40 ml, the chitosan NPs sizes dropped down from 800 to 600 nm [58]. Madani et al, studied the impacts of solvent/non-solvent phase ratio on the size of PLGA NPs and discovered that by maintaining a constant volume of non-solvent and increasing the amount of organic solvent phase from 1 to 3 ml, a decreasing size in the range of 478 to 300 nm was produced. This might be due to a reduction in organic phase viscosity and polymer concentration, resulting in smaller NPs. It was suggested that this was due to Ostwald ripening that over period of time solid particles change their inhomogeneous structure, because solvent evaporation would take longer in this circumstance, giving NPs more time to develop [64].

1.5.2.4 Effect of solvent type

The type of the solvent has a significant impact on the size of the NPs, and this is the most critical parameter. In nanoprecipitation, polymer solubility in organic solvent and organic solvent miscibility in water are critical for determining NPs size. Smaller NPs are produced by the solvent that has a higher miscibility in water. Because of the increased miscibility, the solvent migration from the organic phase to the aqueous phase is rapid, and the polymer forms itself into a smaller size.

Beck-Broichsitter et al, observed the size of PVA nanoparticles in different organic solvents such as methanol, ethanol, 1-propanol, 2 propanol. The PVA with methanol produced the highest sizes and PVA in 2-propanol produced lowest sizes. The nanoparticles were 100-500 nm in the range. They said that organic solvents having a higher affinity for a polymer but a "lower affinity for water led in the formation of larger polymer nanoparticles. Smaller nanoparticles are expected upon faster (more intense) mixing, because the polymer (dissolved in the organic solvent) would partition more effectively into the non-solvent phase [65]. In another research Luque-Alcaraz et al, produced chitosan nanoparticles dissolved in 2% acetic acid solution and 3% sodium formaldehyde bisphosphate. The chitosan particles dissolved in 2% acetic acid solution and 3% sodium formaldehyde bisphosphate were between 850-700 nm and 600-450 nm respectively. They concluded that if the diffusion coefficient of the solvent is high, small NPs with narrow size

distributions are formed. Larger NPs with broad size distributions are formed when the diffusion coefficient is low [58].

1.5.2.5 Effect of polymer molecular weight

There has been multiple research that shows various trends of observation on the influence of NP sizes on molecular weight. Öztürk et al, synthesized PLGA nanoparticles and chitosan coated PLGA nanoparticles and loaded them with clarithromycin. To make bare PLGA NPs, three different molecular weights of PLGA were used- 7000-17000, 24000-38000, and 38000-5400 Da. When the highest molecular weight PLGA was utilized, the particle size fell from 154 to 142 nm. The reason might be an increase in polymer hydrophobicity caused by an increase in the number of aliphatic chains with higher molecular weight [63]. Banderas et al, noticed a similar pattern of reducing NPs size with rising molecular weight, where raising the M.W from 12000 to 48000 Da resulted in a drop in particle size from 311 to 89 nm [64].

1.6 Zeta potential

There is no reliable method for determining the surface charge of tiny particles in liquid. The standard procedure is to locate the electric potential of a particle anywhere in the diffuse layer, far from the particle surface. The sliding or shear plane is the term used to describe this area in relation to particle movement in liquid. Zeta potential, a crucial characteristic for colloids or nanoparticles in suspension, is the potential measured at this plane. It is highly correlated with particle surface morphology and suspension stability [66].

1.6.1 Factors affecting zeta potential

According to Xu, Zeta potential is a property involving not only the particles but also their environment, e.g., ionic strength, concentration of solvent, pH, and even the type of ions in the suspension. Because of this, even though the zeta potential of suspended particles is measured after dilution to produce high resolution and accurate results, in many cases, these results would differ greatly from their true values in the original environment and may have little practical usefulness or even misguide the user [67].

Tentra el al, reported the effect of solvent concentration on zeta potential. They measured on four different samples. The results show that there is a concentration range within which the zeta-potential is not affected by nanoparticle concentration. The lower concentration limit for the

system to produce consistent results was dependent on the nature of the sample under study and ranged between 10^{-2} and 10^{-4} wt%. Below this concentration, there was an apparent shift in zeta-potential [68]. In this study for all four nanoparticle suspensions, they reported that the change in zeta-potential values at extreme dilution was thought to be an artifact because it was not caused by any actual modifications to the nanoparticle suspension. This change was believed to have resulted from a rise in the signal contribution coming from the foreign particles present in the liquid medium, which became more noticeable as the concentration of nanoparticles diminished. An increase in the irreproducibility seen among the replicate data sets may also have been caused by this impact. Additionally, it was thought that the intrinsic performance of instrument detector had a role in this irreproducibility.

pH is the most important parameter for zeta potential. For example, adding acid in nanofluid will decrease the pH, which will increase positive charges on the particle surface. Zeta potential will increase. If there are increasing number of OH- ions in the solution, the pH will increase which ultimately decreases the zeta potential. The point of pH at which zero electrophoretic mobility occurs is called an isoelectric point [66].

1.7 Biomedical Applications of Chitosan and Chitosan coated IONPs

In this section biomedical applications of Chitosan NPs And Chitosan coated IONPs will be discussed in detail. In this section, different biomedical applications of chitosan by nanoprecipitation and Chitosan coated IONPs will be discussed.

Huang et al, developed a new biodegradable amphiphilic copolymer containing a hydrophobic PLA moiety and a hydrophilic chitosan segment. Nanoprecipitation and emulsion/solvent evaporation were used to create imidacloprid-loaded copolymer submicron particles ranging from 180-230 nm. They postulated that smaller particles were synthesized by nanoprecipitation method and when chitosan-PLA copolymer solution in acetone was injected into an aqueous solution of imidacloprid, nanoprecipitation occurred after solvent evaporation, producing a single-layer submicron sphere. The chitosan-PLA copolymer and imidacloprid were dissolved in methylene chloride before being evaporated using the emulsion/solvent evaporation technique. Sonication in aqueous solution with polyvinyl alcohol (PVA) emulsified the mixture, and submicron particles were produced following solvent evaporation. Preliminary investigations of the novel copolymer submicron particles revealed that the fabrication method of the imidacloprid-loaded submicron particles, as well as the mass ratio of copolymer to imidacloprid, had a significant impact on particle size, size distribution, imidacloprid loading content, and imidacloprid release behavior. Because of the amphiphilic nature of copolymer, submicron particles can prolong pesticide release period [69].

Rajan et al, introduced a new approach for producing curcumin-loaded nanoparticles by nanoprecipitation utilizing chitosan (2.5%) and BSA (2%). This process produces nanoparticles with particle sizes ranging from 200 to 300 nm, which can be employed for passive drug targeting. Polydispersity index (PDI) results in the range of 0.2-0.6 revealed that the nanoparticles were polydispersive in nature as the concentration of polymers and drugs increased [70].

Mitomycin C (MMC) was encapsulated in PCL-based nanoparticles covered with chitosan by Bilensoy et al, by dissolving the hydrophilic drug in the aqueous phase. Chitosan (CS), poly-ε-caprolactone coated with chitosan (CS-PCL) and poly-ε-caprolactone coated with poly-l-lysine (PLL-PCL) were the three different particles. The sizes of the nanoparticles ranged from 180 to 340 nm, depending on the polymer utilized for synthesis and coating. Because MMC is water-

soluble, the efficacy of MMC encapsulation was dependent on the hydrophilicity of the polymers. The hydrophilic coating enhanced encapsulation by 2-fold for CS-PCL and 3-fold for PLL-PCL. Only CS-PCL nanoparticles were used to achieve complete drug release [71].

Luque-Alcaraz et al, studied the feasibility of binding nobiletin to chitosan nanoparticles and evaluating their antiproliferative efficacy. The loading and association efficiencies are 69.1% and 7.0%, respectively. The formation of an imine bond through Schiff-base between chitosan amine groups and the carbonyl group of nobiletin is suggested. Nobiletin-loaded chitosan nanoparticles inhibit cancerous cells significantly (IC_{50} = 8 g/mL), indicating their enormous potential for use in cancer treatment. The particle size distribution of chitosan nanoparticles and nobiletin-loaded chitosan nanoparticles gave approximate average sizes of 280 and 500 nm, respectively [72].

Correa-Pacheco et al, synthesized edible propolis chitosan films for food packaging and studied the physicochemical and antimicrobial activity of those films. The chitosan propolis-containing films had an inhibitory effect on several microbial communities including *Listeria monocytogenes* and *E. coli*. The chitosan particles sizes were measured 28.42 ± 7.43 nm which was observed from transmission electron microscopy (TEM). The films were made of five different concentration of chitosan (C1 -C5) and other characterizations of the chitosan-propolis were measured such as moisture content, coating thickness, degree of swelling etc. They observe when nanoparticles were added to the formulations and the propolis concentration rose, swelling and water solubility reduced and increased antimicrobial activity when the chitosan content in those films increased [73].

Shikida et al, prepared arginine conjugated chitosan NPs for treatment of wounds. The particles were made by modified nanoprecipitation method. The hydrodynamic sizes and zeta potentials were around 177 ± 35 nm and 30 ± 6 mV respectively at pH 6.1. Encapsulating arginine in conjugated NPs increased 1.5-fold the size of the nanoparticles while reducing the pH of the dispersions to 5.5. Argenine conjugated chitosan NPs contained around 10% arginine. After a rapid release of approximately 20%, the release of arginine remained steady and slow [55].

Chitosan coated IONPs have also been synthesized for various biomedical applications. Pérez et al, synthesized chitosan-coated magnetic iron oxide nanoparticles as magnetic nano-adsorbent for obtaining purified DNA and recombinant proteins. The particles were 14 ± 4 nm in sizes which was characterized by SEM. The Redlich-Peterson isotherm fitted the DNA experimental

adsorption capacity well, yielding a maximum of 98 mg/g. An adsorption capacity of 440 mg/g for DNA was found [74].

Araujo et al, studied nanocarriers composed of chitosan coated iron oxide loaded with chlorhexidine. The antimicrobial and antibiofilm effects were studied on different microbial organisms. The average diameter of the IONPs-CS compound was estimated at 29.9 ± 10.7 nm and chlorhexidine loading IONPs were 33.6 ± 10.7 nm. Iron oxide nanoparticles were coated with chitosan (CS) and loaded with chlorhexidine at 31.2, 78 and 156 μg/mL. Antimicrobial effects were estimated by determining the minimum inhibitory concentration. They observed the highest reductions in total biofilm biomass and metabolism when CS-IONP nanocarrier contained 156 μg/mL chlorhexidine. After 24 and 48 h of exposure, the nanocarrier reduced chlorhexidine toxicity to the cell at low concentrations [75].

This introductory section provided an overview of IONPs and biopolymers such as chitosan, including their physicochemical features and production technique. Various approaches for producing polymeric NPs were also addressed. The mechanics of nanoprecipitation, as well as the variables that influence the size of the NPs, were thoroughly explored. The biomedical uses of chitosan and chitosan coated with IONPs were discussed at the end of this section.

2. Materials and Methods

2.1 Materials

Chitosan was collected from the Biopolymer NMR lab of the department of Biotechnology, NTNU. Two types of chitosan were collected. The sample from (Fig 7a) were made from shrimp shells which are demineralized (HCl), deprotonized by treating with NaOH and deacetylated and are precipitated at alkaline pH, so the amino group of the polymer is not charged. This means it is not soluble in water. Three types of water insoluble chitosan were collected, and they have different molecular weight (198kDa, 307 kDa and 604kDa) and degree of deacetylation (DA) (0.2, 0.18 and 0.17) respectively.

The chitosan in (Fig 7b) was dissolved in 0.2 M acetic acid, dialyzed against NaCl and then against distilled water before freeze drying. This means that the amino groups will have Cl- as counter ion and therefore is soluble in water. The molecular weight is 198 kDa and DA 0.18.

Acetic acid was used to dissolve the chitosan (Fig a) and Milli Q-water was used for dissolving chitosan (Fig b). Tween 20 (100%) and tween 80 (100%) were used separately as surfactant. Tween 20 and 80 were purchased from Sigma Aldrich, Germany.

Iron (III) chloride hexahydrate ($FeCl_3.6H_2O$), iron (II) chloride tetrahydrate ($FeCl_2.4H_2O$) and 25% ammonia solution were used for the synthesis of magnetite which were purchased earlier from. Sigma Aldrich, Germany. Milli Q-water was used for the synthesis of magnetite.

For the preliminary studies, PLGA (poly lactide-co-glycolide acid) with molecular weight of (30000-60000), DMSO and pluronics F127 were used.

Note: The chitosan which is insoluble in water is named chitosan A and chitosan which is soluble in water is named chitosan B. It will be addressed for the rest of this report.

(a) (b)

Figure 7: a) water insoluble chitosan A with molecular weight of 198kDa, 307kDa and 604kDa and different degree of deacetylation (FA =0.20, 0.18 and 0.17 respectively). And b) water soluble Chitosan B with 198kDa molecular weight and degree of deacetylation FA = 0.18.

2.2 Synthesis Methods

In this section, for preliminary studies the procedure of bare PLGA NPs and PLGA-IONPs were performed. Then we followed to synthesize bare chitosan NPs by nanoprecipitation method, IONPs by co-precipitation and Chitosan coated IONPs by nanoprecipitation are highlighted.

2.2.1 Synthesis of bare PLGA NPs by nanoprecipitation

For the synthesis of PLGA NPs, nanoprecipitation technique was used according to master's thesis (A Bin Ashar, 2021) [37]. Firstly, 20 mg of poly (lactide-co-glycolide acid) (Mw-30000-60000) were weighed in different vials and 1 ml DMSO was added in each vial. PLGA were dissolved in DMSO under constant stirring. Secondly, a stock solution of 5mg/ml aqueous pluronics F127 was prepared. 20 ml of solution was poured from the stock solution in each vial. Using a syringe pump and a flowrate of 4.5 ml/h, the 1 ml polymeric solution for each PLGA was injected dropwise into the aqueous pluronics F127 solutions. The polymeric mixtures were then continuously stirred at 500 rpm for 5 hours. Then the solutions were aliquoted in eppendorf tubes and centrifuged for 20 minutes at 14500 rpm. At the bottom of the eppendorf tube, PLGA NPs were collected, and the

supernatant was discarded. The NPs at the bottom were redispersed into a known amount of MQ water and characterized using DLS.

2.2.2 Synthesis of bare chitosan NPs by nanoprecipitation

2% aqueous acetic acid solution was added to dissolve Chitosan A according to the paper Luque-Alcaraz et. Al [58]. 100ml of chitosan solution was made with chitosan A at different concentration (2mg/ml, 0.5mg/ml). For 2mg/ml conc. Chitosan, 200 mg of chitosan were measured and transferred in Schott bottle. Then 100 ml 2% aqueous acetic acid solution was added in the bottle. Then sonication was done 30 minutes to 1 hour accordingly.

For chitosan B Milli Q-water was added to dissolve the polymer. For 2mg/ml conc. Chitosan solution, 200 mg of chitosan were measured and transferred in Schott bottle. Then 100ml Milli Q-water were added in the bottle. Then the bottle was placed on a stirring plate and left for stirring for 12-14 hours until dissolved completely.

For bare chitosan nanoprecipitation, two phases are needed. One is solvent phase which is chitosan in acetic acid or water and another is non-solvent phase which is methanol and 0.05% tween as a surfactant. 10ml of that methanol solution was taken in a glass vial and placed on a magnetic stirrer at 500 rpm.

For nanoprecipitation, the chitosan solution was added dropwise in the methanol solution. In order to do that, first the flow pump was calibrated at 58.06 ml/h. Then 1 ml of chitosan solution was added to 10-25 ml of methanol solution via flow pump.

After that, the solution was taken to do either centrifugation or rotary evaporation to remove the methanol from chitosan solution. Then Milli Q-water was added for redispersing the chitosan NPs for further characterization.

2.2.3 Synthesis of IONPs by co-precipitation

For the synthesis of IONPs by co-precipitation, 84.6 mg of MQ water was weighed in a beaker and 15.4 ml of 25% (vol%) ammonia solution was added into it. 4 g of $FeCl_2.4H_2O$ and 10.8 g of $FeCl_3.6H_2O$ were weighed carefully and dissolved in MQ water in a 50 ml volumetric flask. The mixture was shaken well until no undissolved traces were left in the solution. 10 ml from the prepared solution of iron precursors was then added dropwise using a burette into 100 ml of 1M aqueous ammonia solution under constant agitation. It was observed that the iron oxide NPs readily

started to form as the iron mixture was added into the ammonia solution. The obtained IONPs were then magnetically separated and washed three times with MQ water. Finally, IONPs were dispersed in 12 ml MQ water. The NPs were then characterized using DLS, VSM, Lumisizer and TEM.

The picture of the setup for IONPs synthesis and magnetic separation step is shown below:

(a) (b) (c)

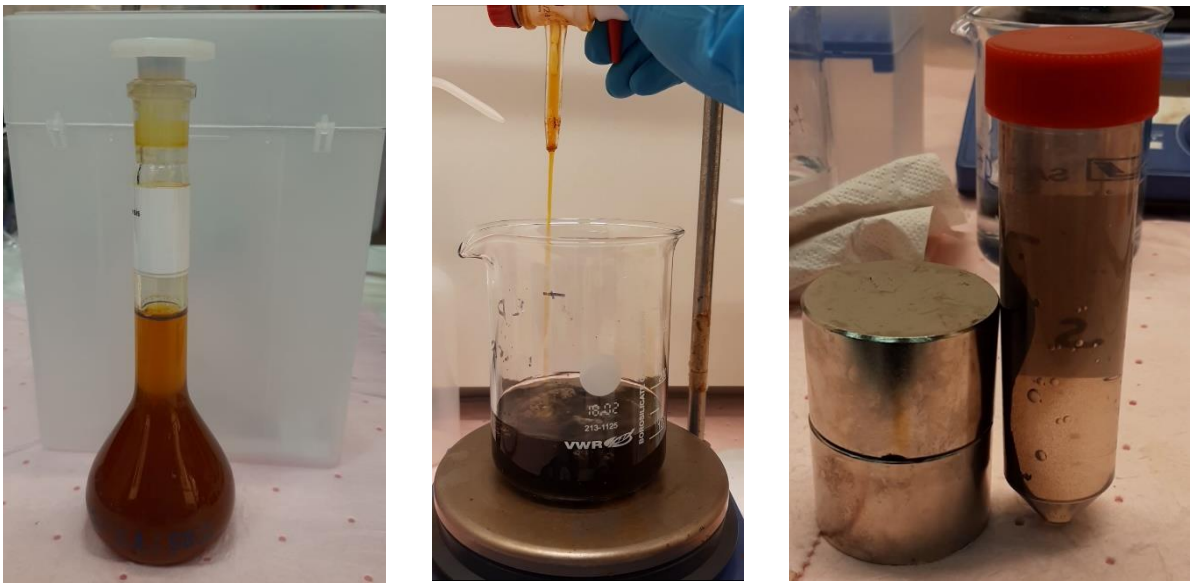

Figure 8: (a) The iron mixture solution, (b) the setup of synthesis of IONPs and (c) magnetic separation of IONPs during washing steps.

2.2.4 Synthesis of PLGA-IONPs by nanoprecipitation

Nanoprecipitation was used to encapsulate IONPs produced using the co-precipitation technique in PLGA (Mw – 30000-60000). For this procedure, 1 ml of 4 mg/ml concentrated IONPs (synthesized method from 2.2.3 section) was used and was magnetically separated in an eppendorf tube. After adding 1 ml of 20 mg/ml concentrated polymeric solution (polymers dissolved in DMSO), IONPs were dissolved into the solution by vortexing the eppendorf tube three times for 20 seconds each. Then, using a syringe pump and a flow rate of 4.5 ml/h, the mixture of IONPs and polymer was dropped into the pluronics F127/water solution. It was then stirred for 5 hours. During PLGA-IONPs nanoprecipitation, magnetic separation was conducted in two phases. First, a 30 second magnetic treatment was done to separate the unbound IONPs and polymer from the

polymer coated IONPs. The supernatant was transferred in separate vial. Then the supernatant containing PLGA-IONPs were treated with 2 min magnet separation three times and 3 washes only for screening out the PLGA-IONPs.

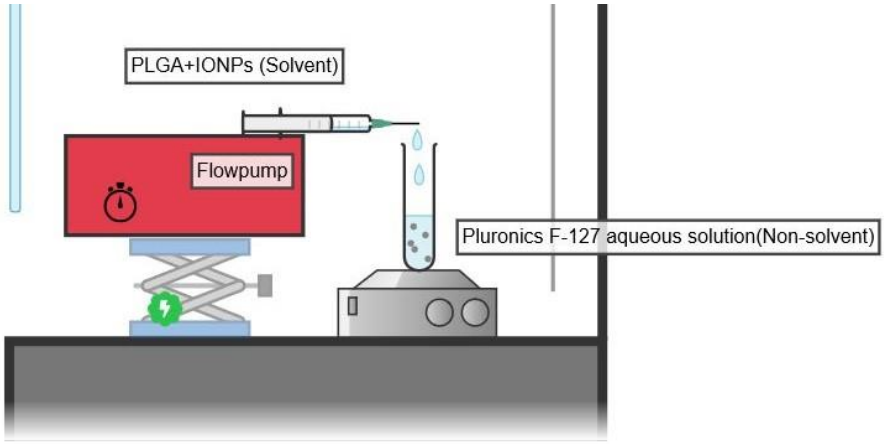

Figure 9: Illustration of PLGA-IONPs synthesis by nanoprecipitation

2.2.5 Synthesis of Chitosan coated IONPs by nanoprecipitation

Nanoprecipitation was used to coat IONPs produced using the co-precipitation technique in Chitosan, here chitosan B was used. For this procedure, 1 ml of 5 mg/ml concentrated IONPs (synthesized method from 2.2.3 section) was used and was magnetically separated in an eppendorf tube. After adding 1 ml of 2 mg/ml concentrated polymeric solution (polymers dissolved in water), IONPs were dissolved into the solution by vortexing the eppendorf tube three times for 20 seconds each. Then, using a syringe pump and a flow rate of 58.06 ml/h, the mixture of IONPs and polymer was dropped into the Tween/methanol solution. During chitosan coated IONPs nanoprecipitation, magnetic separation was conducted in two phases. First, a 30 second magnetic treatment was done to separate the unbound IONPs and polymer from the polymer coated IONPs. Then the supernatant was discarded. Then the NPs separated by magnet washed 3 times and characterized using DLS and other techniques such as FT-IR, SEM etc.

2.3 Characterization

2.3.1 Dynamic Light Scattering

Malvern Zetasizer Nano ZS© and later Anton Paar litesizer 500 were used to measure the hydrodynamic size and zeta potential of PLGA, chitosan NPs, PLGA encapsulated IONPs and chitosan coated IONPs. The variation of these conditions was performed in Anton Paar 500 by changing the refractive Index of the SOP (Polystyrene latex and Unknown material discussed in appendix E) and measurement angle of the system (10°, 90° and 175°). For bare chitosan samples, the measurement angle was varied from back scattering 175° to side scattering 90° and its effects on sample size was observed. For chitosan coated IONPs three different measurement angles were measured once to check the size difference, usually back scattering 175° angle was used. The solvent used for all the samples was MQ water. All values were generated in triplicates and the average was taken.

2.3.2 Lumisizer

LumiSizer Dispersion Analyser was used to measure the particle size distribution of chitosan NPs, IONPs and chitosan coated IONPs. The particle size distribution is volume weighted which means distribution per volume of the particle sizes, shown as a differential of total volume of all counts. Volume is a cubic function of the particle size which is representative of the distribution in a column fill. The particles were measured in either constant time or constant position.

2.3.3 Vibrating Sample Magnetometry

Magnetic measurement of IONPs were carried out using MicroMag™ 3900 vibrating sample magnetometer (VSM). MicroMag™ 3900 was operated at room temperature with maximum applied magnetic fields of 1 T and the magnetization of the samples were recorded. Dried IONPs sample was used for VSM.

2.3.4 Fourier Transform Infrared Spectroscopy

FT-IR spectra were recorded with a Bruker Vertex 80v ATR-FT-IR spectrometer in the range 500–4000 cm^{-1} to observe chemical properties of chitosan NPs, IONPs and chitosan coated IONPs. In this technique, one drop of concentrated sample was placed onto the ATR crystal and infrared light was absorbed by the sample emitting different wavelength of spectrum according to the

configuration of the sample. The functional groups of each sample were observed and confirmed by literature review.

2.3.5 Scanning Transmission Electron Microscope (STEM)

Scanning transmission electron microscopy (STEM) images were taken of chitosan NPS, IONPs and chitosan coated IONPs. The samples were diluted and drops of the diluted samples (~ 10 µL) were put on a Formvar carbon coated copper grid. STEM Imaging was performed on IONPs, chitosan NPs and chitosan coated IONPs. Two types of staining were used for those NPs. Uranyl acetate and Phosphotungstic acid. 30 kV was used for imaging the NPs. For Uranyl acetate staining the NPs were incubated with the solution for 30 mins and then 6µl of that solution was put on the grid for 5 min. For Phosphotungstic acid staining, 10µl NPs were added on the grid for 5 mins and then soaked off excess samples with filter paper. Then 6µl staining solution was added on the grid for 1/2 mins before soaking them from the grid.

2.3.6 Transmission Electron Microscope (TEM)

Transmission electron microscopy (TEM) images were taken using the Thermo Fisher - Tecnai 12 transmission electron microscope for imaging IONPs. The samples were diluted and drops of the diluted samples (~ 10 µL) were put on a Formvar carbon coated copper grid. Then the samples were stained with Phosphotungstic acid. 30 kV was used for imaging the NPs. The staining procedure was done like STEM (section 2.3.5).

3. Results and Discussion

The preliminary studies were done on PLGA, to see how concentration, flowrate changes hydrodynamic sizes and zeta potentials and how PLGA encapsulate IONPs are different in hydrodynamic sizes and zeta potentials by nanoprecipitation method. These results gave ideas how to proceed synthesizing chitosan NPs and chitosan coated IONPs by nanoprecipitation method and then optimizing the synthesis parameters to get better sizes. Our main study is about synthesis and different characterization of chitosan and chitosan coated IONPs.

In this section all the results obtained from different studies are discussed in detail with reference to present literature on similar studies. The first section (3.1) starts with the preliminary studies of synthesis of PLGA NPs using nanoprecipitation. The next section (3.2) is the synthesis of chitosan NPs using nanoprecipitation. Then section 3.3 is the results of IONPs by co-precipitation methods. The last two chapters (3.4 and 3.5) are the results of coated IONPs with PLGA and chitosan respectively.

3.1 Synthesis of PLGA NPs by nanoprecipitation (Preliminary study)

PLGA NPs nanoprecipitation and PLGA-IONPs nanoprecipitation syntheses were done to understand the principle of nanoprecipitation and characterize the hydrodynamic sizes and zeta potential by DLS, as preliminary studies for the project. In this section, the results of PLGA NPs are discussed and PLGA-IONPs results will be discussed later in section 3.4.

The hydrodynamic sizes and zeta potentials were observed in three different concentrations (5mg/ml, 10mg/ml and 20mg/ml) of PLGA solution and at two different flowrates 4.5 ml/h and 2.5 ml/h.

3.1.1 Effect of PLGA concentration

Three different PLGA concentrations were used to see the difference between sizes and zeta potentials. The different concentrations were 5 mg/ml, 10 mg/ml and 20 mg/ml.

The polymer concentration has significant effects on sizes as the concentration of the polymer increases the sizes of the NPs also increase. Higher polymer concentration possibly increases super-saturation and the number of polymer chains in solvent phase. An increased number of

nuclei is formed, and the growth rate of NPs is also fast. Hence increasing polymer concentration increases the growth rate of NPs according to Hernández-Giottonini et al [59].

The negative charge originates from the deprotonated carboxylic groups present in the PLGA made the surface charges negative of the NPs. The sample with 20 mg/ml concentrated PLGA NPs has low negative zeta potential than 10 mg/ml and 5 mg/ml. But it was in the same range of negative zeta potential (from -27 to -25 mV) which suggested the PLGA NPs could be colloidally stable in the dispersion medium regarding different concentrated PLGA solution.

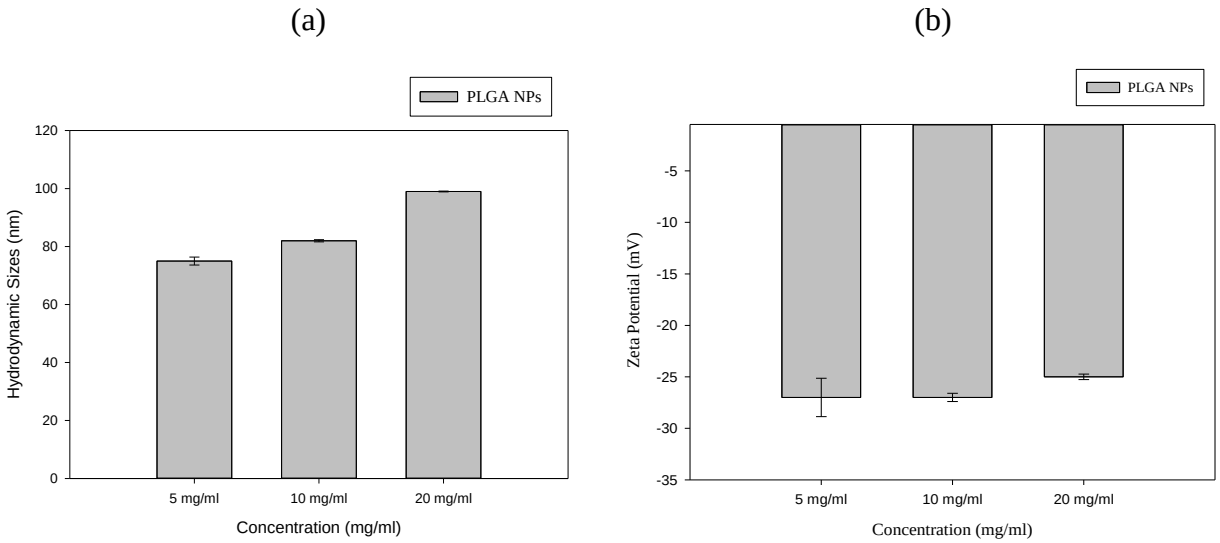

Figure 10: Graph represents the hydrodynamic sizes (a) and zeta potentials (b) of PLGA NPs at three different concentrations.

3.1.2 Effect of flow rate

The aim was to look at differences in both sizes and zeta potentials for the different flowrates. Other parameters were constant. The two flowrates were 2.5 ml/h and 5 ml/h.

The change in flow rates did not give any significant changes in the hydrodynamic sizes. The size range was between 95-110 nm. It has been reported in Zhang et al, that higher stirring rates decrease in particle sizes. The decrease in particle size may be due to enhanced mass transfer and rate of diffusion leading to rapid nucleation and precipitation [60]. Another reason was argued by Mora Huertas et al, that larger NPs are obtained at lower flowrate because of nonhomogeneous mixing of organic and aqueous phase [51].

So, similar sizes might be because of same mass transfer and rate of diffusion in both flow rates. There were no other experiments on the effect of flow rates with PLGA NPs to observe if the sizes actually increase when the flow rate decreases, so there could be some experimental errors also with the result.

The zeta potentials of both particles were in the same negative range (from -27 to -25 mV). which suggested the PLGA NPs could be colloidally stable in the dispersion medium regarding different flow rates.

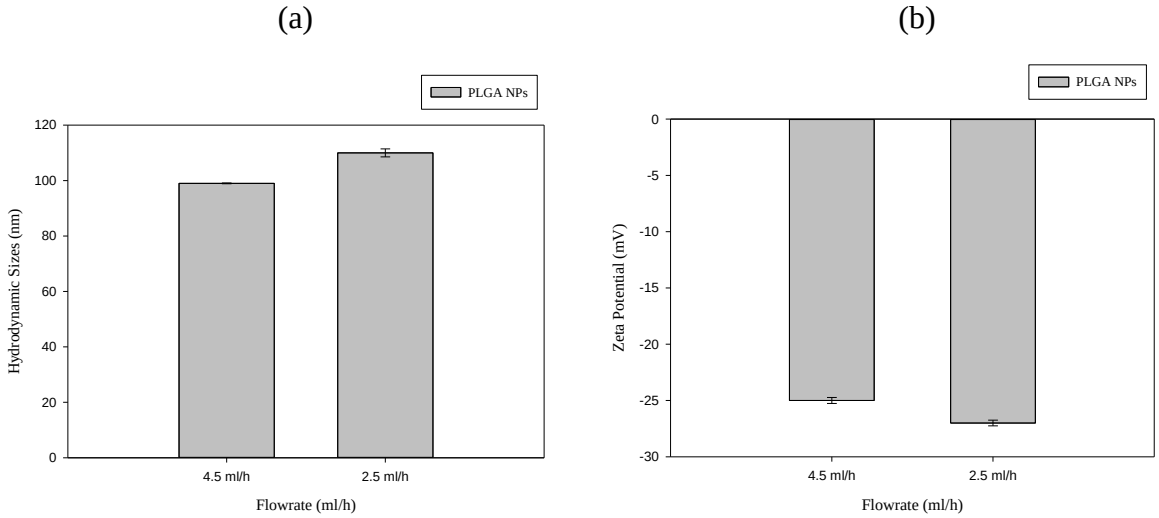

Figure 11: Graph represents the hydrodynamic sizes (a) and zeta potentials (b) of PLGA NPs at two different flowrates.

3.2 Synthesis of bare chitosan by nanoprecipitation

Bare chitosan NPs have been synthesized and the hydrodynamic sizes and polydispersity index (PDI) were measured in Dynamic Light Scattering (DLS) by measuring the Brownian motions of the NPs and zeta potentials were determined in Laser Doppler Velocimetry (LDV) by measuring the electrophoretic mobility of the NPs. Different synthesis parameters were changed to see their effects on the physicochemical properties. In these experiments, chitosan A with three different molecular weights (198 kDa, 307 kDa and 604 kDa) were used. Then chitosan B was introduced later on. It was mentioned earlier (section 2.1), the chitosan A was precipitated at alkaline pH and the amino group is not charged making the polymer insoluble in water. On the other hand, chitosan B has the amino groups will have Cl- as counter ion making it soluble in water as it was dialyzed

against NaCl. For methanol removal, centrifugation was the first extraction method which was tried. But it was not well-suited extracting technique for bare chitosan NPs which will be discussed later. Then rotary evaporation technique was used for removing the methanol in chitosan NPs solutions.

3.2.1 Synthesis of chitosan NPs with Chitosan A

NPs from chitosan A were measured by DLS. Different synthesis parameters were used and observed the size of NPs on those parameters. Optimized studies of DLS were also performed.

Water insoluble chitosan A (method Figure a) was first used for making chitosan NPs. Three different molecular weights (198kDa, 307kDa, 604kDa) and DA of chitosan A were used. 2% acetic acid aqueous solution was used for dissolving chitosan A. Centrifugation was used for extracting chitosan NPs from methanol + tween 20 solution at 1500 rpm for 20 mins. Later on the study, rotary evaporator was used to be able to remove methanol completely from chitosan solution after nanoprecipitation.

The molecular weight of chitosan, concentration of chitosan solution, flowrate and stirring time duration of magnetic stirrer are the synthesis parameters which were varied to see the effects of sizes. Homogeneity and surface charge of the NPs were measured by PDI and zeta potentials respectively.

The synthesis parameters (molecular weight, concentration of chitosan, stirring time and flowrate) of the experiments were varied to see the effects on the hydrodynamic sizes. Centrifugation method was used for removing methanol from the chitosan A NPs solution. According to centrifugation mechanism, the centrifuge machine uses centrifugal forces to separates the particle from solution according to size, density etc. After centrifugation even if there was no precipitated NPs were seen clearly, as chitosan NPs were supposed to be solid, it was assumed that the solution containing chitosan NPs should be at the bottom of the 11 ml solution (1ml solvent + 10 ml non-solvent). So, 10 ml of the solution was discarded, and the remaining 1 ml of the solution was taken to an Eppendorf tube and used for DLS measurements. As there was no pallet of chitosan NP seen at the bottom of the centrifuge tube, it was not sure whether 1ml of that solution contain chitosan NP completely and not contain any methanol solution. So, traces of methanol solution in the chitosan

NP solution might have some influence in the DLS sizes which might contradict the size trends discussed in the literature below.

3.2.1.1 Control Test on surfactants (tween 20 and tween 80)

After nanoprecipitation of the chitosan A NPs, centrifugation method was performed before shifting to rotary evaporator for removing non-solvents and as mentioned (section 3.2.1), out of 11 ml of the solution, 10 ml were removed. There might be a possibility that the hydrodynamic sizes in Table A1 (Appendix A) measured by DLS were not actually polymer NPs rather than surfactant particles. So, a control experiment was done where polymer was absent in the organic phase and organic solvent was added to the non-solvent.

(Figure 12) represents the hydrodynamic sizes of surfactant (tween 20 and 80). The hydrodynamic sizes were between 25-55 nm which were lot less than the sizes measured for the polymer containing solution. This might confirm that those samples contain chitosan NPs even if the amount is low.

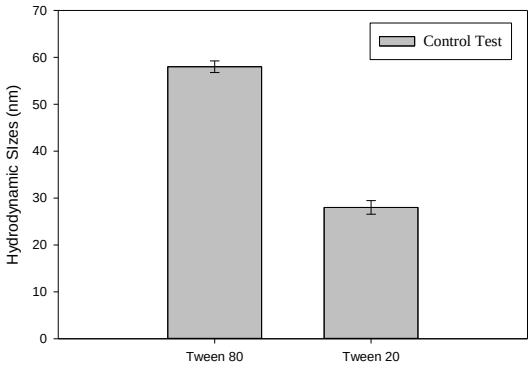

Figure 12: The graph represents the hydrodynamic sizes of samples from control experiment

3.2.1.2 Effects of Molecular weights

(Figure 13) represents the hydrodynamic sizes of chitosan NPs for three different molecular weights. Keeping other parameters constant (concentration of polymers, flowrates, stirring time) no significant changes in hydrodynamic sizes observed by changing molecular weight of the chitosan and they were between 230-250 nm. In most cases, a general trend with respect to

molecular weight has not been observed. There are some nanoprecipitation studies that observed a decreasing in sizes when the molecular weight of polymer is higher. Öztürk et al, and Banderas et al, both find decreasing trend on NPs sizes when they used higher molecular weight polymer. Öztürk et al synthesized chitosan coated PLGA NPs and loaded them with clarithromycin. PLGA with three different molecular weights 7000-17000, 24000-38000 and 38000-5400 Da were used to synthesize chitosan coated PLGA NPs. They found that the NPs size decreased from 154 to 142 nm. They used 90 mg/ml concentrated PLGA solution [63]. Similarly, Banderas et al, increased the M.W from 12000 to 48000 Da of PLGA polymer and observed NPs size from 311 to 89 nm. They used 5 ml PLGA solution. They postulated that the higher M_w polymer has high hydrophobicity due to large number of aliphatic chains which can decrease the NP sizes [64].

In our study, the hydrodynamic sizes did not follow any of the trends. The amount of the chitosan was lot less (2 mg/ml) in the solution than what were shown in other studies and presence of surfactant in the solution are some experimental differences which might cause not following the trends. The presence of methanol in the solution could influence the size of the NPs also.

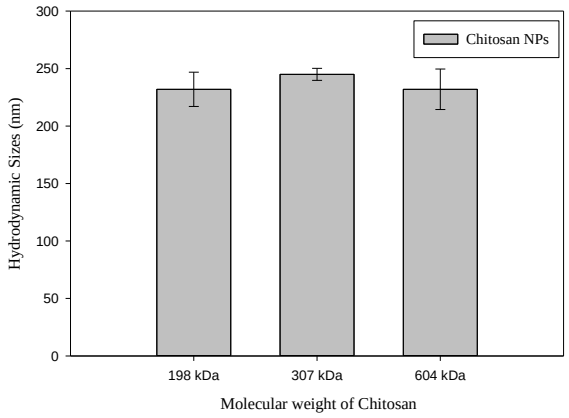

Figure 13: The graph represents the hydrodynamic sizes of chitosan NPs of different molecular weights

3.2.1.3 Effects of polymer concentration

Polymer concentration has effects on polymer NPs sizes. In our studies, Chitosan concentration was changed from 0.5 to 2 mg/ml and an increase in size from 230 ± 10 to 320 ± 7 nm was obtained. (Figure 14) represents the changes of hydrodynamic sizes of chitosan NPs based on concentration of chitosan. The size change can be explained by classical nucleation theory described by

Kalikmanov where there will be more super-saturation since there are more polymer chains in the solvent phase. There will be more nuclei created, and NP growth rate will accelerate as well [76]. The second reason is the rise in organic phase viscosity brought on by higher polymer content. Since the amount of polymer in the drop will substantially increase, the precipitation of polymer from the solvent will be hindered due to slower diffusion of solvent into the nonsolvent phase which results in larger NPs. Hernández-Giottonini et al, observed that increasing the PLGA concentration from 5 to 15 mg/ml the NPs sizes were increased from 150 nm to 190 nm [59].

The possible reason of increased chitosan NP size could be because of extra polymer chains in the solvent phase as a result of increased supersaturation in the medium or slower diffusion of solvent into non-solvent phase resulting bigger chitosan NPs in size.

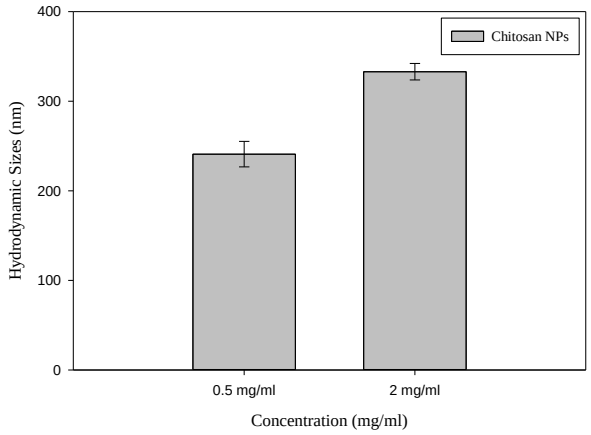

Figure 14: The graph represents the hydrodynamic sizes of chitosan NPs of different concentration

3.2.1.4 Effects of stirring time

No evidence was found whether duration of stirring can also change the NPs sizes or not. (Figure 15) represents hydrodynamic sizes of chitosan NPs in three different durations of stirring (1h, 3h and 5h). After the chitosan solution was added to the non-solvent phase (methanol and tween20), it remained under stirring for 5h. The sizes decreased after 3h but increased after 5h. The possible reason could be after 1h the polymer starts to breakdown into smaller pieces because of constant agitation and swirl together in the solution. But as the time went by after 3h the NPs had enough

time to grow bigger and start aggregate. As it was mentioned earlier (section 3.2.1) that the samples might contained methanol and unbound tween, which could influence the hydrodynamic sizes of the NPs. The experiments might have variable issues such as slightly varied non-solvent or solvent volume, concentration of surfactant or some experimental errors for preparing samples for DLS could also influence the hydrodynamic sizes.

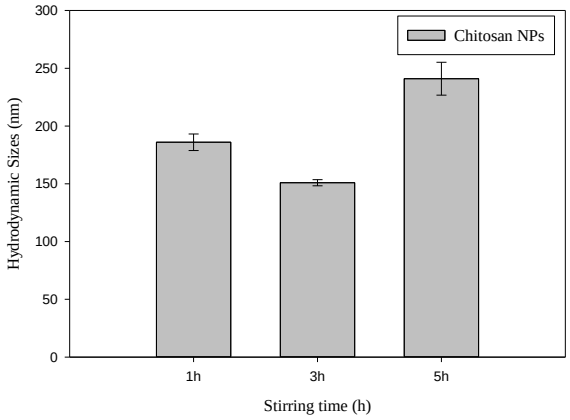

Figure 15: The graph represents the hydrodynamic sizes of chitosan NPs of different stirring time

3.2.1.5 Effects of flow rate

There are different opinions on flowrates effects on NP sizes. Wang et al, investigated the effect of addition of PLGA by using different flowrate rate (2-2000 µl / min) but they did not observe any significant sizes changes. They explained flowrates have no effect over diffusion rather they only affect the rate of mass transport. But Lince et al, observe increasing size of poly-ε-caprolactone when the flowrate decreases from 120 ml/min to 3 ml/min. They observe sizes decrease from 400 nm to 200 nm. They explained that better mixing of the two phases, which resulted in a greater nucleation rate and smaller NPs in a large population, is likely what caused NPs to get smaller [77]. (Figure 16) represents hydrodynamic sizes of chitosan NPs in different flowrates. When the flow rate increased from 29.05 ml/h to 116.1ml/h, the size of the NPs increased from 139 nm to 326 nm. In nanoprecipitation the solvent phase starts to break down into smaller and smaller droplets resulting in dissolution of solvent into non-solvent phase and

precipitation of polymer as NPs. The higher flowrate might produce larger sizes because of nonhomogeneous mixing of organic and aqueous phase.

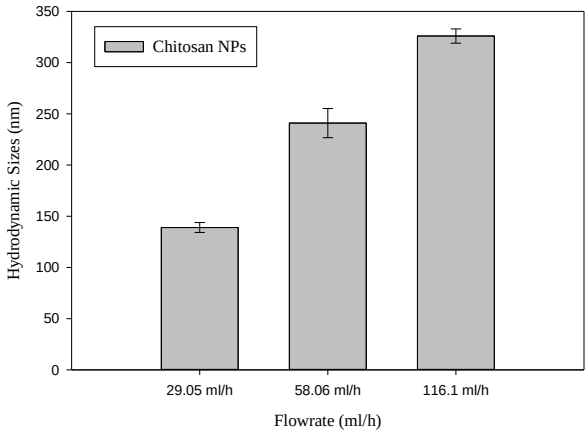

Figure 16: The graph represents the hydrodynamic sizes of chitosan NPs of different flow rate

The results of hydrodynamic sizes of the chitosan A NPs were shown in sections (3.2.1.2 -3.2.1.5). It should be noted that centrifugation method was used for removing methanol from the chitosan A NPs solution of previous sections. According to section 2.2.2, 1ml chitosan solution was added to the non-solvent phase dropwise so after centrifugation method, only 1ml of the solution was taken and rest of the solution was discarded. But no pellet of chitosan NPs were seen evidently in the centrifuge tube (Figure 17a) and freeze-drying method was also tried on that chitosan NP solution to see if any dried particles were found (Figure 17b). But there were no particles to be found.

Then rotary evaporator was introduced to remove methanol from the chitosan NP solution. The next section is the results obtained from the DLS of chitosan NPs which were measured after rotary evaporation.

(a) (b) (c)

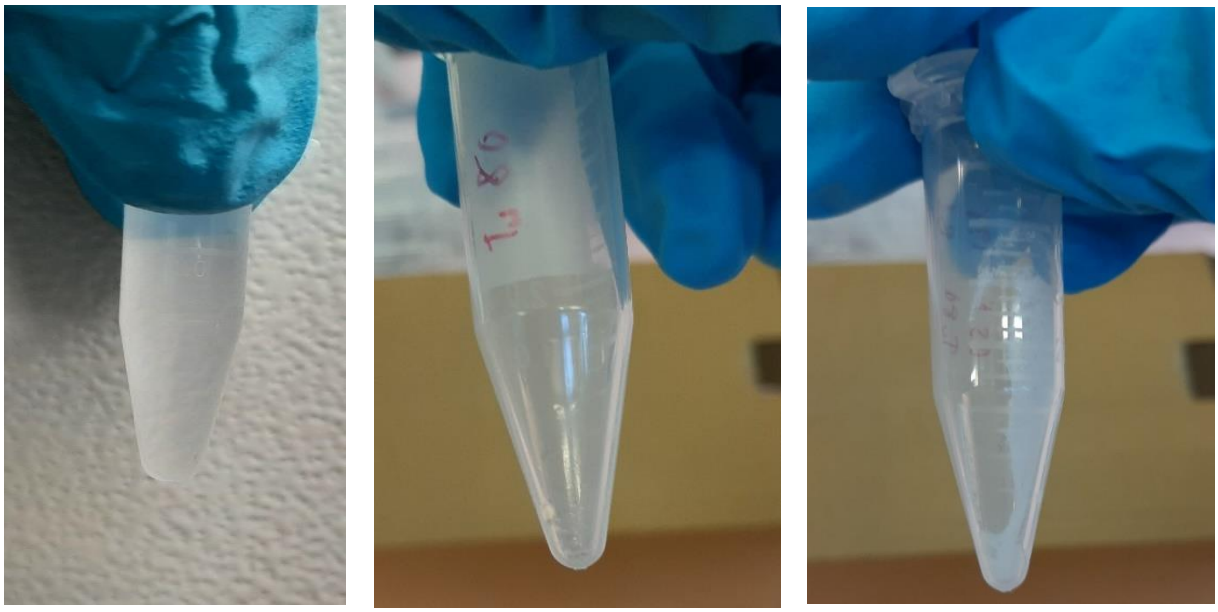

Figure 17: a) No clear pellet of chitosan were found after centrifugation method b) Nothing left in the tube after freeze drying and c) Chitosan particles after freeze drying. (a) and (b) were after centrifugation and (c) after rotary evaporator

3.2.1.6 Effects of different non-solvent removal technique

During the preliminary study of PLGA NPs, centrifuge technique was performed to separate the NPs from the aqueous phase. It was also repeated for removing methanol in chitosan NP synthesis. But there was no evidence of separating chitosan NPs in the solution. Then rotary evaporation was introduced for removing the methanol from the solution rather than chitosan NPs to form pallets and separate them. To prove this technique was working, freeze drying was done to see if the solution contains chitosan NPs and particles were seen (figure 17c). The solid chitosan particle could contain surfactant on the surface. Then further studies were continued on chitosan A NPs. Centrifugation was replaced by rotary evaporation in chitosan NPs synthesis.

Four set of experiments were done on chitosan A NPs. Two different molecular weight chitosan A (198_kDa and 604_kDa) at two concentrated (0.5 mg/ml and 2mg/ml) solutions were used. At low concentration, different molecular weight of chitosan has shown less or no effect on sizes but on higher concentration higher molecular weight chitosan has bigger sizes than lower molecular

weight chitosan. Experiments were done in triplets. All the sizes of the NPs were between 150-170 nm except the 2 mg/ml 604_kDa chitosan NPs. The bigger sizes could be because of nonhomogeneous mixing of the solvents to non-solvents during nanoprecipitation. Another reason could be increased super saturation of those samples because of increased number of polymer in the solution.

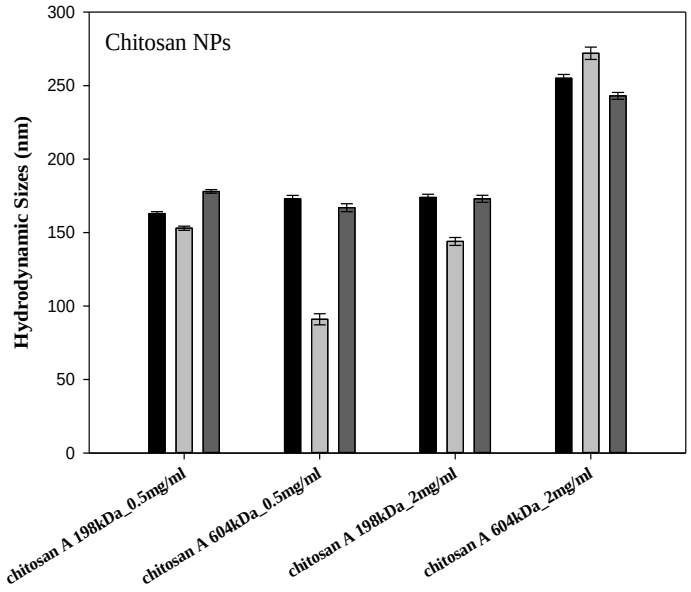

Figure 18: The graph represents the hydrodynamic sizes of the Chitosan NPs on two different molecular weights (198kDa and 694kDa) and concentrations (0.5 mg/ml and 2mg/ml).

3.2.1.7 Effects of different surfactants on chitosan A NPs

Chitosan A_198 kDa at 2 mg/ml conc was synthesized by two surfactants (tween 20 and tween 80) of 0.05% w/v and hydrodynamic sizes of the NPs were measured. When tween 20 was added in the non-solvent phase, the chitosan NPs sizes were between 530-560 nm and when tween 80 was added in the surfactant the sizes were around 450 nm and less. Surfactants are used to reduce particle surface tension at nonsolvent surfaces in order to prevent particle aggregation. Shkodra-Pula et al, observed the effects of surfactants on the size of PLGA NPs. Particle with tween 20 gave 152 ± 4 nm and tween 80 gave 159 ± 2. The concentration of the surfactant in the non-solvent

was 3% w/v and acetone as non-solvent phase. The sizes were increased a little when they used tween 80 in non-solvent.

In our study, the NPs sizes were decreased when tween 80 was used. The reason might be because of using different parameters such as concentration of the surfactant and different non-solvent phase.

Table 1. DLS results of hydrodynamic sizes chitosan A_198 kDa at 2 mg/ml concentration for two different surfactants.

Tween 20 as surfactant		**Tween 80 as surfactant**	
Sample	**Hydrodynamic sizes (nm)**	**Sample**	**Hydrodynamic sizes (nm)**
1	560 ± 3.23	1	273 ± 2.4
2	553 ± 1.45	2	450 ± 1.27
3	538 ± 5.62	3	437 ± 4.85

3.2.1.8 Polydispersity of Chitosan A NPs

The polydispersity index (PDI) is a measure of the heterogeneity of a sample based on size (Mudalige et al). According to many papers, if the polydispersity index (PDI) is < 0.05 of a sample than it is a monodispersed sample. The PDI range of the samples in Table A1 (appendix A) is between 0.3-0.5 value indicates that the samples do not have homogeneity, but it is within the range of reliability for DLS (PDI < 0.5) (Sawtarie et al). Nevertheless, there was a significant difference in PDI from being monodispersed.

3.2.1.9 Surface characterization of Chitosan A NPs

The zeta potential of the chitosan NPs was measured in DLS which indicates the surface charge of the particles. The solution containing chitosan NPs probably contained methanol and free chitosan that did not precipitate out might affect zeta potentials.

Chitosan is a positively charged polymer and chitosan A was deprotonated (H^+ Ion) (section 2.1) and according to Clogston et al, the zeta potential should be positive for cationic NPs [78]. But in figure 6, zeta potentials were negative in all the experiments and Kosmulski et al, suggested that zeta potential of a solution will decrease if the solvent contains 30% methanol than pure aqueous solution [79]. A possible reason for decreasing the zeta potential is the increasing number of OH^- ions in the solution which shifts the pH of the towards basic solution. So that will decrease the

positive charge of the surface of the NPs affecting the zeta potentials. This might be because several other elements like methanol or tween 20 were also in the solutions apart from chitosan NPs.

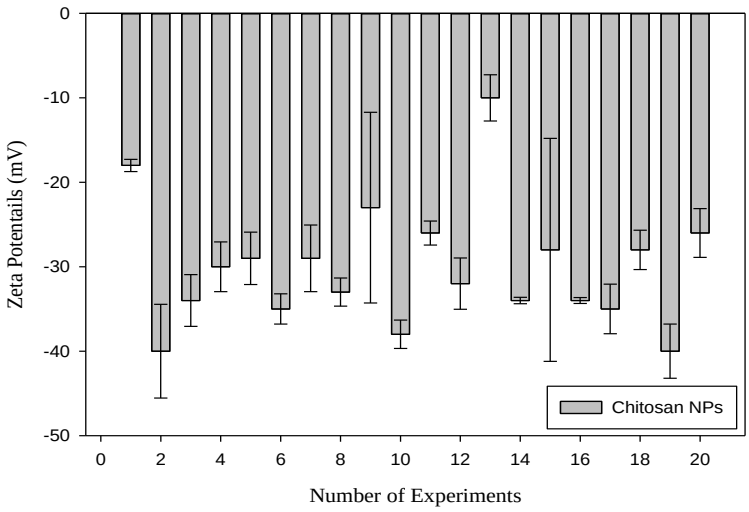

Figure 19: The graph represents the zeta potentials of the chitosan NPs from chitosan A. All experiments were measured after centrifugation technique was performed to remove methanol from those samples.

During the nanoprecipitation method of chitosan, 1 ml of solvent (organic solvent+ polymer) was dropwise added at fixed flowrate into 10 ml methanol + tween 20 solution and according to nanoprecipitation mechanism reported by Quintanar al el, the different surface tension from two phases creates surface turbulence which leads to counterflow formation at the interface of both phases. These counterflow result in increased mass transfer from one phase to another. Since chitosan is non-miscible in methanol, the polymer chains began to disintegrate into smaller pieces resulting in dissolution of chitosan polymer into methanol and precipitation of chitosan polymers as NPs [80].

The zeta potentials of chitosan NPs from (Figure 19) did not follow any trend or repeatability on same parameters. The reason could be presence of methanol in the chitosan solution as the centrifuge method was not working to separate the particles.

So, rotary evaporator method was introduced to remove the methanol from the chitosan NPs solution. After rotary evaporation, the zeta potential of the NPs was measured. Four sets of experiments were done. All experiments were done in triplicates. The zeta potentials were positive (figure 20) which might indicate that the positive surface charge of the chitosan NPs and not having methanol in the solution as well.

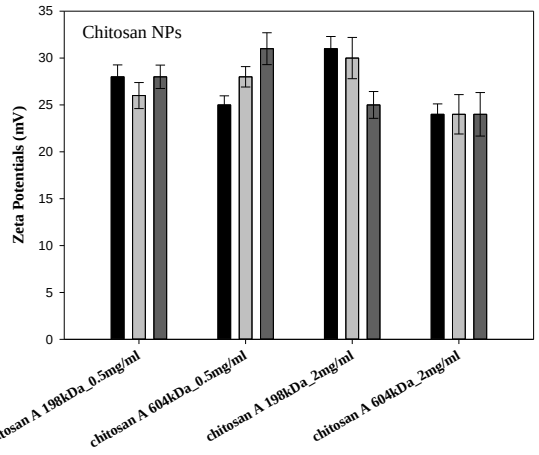

Figure 20: The graph represents the zeta potentials of the Chitosan NPs on two different molecular weights (198kDa and 694kDa) and concentrations (0.5 mg/ml and 2mg/ml).

3.2.1.10 Optimization of DLS measurements for chitosan A NPs

According to DLS procedure, if the concentration of a particle is too low then photon of light scattering from the particle will be weak and there will be noise in the measurement. Adding 100µl sample in 1.9 ml of water was the starting process for preparing the DLS sample. But as the concentration was already very low for the chitosan A sample (0.5 or 2 mg/ml) so to remove any noise and up concentrate the particle, sample without any dilution were used later on the study as an optimization study.

For both Chitosan A_198kDa and Chitosan A_604kDa NPs hydrodynamic sizes of direct samples were almost 3/4 times larger than diluted samples. The possible reason for getting bigger sizes could be because of increased polymer concentration on the direct samples which explained earlier (section 3.2.1.3). Positive zeta potentials were also higher in direct samples even if there is no direct relation of zeta potential with polymer concentration.

Table 2. DLS results of sizes and zeta potential of chitosan A 198 and 604 kDa at 2 mg/ml concentration.

Chitosan A_198 kDa					
Direct Sample	**Hydrodynamic Size (nm)**	**Zeta potential (mV)**	**Diluted sample (100 µl in 1.9 ml)**	**Hydrodynamic Size (nm)**	**Zeta potential (mV)**
1	560 ± 2.52	52 ± 1.87	1	152 ± 1.90	35 ± 2.12
2	553 ± 3.12	54 ± 1.26	2	142 ± 2.12	29 ± 1.98
3	538 ± 2.34	41 ± 0.98	3	167 ± 2.32	34 ± 0.78
Chitosan A_604 kDa					
Direct Sample	**Hydrodynamic Size (nm)**	**Zeta potential (mV)**	**Diluted sample (100 µl in 1.9 ml)**	**Hydrodynamic Size (nm)**	**Zeta potential (mV)**
1	1905 ± 2.72	49 ± 1.22	1	305 ± 1.23	32 ± 1.88
2	1389 ± 1.58	47 ± 1.31	2	246 ± 1.79	33 ± 1.26
3	1809 ± 1.29	52 ± 0.95	3	232 ± 1.49	31 ± 2.21

3.2.1.11 STEM characterization of chitosan A NPs

The point of characterizing the chitosan NPs was to observe the size of the chitosan A NPs. The STEM images (figure 21) might suggest polydispersity of the chitosan NP solution. The white particles are the chitosan NPs and shadows surrounding the particles are staining and from (figure 22a) NP (in white), the yellow line is the path of the beam, and the graph below (figure 22b) is the elemental analysis along the yellow line. At the edges of the NPs the elements listed in the legend increase, before dropping in the center of the NP and increasing again at the other edge of the NP. This could be because of staining particles. Renz et al, prepared their polymeric nanoparticles for characterizing in electron microscopes (TEM) with uranyl acetate (UA) and other staining. They observed darker edges of the particles when using UA and suggested UA inverts the contrast increasing the visibility of the nanoparticles [81]. The largest chitosan particles were more than 2µm in size. These are the probable large particles which were assumed in some earlier sections.

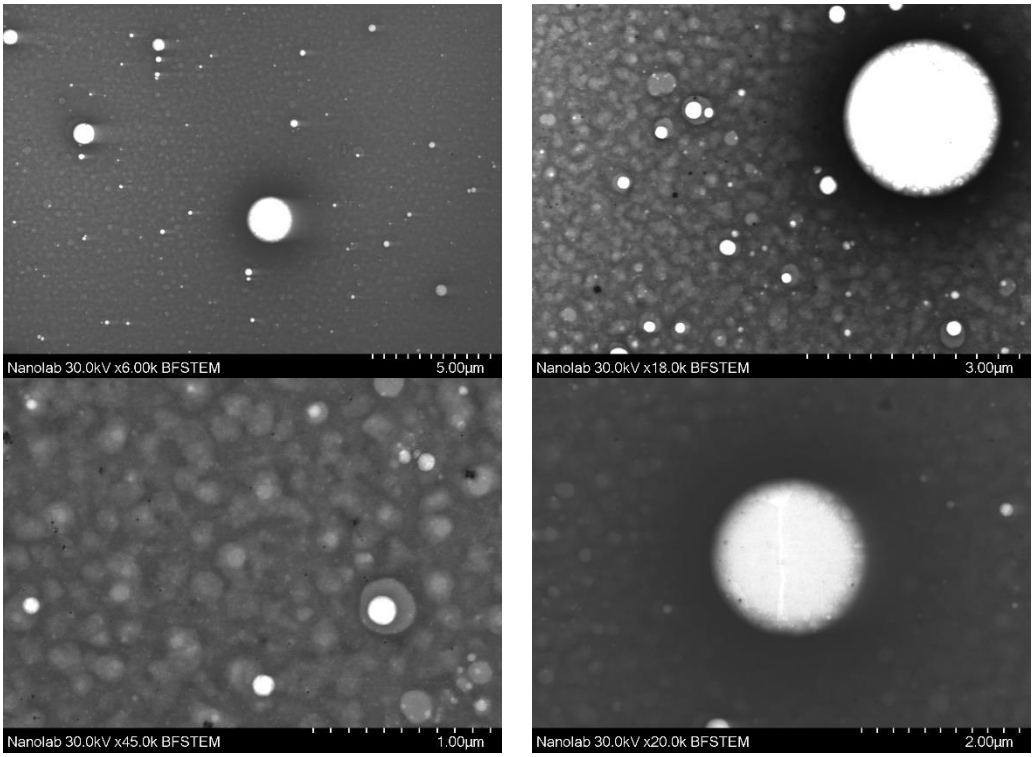

Figure 21: STEM images showing the chitosan NPs stained in Uranyl acetate

(a)

(b)

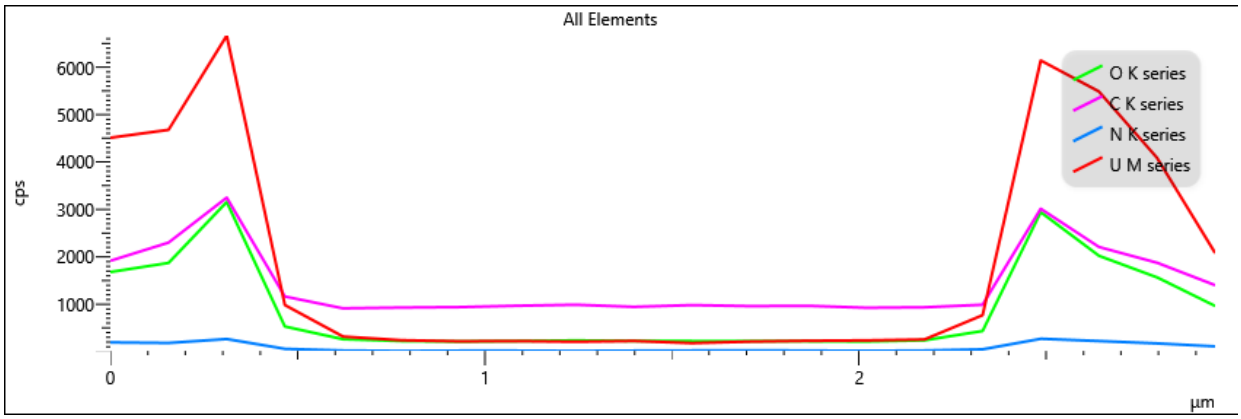

Figure 22: EDX of chitosan NPs

3.2.2 Synthesis of chitosan NPs with Chitosan B

With chitosan NPs from Chitosan A, the synthesis parameters studies on hydrodynamic sizes were observed, methanol removal technique was changed from centrifugation to rotary evaporation and optimization of DLS measurement was done. It was discussed earlier (section 2.1) that chitosan B was introduced and decided to synthesize chitosan NP and later use for the polymer coating for IONPs. It was dialyzed against NaCl and then against distilled water before freeze drying which means the amino groups will have Cl- as counter ion and makes it easier to dissolve in water than chitosan A.

Water soluble chitosan B (M_w = 198kDa, DA = 0.18) was introduced to do further studies on chitosan NPs. Chitosan B NPs were synthesized by nanoprecipitation and methanol were removed using rotary evaporator. Then direct sample was measured without any dilution in DLS. The effect of different concentration of polymer, size distribution, FT-IR. These will be discussed in the following sections.

3.2.2.1 Hydrodynamic sizes and size distribution of chitosan B NPs

The chitosan B NPs were synthesized in two different concentrations (0.5 and 2 mg/ml) and hydrodynamic sizes were measured in DLS. The hydrodynamic sizes were bigger when the concentration increased. When the polymer concentration was 0.5 mg/ml the hydrodynamic sizes of the NPs were between 500-550 nm and when concentration increases to 2 mg/ml the hydrodynamic sizes were between 900-1100 nm. The effect of concentration was seen in these

NPs hydrodynamic sizes. The similar effect was also observed with chitosan A NPs. The possible reason for the increased might be as a result of increased super saturation in the solution described earlier in section (3.2.1.3).

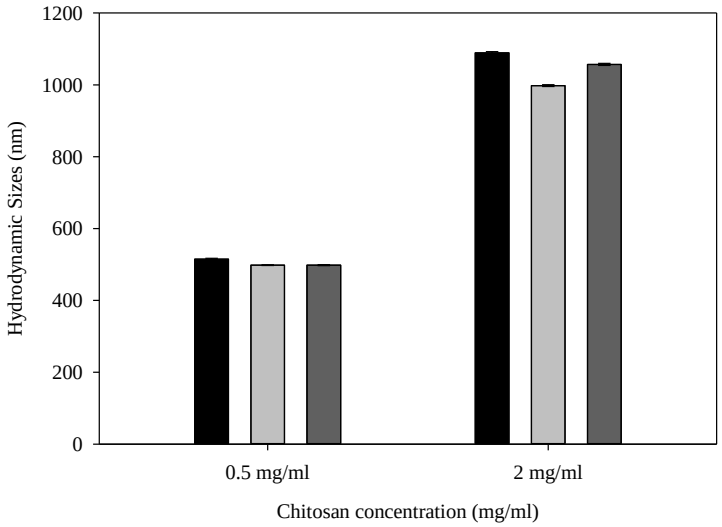

Figure 23: The graphs represent the hydrodynamic sizes of the chitosan B NPs in different concentrations.

The size distribution of Chitosan B NPs was characterized using lumisizer.

Table 5 represents the particle hydrodynamic size distribution of sample measured by lumisizer. The concentration of the chitosan NPs was 5mg/ml. The smallest size of chitosan NPs is 370 nm which is less or equal 10 % of the total population and the largest size in 3920 nm. The mean size of the particle is around 1271 nm. The concentration of the NPs was 0.5 mg/ml. The lumisizer uses STEP technology (Space- and Time-resolved Extinction Profiles). It is the combination of centrifugation and laser technology. This process allows to analyze the whole sample instantaneously from top to bottom and provide the particle size and particle distribution. In this process, the sample was rotating at specific rpm in specific intervals (SOP in table B2 -Appendix B) that the larger particles would sediment first and as the process goes by the smallest particles settle down. During the whole sedimentation process, the machine will analyze the particle sizes. From the irregular points on size distribution curve (figure 24) and noises on time lapse sedimentation graph (B2 – Appendix B), it can be said that the sample has difficult to settling down. That can manipulate the size measurements. It should be noted that the chitosan NPs were not able to separate from the non-solvent phase after centrifugation.

At 2 mg/ml polymer concentration, the hydrodynamic sizes measured by lumisizer were 1271 nm and 900-1100 nm in DLS. The sizes from lumisizer were larger than DLS. In DLS the machine can measure the particle size in single measurement angle (back, side or forward scattering) but lumisizer can analyze the whole sample and provide size distribution. In a single measurement angle, there might be a possibility not to measure the whole sample which could lower the average size. For example, in 175° back scattering angle the scattering light of the smaller particles could missed out during the DLS measuring. This could be a possible reason to get smaller sizes in DLS than lumisizer. The measurement techniques of DLS and lumisizer could be another possible reason to get different sizes. DLS represents the average hydrodynamic sizes which were determined by light scattering of the NPs. On the other hand, lumisizer represents the hydrodynamic size distribution of the NPs determined by analyzing the whole sample instantaneously from top to bottom.

Table 3. Hydrodynamic size distribution of chitosan NPs characterized by Lumisizer

Size distribution	10% ≤ in nm	50% ≤ in nm	90% ≤ in nm
Hydrodynamic size	371	1271	3920

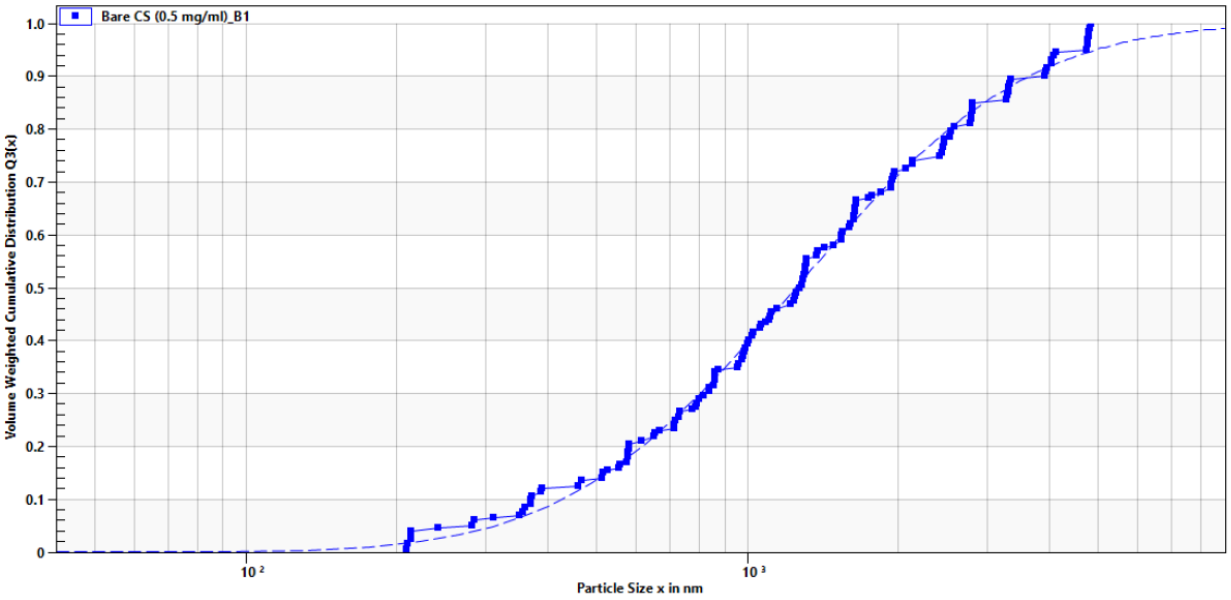

Figure 24: Volume weighted cumulative distribution vs size distribution graph of chitosan NPs

3.2.2.2 FT-IR characterization of chitosan B NPs

FT-IR was done as a confirmation test to observe the molecular structure of chitosan NPs and presence of the surfactant tween80 in the surface of the chitosan NPs. Tween80 was used to provide stability for NPs synthesis during nanoprecipitation method.

In this (figure 25), two FT-IR spectra represent two chitosan NPs sample where surfactant is present (black) and absent in another one (red). The spectrum of the chitosan shows more broad absorption bands at 3291 cm^{-1} (surfactant present) and 3361 cm^{-1} (surfactant absent). This broad band might be corresponded to – OH stretching vibrations of water, hydroxyls and NH2 stretching vibrations of free amino groups according to Ali et al. The two bands observed at 2923 and 2856 cm^{-1} correspond to asymmetric stretching of CH3 and CH2 in both chitosan sample [82]. In the spectra of chitosan with Tw 80 NPs a small peak of 1735 cm^{-1} was observed which could be a C=O stretching bond of ester which can be found in Tween80 [83]. This peak was not observed in the chitosan NPs where surfactant was not used. 1087 and 1068 cm^{-1} two strong peaks indicate a possibility of C-O bonds [82].

The chitosan has primarily an amine ($-NH_2$) and a hydroxyl group in its molecular configuration and Tween80 has ester bond. By observing the peaks from the FT-IR data, this proved that chitosan NPs were present in the solution and the coating of Tween80 was also found in the chitosan NPs when chitosan was added on the non-solvent with surfactant solution for synthesizing NPs by nanoprecipitation.

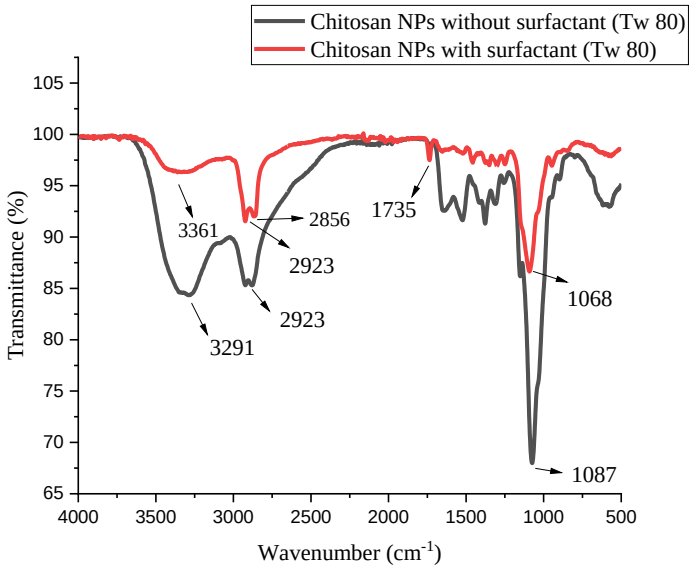

Figure 25: Graph representing the spectrum of chitosan NPs with and without surfactant Tw 80

3.3Synthesis of IONPs by Co-precipitation

In this section, characterization of IONPs synthesized by co-precipitation method are presented. The entire section is divided into two subsections. Firstly, the hydrodynamic sizes, zeta potential and size distribution, along with the image obtained from TEM of the IONPs is presented and discussed with some literature. Secondly, configuration, and magnetic characterization of IONPs systems using FT-IR and VSM is shown.

3.3.1 Size characterization by DLS, TEM and Lumisizer

IONPs were synthesized by co-precipitation method (described in the IONPs co-precipitation method). These IONPs were characterized using Zeta Sizer, Lumisizer and TEM. The TEM image of IONPs is presented in figure 5. The hydrodynamic size and zeta potential of IONPs was obtained by zeta sizer i.e., 176 ± 4 nm and -32 ± 0.3 mV (table 4), respectively. IONPs have FeO^- (figure 27b) on the surface which might be the reason for possessing negative zeta potential. The average IONPs size was also estimated by counting 100 particles using the software ImageJ and the average size was estimated to be 10 ± 3 nm. The TEM samples were stained with Phospotungstic acid to invert the contrast and increase the visibility of the nanoparticles. The difference in hydrodynamic size obtained from zeta sizer and TEM images is almost ten times and this could be because of the two main reasons. The first reason is that the zeta sizer estimates the hydrodynamic size based on hypothetical sphere which is then calculated using Stoke-Einstein equation. while in HR-TEM gives dry particle size. The second reason could be the aggregation of IONPs due to their close interactions inside the zeta sizer cell during the hydrodynamic size measurements. Cheraghipour et al. also stated that IONPs aggregation occurs because of their hydrophilic nature and sufficient repulsive interactions are required to prevent aggregation [84]. As evident from figure 26b, IONPs synthesized by co-precipitation seem to be aggregated, this could probably be because of the three main reasons. The first reason is that there are magnetic dipolar interactions among the formed NPs, and this may lead to aggregation which was reported by Easo et al. The second reason could be the uncoated surface of IONPs, since the IONPs does not have capping agents on the surface. They could easily interact due to inter-molecular forces. Hence the surface needs to be electrostatically or sterically stabilized using different functionalizing agents [85]. Dave et al observed that the IONPs have a negative zeta potential because of the presence of hydroxyl groups

on the surface of IONPs. These hydroxyl groups make IONPs hydrophilic, and they are dispersed well in water. The value obtained for zeta potential is high which means that the IONPs are colloidally stable [86].

The concentration of the IONPs batch was also estimated by weighing 300 µl of IONPs solution in eppendorf tubes after drying them overnight in an oven. The average concentration of IONPs batch was calculated to be 56 mg/ml.

Table 4. Hydrodynamic size and Zeta potential of IONPs

Hydrodynamic Sizes (nm)	Standard Deviation	Zeta Potential (mV)	Standard Deviation
176	4.701	-32	0.265

Table 5. Hydrodynamic size distribution of IONPs characterized by Lumisizer

Size distribution	10% ≤ in nm	50% ≤ in nm	90% ≤ in nm
Hydrodynamic size	24	30	39

Table 5 represents the particle hydrodynamic size distribution of sample measured by lumisizer. The concentration of the IONPs was 5mg/ml. The smallest size of IONPs is 24 nm which is less or equal to 10 % of the total population and the largest size in 39 nm. The mean size of the particle is around 30 nm. The average size of IONPs were lot bigger in DLS than lumisizer. The reason is DLS measured all the particle sizes of a sample and if there the sample is not homogenous and contain very large particles even if for a very small percentage, the average size of the whole sample population will increase to a large extent. But lumisizer can measure the size distribution and clearly in (table 5) it was observed that less or equal than 90% of the sample population is 39 nm. So, maybe less than 10 % of the sample contains large, aggregated particles which were measured by DLS and enhance the average size of the sample.

(a)

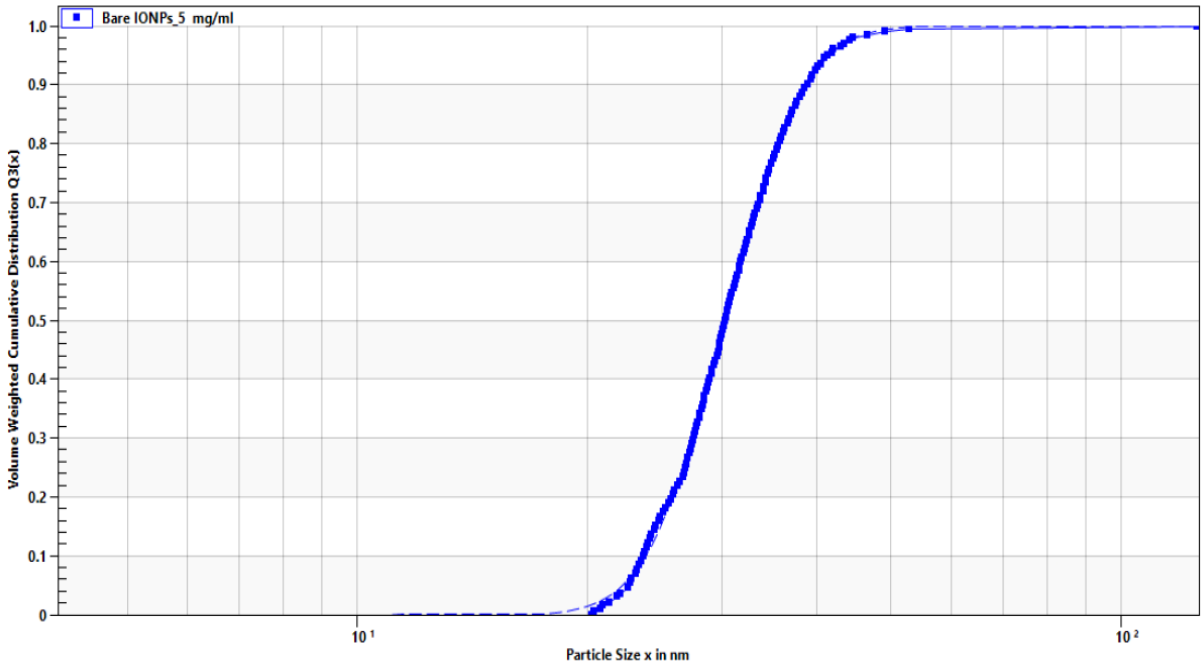
Bare IONPs_5 mg/ml
Volume Weighted Cumulative Distribution Q3(x)
1.0
0.9
0.8
0.7
0.6
0.5
0.4
0.3
0.2
0.1
0
10 1
10 2
Particle Size x in nm

(b)

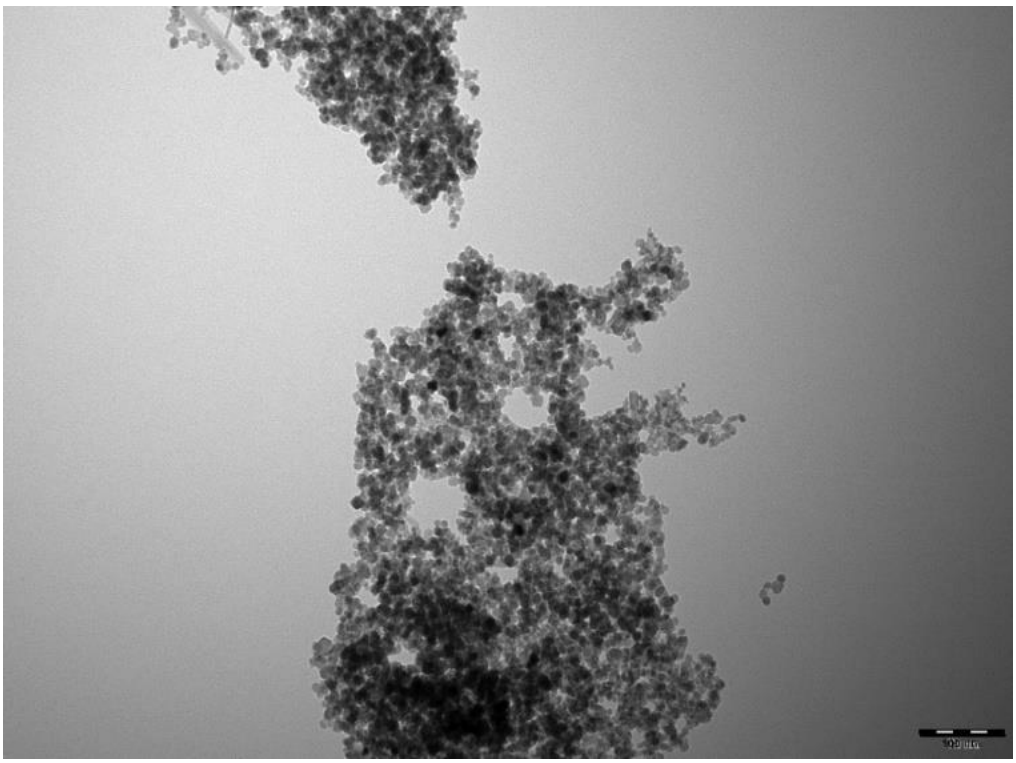

Figure 26: a) Volume weighted cumulative distribution vs size distribution graph of IONPs (5mg/ml) by lumisizer and b) TEM pics of IONPS staining by Phosphotungstic acid

3.3.2 FT-IR and magnetic characterization of IONPs

FTIR is one of the analytical techniques used to disclose the functional groups present in the sample and also to learn the microcrystalline nature of the particles. In this (figure 27b), FT-IR spectra reveal one very strong peak at 567 cm^{-1} and a very weak peak at 1408 cm^{-1}. The bands in the region of 400–650 cm−1 are attributed to the Fe-O bonds and the bands on 567 cm^{-1} indicates the Fe-O bonds of magnetite nanoparticles which are close to the studies of Basavegowda et al. The metal-oxygen band at 557 cm−1 corresponded to intrinsic stretching vibrations of metal at the tetrahedral site [87]. 1408 cm^{-1} peak is situated in the fingerprint region and a very small peak. So, there is no confirmational evidence of this peak and it could be a noise in the sample.

VSM system is used to measure the magnetic properties of IONPs as a function of the magnetic field, temperature, and time. The IONPs synthesized by co-precipitation method were analyzed by VSM to explore the magnetic property. The magnetic moment versus applied magnetic field (emu/g–Oe) curve of IONPs was carried out at room temperature and the graph is shown in (Figure 27a). There is no hysteresis in the hysteresis loop which suggests that the synthesized IONPs are superparamagnetic in nature with zero remanence and coercivity [88]. Magnetic moment was calculated 56.7 emu/g.

a) b)

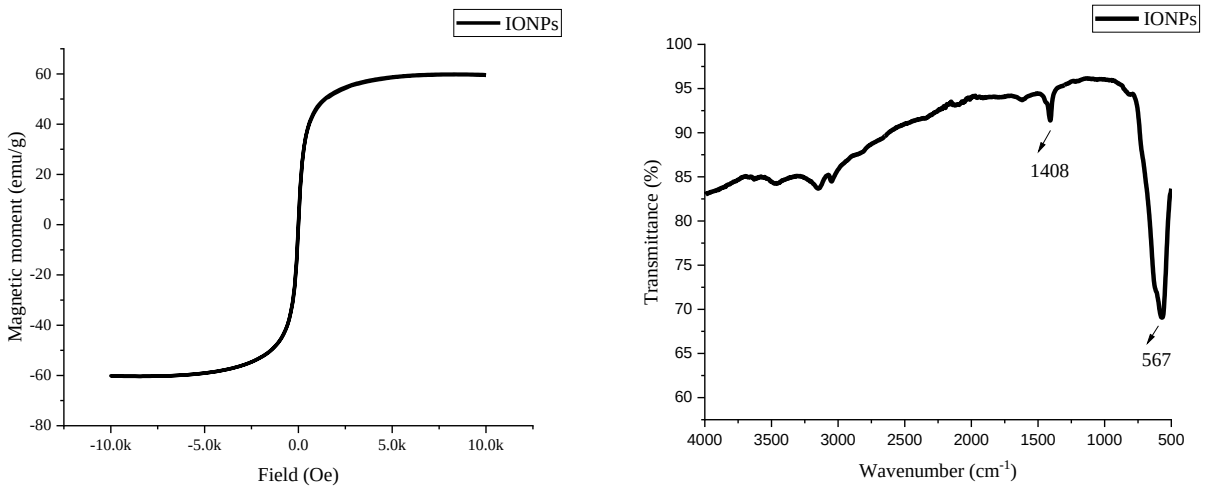

Figure 27: a) Magnetic hysteresis (M-H loops) of IONPs particles using VSM at room temperature and b) Fourier-transformed IR spectrum of IONPs

3.4 Synthesis of PLGA-IONPs by nanoprecipitation (Preliminary study)

Before synthesizing chitosan coated IONPs, preliminary study of PLGA-IONPs were done for better understanding the polymer coating IONPs synthesis process by nanoprecipitation and observe the hydrodynamic sizes and surface charge. For PLGA-IONPs nanoprecipitation, PLGA of 30000-60000 Mw and 4 mg/ml conc IONPs were used. PLGA was dissolved in DMSO. Pluronics 127 aqueous solution was the non-solvent phase.

The experiments were done in triplets (Batch 1, 2 and 3). The hydrodynamic sizes were between 380-320 nm which was higher than bare PLGA NPs and the possible reason could be because PLGA encapsulated the IONPs during nanoprecipitation. The negative zeta potentials for PLGA-IONPs (-25 mv) suggests that the surface might have IONPs and PLGA as they both have negatively charged functional group OH^- (IONPs) and terminal carbonyl group (PLGA) [37].

(a) (b)

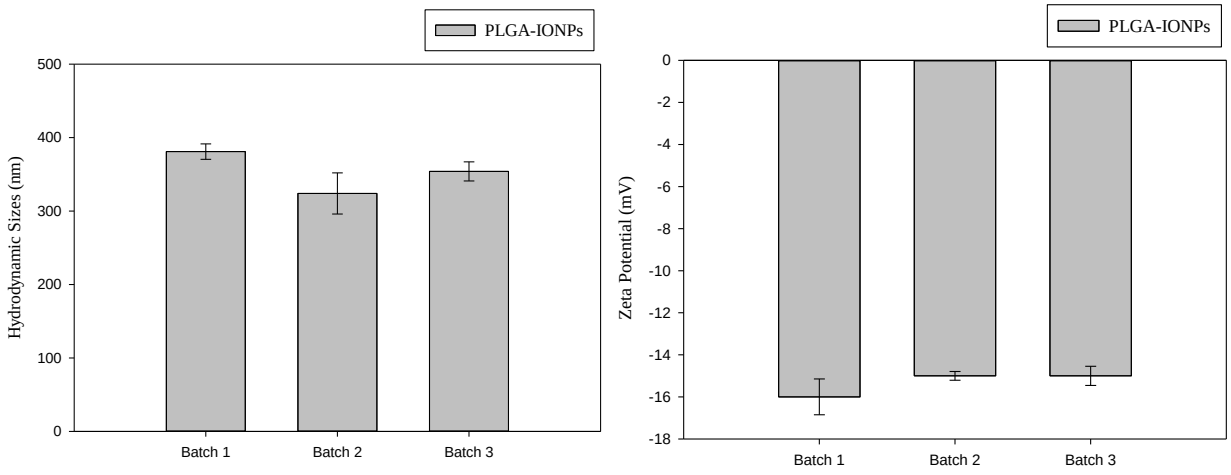

Figure 28: Graph represents the hydrodynamic sizes (a) and zeta potentials (b) of PLGA-IONPs

3.5 Synthesis of Chitosan coated IONPs nanoprecipitation

For chitosan coated IONPS, water soluble chitosan B_198kDa and 5 mg/ml conc IONPs were used. Comparison study of the chitosan coated IONPs by nanoprecipitation and mixing are in section 3.5.1. The size characterization by DLS, STEM and Lumisizer will be discussed in the next

to section 3.5.1 and 3.5.2 followed by surface characterization of these particles by determining the iso-electric point and FT-IR spectrum (3.5.3). Some optimizations of these particles during washing steps are discussed in section 3.5.4. Later a statistical design of experiment of CS coated IONPs will be discussed in section 3.5.5.

3.5.1 Comparison of chitosan coated IONPs by mixing and nanoprecipitation

To observe if the IONPs and chitosan particles aggregate before reaching into organic phase and whether chitosan NPs coat or encapsulate IONPs properly before putting them drop wisely into the non-solvent organic phase, this control test was also done. The hydrodynamic sizes, zeta potentials and STEM images of these samples were compared with the nanoprecipitated samples.

Chitosan coated IONPs were prepared by nanoprecipitation method. IONPs were mixed with chitosan solution in the solvent phase then it was added to the non-solvent phase dropwise. Then the particles were separated by magnet (section 2.2.5) and the hydrodynamic sizes and zeta potentials of chitosan coated IONPs were measured. STEM images of the NPs after staining with uranyl acetate (UA) were also taken to see the configuration of the NPs and as a confirmation of any polymer coating IONPs.

Figure 29 represents the hydrodynamic sizes and zeta potentials of the polymer coated IONPs by nanoprecipitation and mixing process. The experiments were done in triplicates. The hydrodynamic sizes and zeta potentials were between 1200-2000 nm and 25-30 mV respectively. The hydrodynamic sizes were lot bigger than bare IONPs (table 4), which indicates chitosan might be coating IONPs. The surface charge of the NPs was positive which could suggest chitosan is on the surface of the IONPs as chitosan has positive surface charge.

For the mixing process, two different concentrations of IONPs solution (2.5 mg/ml and 5mg/ml) and 2 mg/ml conc chitosan solution were used. The samples were mixed to be homogenous for 20 minutes by shaker. Then hydrodynamic sizes and zeta potentials of the NPs were measured (figure 29). The samples were washed 3 times to get rid of the excessive chitosan. The experiments were done in triplicates. The hydrodynamic sizes of the NPs from mixing were between 1000-3000 nm in range, one sample was above 7500 nm. The zeta potentials were all positive and between 25-35 mV, which might indicate the positively charged particles are on the surface of the particles.

The hydrodynamic sizes of the nanoprecipitated NPs could indication of synthesizing smaller sizes by nanoprecipitation technique. But DLS can only measure the hydrodynamic sizes, but it was not possible to tell that the particles were aggregated and those results cannot differentiate them from nanoprecipitated out samples.

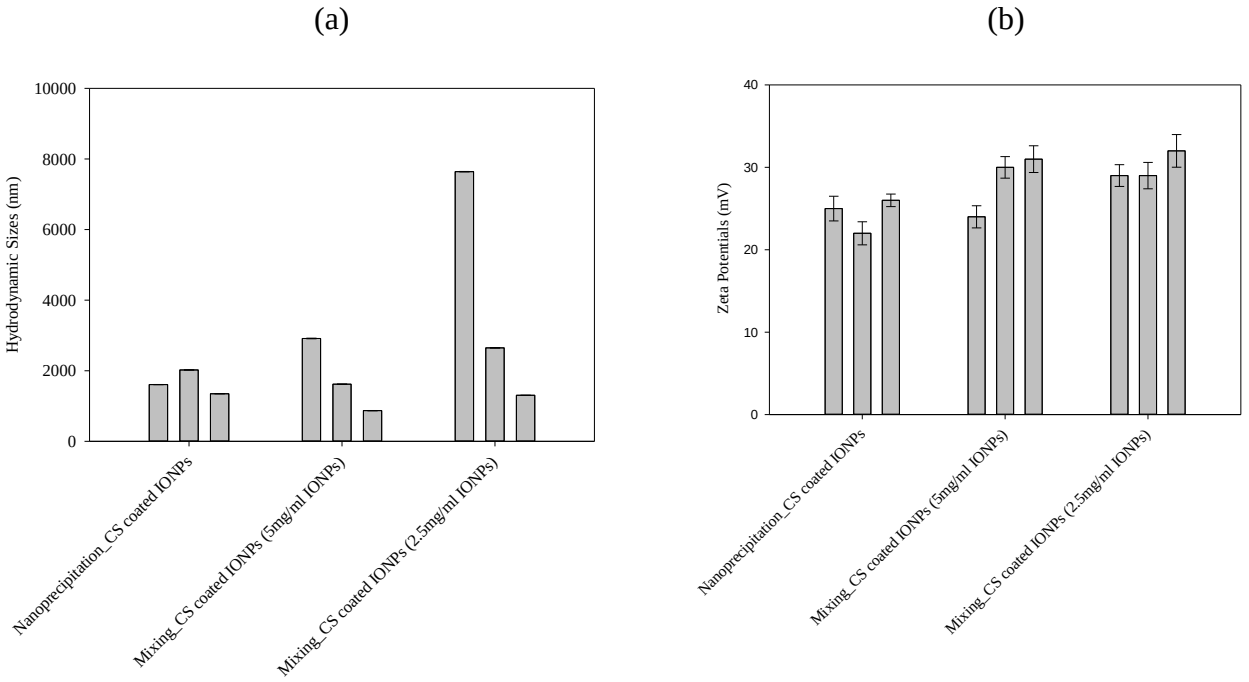

Figure 29: Graph represents the hydrodynamic sizes (a) and zeta potentials (b) of chitosan coated IONPs by nanoprecipitation and Mixing process.

STEM images of these NPs would be another strong argument to whether nanoprecipitation would coat the IONPs with chitosan or not. Figure 30 shows the STEM images of IONPs coated with chitosan. The particle sizes were between 10-100 nm. Light and dark aggregated particles are detected in the images. The black particles would be IONPs, and white particles wrapped around the IONPs might be the polymer NPs. The shadow occurred due to staining particle to create contrast between the particles and the background.

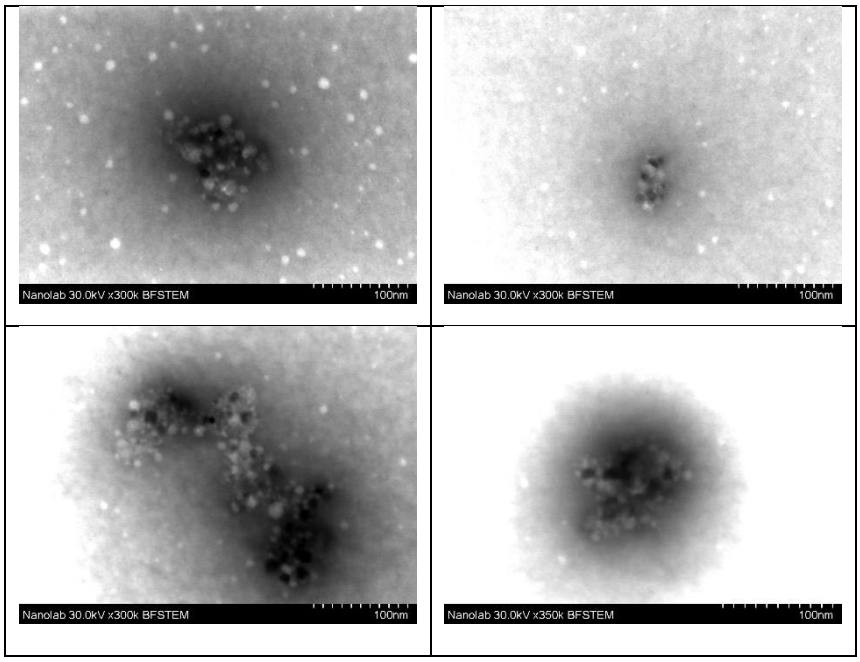

Figure 30: STEM image showing the chitosan coated IONPs stained by Uranyl Acetate.

The mixing process samples were also characterized in STEM by co-supervisor Nesrine Bali. The control particles were irregular in shape (figure 20) and size were ranged between 1-10 µm (figure 31). IONPs or chitosan NPs were not identified distinctively from these images. The nanoprecipitate particles (chitosan-IONPs) were spherical in shape (figure 30) and smaller compared to the mixing samples. By comparing the STEM images of control sample and nanoprecipitate sample of chitosan-IONPs, it would suggest that nanoprecipitation method should be more appropriate to synthesize chitosan coated IONPs than just mixing the particles together.

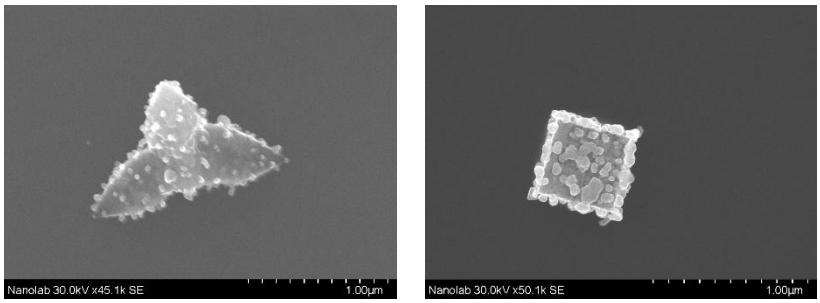

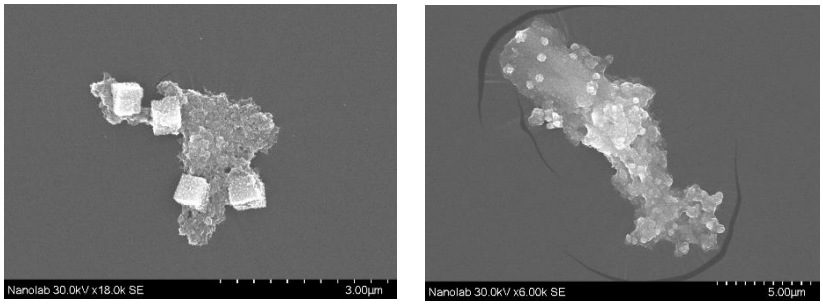

Figure 31: STEM images of chitosan-IONPs particles (mixing process) stained by Uranyl Acetate.

It was proven earlier in the section that chitosan coated IONPs can be synthesized by nanoprecipitation method and sizes were characterized by DLS and STEM. But the NPs sizes were very different, and these two techniques do not give the size distribution of the particles. For observing the size distribution as different insights of the NPs characterization, they were characterized by lumisizer. Both lumisizer and DLS measured the hydrodynamic sizes and STEM characterized only dry particles. But DLS calculates the hydrodynamic size based on a hypothetical sphere, which is then determined using the Stoke-Einstein equation and lumisizer, on the other hand, analyzes the whole sample instantaneously from top to bottom and provides the particle size and particle distribution.

Table 6 represents the particle hydrodynamic size distribution of chitosan coated IONPs sample. The concentration of the IONPs was 5mg/ml and chitosan were 0.5 mg/ml. The smallest size of polymer coated IONPs is 58 nm which is less or equal 10 % of the total population and the largest size is 261 nm. The mean size of the particle is around 91 nm. The average size of polymer coated IONPs were lot bigger in DLS than lumisizer. The reason is DLS measured all the particle sizes of a sample and if there the sample is not homogenous and contain very large particles even if for a very small percentage, the average size of the whole sample population will increase to a large extent. But lumisizer can measure the size distribution and clearly in table 6 it was observed that less or equal than 90% of the sample population is 261 nm. So, maybe less than 10 % of the sample contains large, aggregated particles which were measured by DLS which could influence the average size (1200-2000 nm) of the sample. Another reason might be polymer coated IONP aggregation caused by intimate contacts inside the DLS cell during hydrodynamic size measurements. According to Cheraghipour et al., IONP aggregation occurs due to their hydrophilic

nature, and adequate repulsive interactions are necessary to avoid aggregation [84]. The chitosan B (water soluble) used for IONPs coating was also hydrophilic in nature, chitosan coated IONPs could be also hydrophilic and aggregated inside the DLS cell which could cause large particles. As STEM measures dry diameter of the particle, they gave smaller sizes within 10-100 nm (figure 30) and DLS and lumisizer estimates the hydrodynamic diameter, which includes hydrated layers on the NPs surface gave large particle sizes. By using DLS, STEM and lumisizer, it was possible to measure different category size (dry size or hydrodynamic size) of the NPs.

Table 6. Hydrodynamic size distribution of chitosan coated IONPs characterized by Lumisizer

Size distribution	10% ≤ in nm	50% ≤ in nm	90% ≤ in nm
Hydrodynamic size	58	91	261

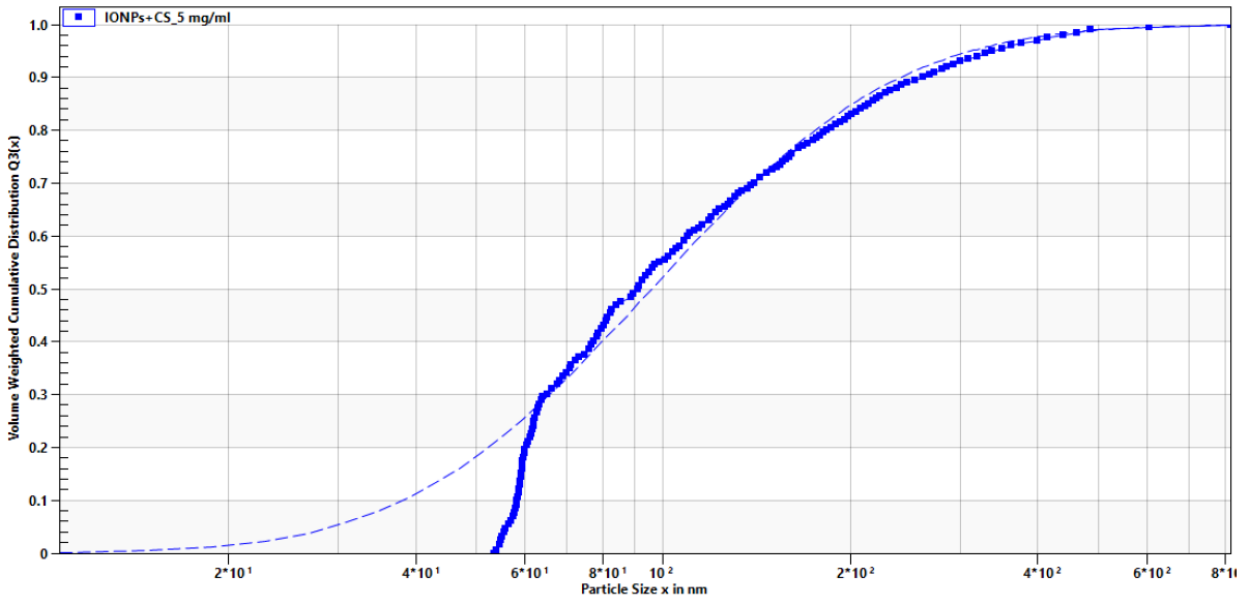

Figure 32: Volume weighted cumulative distribution vs size distribution graph of IONPs by lumisizer

3.5.2 Surface characterization of chitosan coated IONPs

pH study and FT-IR characterization was done to study the surface characterization of the chitosan coated IONPs. The effect of pH on zeta potential was studied to determine the isoelectric point (IEP) of the chitosan coated IONPs (with and without tween80), bare chitosan nanoparticles (with

and without tween80) and bare IONPs. The isoelectric point is the point where there will be no surface charge on the NPs (zero zeta potential). Different functional groups have different isoelectric points. IONPs have OH^- and chitosan has amine as functional group.

Initial (after synthesis) pH was measured for each sample and then zeta potential was measured in each point of the pH changing from (3-10) then according to the pH of the sample, was changed to both high and low pH (table G1). The effect of pH on zeta potentials was discussed in section 1.6.1. Herranz et al, reported the increase of pH of the PEG conjugated IONPs by placing them in acidic solution. They suggested that is it will increase the surface charge and if acid was added to solution the H^+ ion will increase in the solution. It will ultimately increase the positive charge of the surface [89].

The zeta potential decreases when the pH increases in all the samples. The iso-electric point for bare chitosan NPs and chitosan coated IONPs (with or without surfactant) are similar between 8-9 but for bare IONPs the iso-electric point is 4-5 (figure 21).

The reason bare IONPs and chitosan had different isoelectric point might be because they most likely had different functional groups (hydroxyl group for IONPs and amine group for chitosan). The bare chitosan and chitosan coated IONPs showed similar isoelectric point. This can be a proof of having chitosan coating on the surface of the IONPs. The point of choosing with and without surfactant NP sample was to determine the presence of tween80 on the surface of the NPs and if the surfactant on the surface of the NPs had any effect on shifting the isoelectric point of the NPs. The possible reason of not getting any different IEP in those four samples might be because of similar functional region of chitosan and tween80. Another reason could be surfactant might not bind to the surface on the NPs.

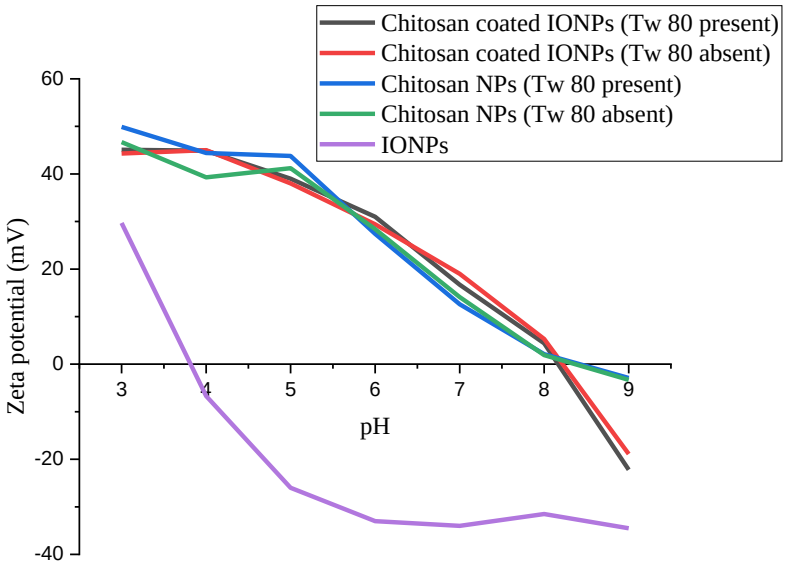

Figure 33: pH dependent zeta potential graphs of polymer NPs, polymer coated IONPs and IONPs

In this (figure 34), two FT-IR spectra represent two chitosan coated IONPs sample where surfactant is present (black) and absent in another one (red). Both FT-IR spectrum reveal one very strong peak at 582 cm^{-1} and two very weak peaks at 1513 cm^{-1} and 3745 cm^{-1}. The bands in the region of 400–650 cm^{-1} are attributed to the Fe-O bonds and the bands on 567 cm^{-1} indicates the Fe-O bonds of magnetite nanoparticles which are close to the studies of Basavegowda et al [87]. 1513 cm^{-1} peak is situated in the fingerprint region and a very small peak and peak in 3745 cm^{-1} is in the functional region which can be an indication of weak -NH_2 bond according to Ali et al [82]. This could be a possible reason for containing chitosan on the surface of the IONPs particles.

FT-IR was done as a confirmation test to observe the molecular structure of chitosan coated IONP and presence of the surfactant tween80 in the surface of the NPs. Tween80 was used to provide stability for polymer coated NPs synthesis during nanoprecipitation method. CS coated IONPs did not show any strong peaks in the functional region and any confirmational peaks for tween80 on the surface. The reason might be both particles muffled the absorption of their respective functional

bonds and not getting any clear peaks. Another reason for not getting any strong peaks is probably because of less concentrated sample.

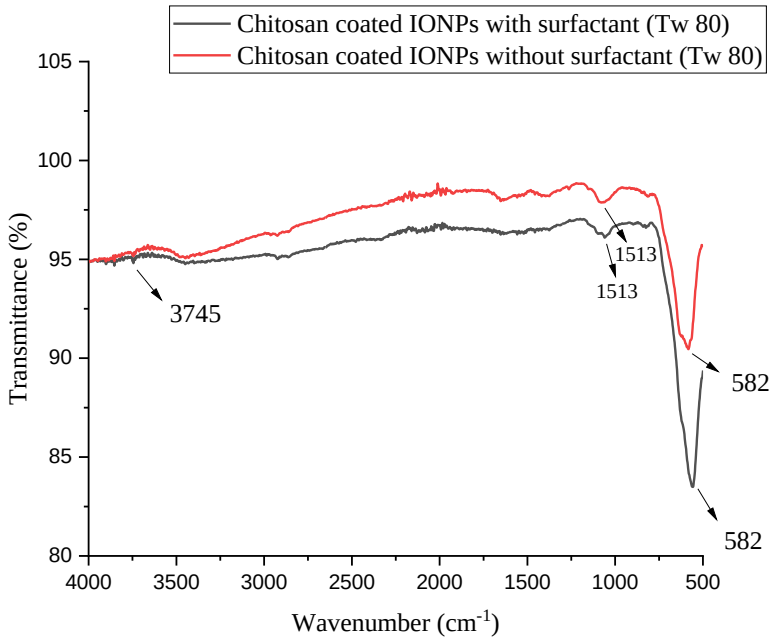

Figure 34: FT-IR Graph representing the spectrum of chitosan coated IONPs with and without surfactant (Tw 80)

3.5.3 Optimization of the washing steps

After the particles in the solvent phase precipitated out in the non-solvent phase during the nanoprecipitation method, they were separated by magnet and followed the same procedure for that as PLGA-IONPs (section 2.2.4). In the solution there should be three populations of particles: unbound IONPs, unbound chitosan and chitosan coated IONPs. The optimization of the washing steps was done to separate chitosan coated IONPs from those two other populations.

The studies from (Culita et al,2019) show that as the mass ratio between chitosan and magnetic nanoparticle increase the saturation magnetization values decrease. That means chitosan coated IONPs could be less magnetic than the uncoated IONPs. But after 30 seconds almost 90-95% of the IONPs were separated (figure 35b, vial 1) and only 3-5% of the IONPs were in the supernatant (figure 35c, vial 2) and the supernatant was transferred to a different vial before discarding the liquid. So, it was difficult to differentiate chitosan coated and uncoated IONPs just after 30 seconds magnet separation. But more chances of getting unbound chitosan should be in the supernatant than in the particles separated by magnets. Both NPs in vials 1 and 2 were redispersed in 1ml of

water and measured the hydrodynamic sizes and zeta potentials. As there were very low number of NPs present in vial 2, adding 1 ml of water made the concentration of that NP solution in vial 2 compared to solution in vial 1.

Table 7. DLS results solution containing chitosan coated IONPs

NPs in vial 1			NPs in vial 2		
Sample	**Hydrodynamic Size (nm)**	**Zeta Potential (mV)**	**Sample**	**Hydrodynamic Size (nm)**	**Zeta Potential (mV)**
1	5496	34	1	117493	-15
2	6736	32	2	69726	-15
3	5826	32	3	63808	19

The NPs in vial 2 have larger hydrodynamic sizes than the NPs in vial 1. Inbaraj et al, 2012 suggested that coating in bare IONPs will increase the sizes [90]. The hydrodynamic sizes of bare IONPs and chitosan B_198 were measured between 175-180 nm and 250-1500 nm range respectively. After chitosan-IONPs mixture added to the non-solvent phase for nanoprecipitation, the chitosan particles should entrap IONPs which can eventually make larger particles respective to bare chitosan NPs and IONPs. According to table 7, NPs from both vial 1 and 2 showed larger sizes. But less magnetic samples show very large sizes and a small amount of IONPs. The concentration of vial 2 solution was much less than vial 1 which could influence the hydrodynamic sizes. Another possibility is of having unbound chitosan NPs in vial 2 solution. Anton Paar can measure size up to 1/2 Å, the chances are in the less concentrated solution there might be very few or no chitosan coated IONPs and more aggregated chitosan polymeric particles. Zeta potentials of both populations were also different. The NPs in vial 1 have positive zeta potential and that could suggest their surface charge is positively charge. IONPs have negative zeta potential (Table 4) and chitosan NPs which were extracted after rotary evaporation, had positive zeta potential (figure 20). So, there might be a possibility that the IONPs present in the vial 1 have chitosan particles bounding them. But NPs in vial 2 have low zeta potentials (2 samples were negative) which could suggest the presence of bare IONPs in the solution and as it was discussed earlier (section 3.2.1.2) that zeta potential measurements can be influenced by slight change of dilution and concentration,

So, it was decided to measure and further study only NPs which were in the wall of the vials separated primarily after 30 seconds magnet separation and discard supernatant. This is the

primary screening of separating coated samples and uncoated samples. Then the magnet separation method was done by washing 3 times for separating any uncoated chitosan NPs.

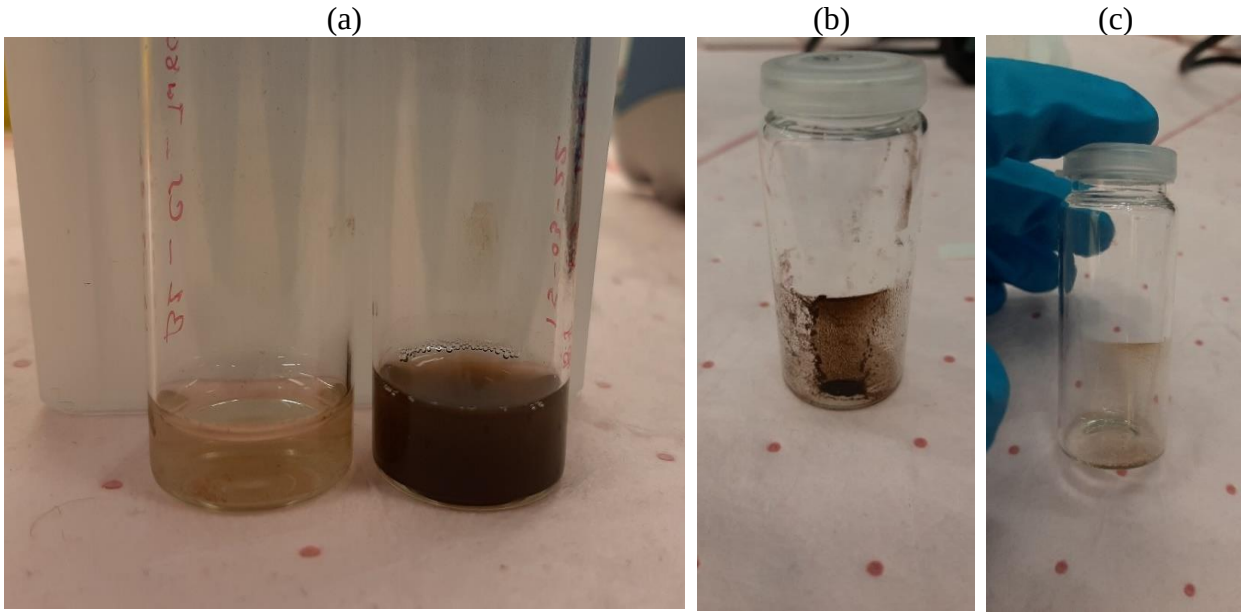

Figure 35: Separation of coated IONPs by magnetic separation. a) NPs redispersed in water in (vial 1) and (vial 2), b) 30 sec magnet separation NPs (vial 1) before redispersing in water and c) NPs of supernatant (vial 2) before redispersing in water.

In order to retrieve all the magnetic chitosan coated IONPs, the separation time on the magnet must be optimized. The magnet separation process of chitosan coated IONPs was not optimized. There is a possibility that three different populations of Chitosan coated IONPs, bare chitosan and free IONPs are present in the samples. For this purpose, three different magnet time were chosen in order to optimize the magnetic separation time and retrieve all the polymer coated IONPs. Three different times were 30 second, 20 second and 10 second. Primary separation of solid particles was done by 30-10 seconds and supernatant was discarded as there was trace amount of IONPs present (figure 35c).

The chitosan solution concentration was 2 mg/ml and IONPs concentration was 5 mg/ml. The experiments were done in triplicates (B1, B2 and B3).

The range of hydrodynamic sizes of the particles were between 1000-3500 nm except for one sample in 20 sec magnet separation (figure 36). The zeta potential was between 25-35 mV which

indicates they might have positive charged particles on the surface. In all the cases, variation in the NPs hydrodynamic size is seen and no probable trend is observed. The possible reasons might be presence of different populations of NPs in different frequency in each batch. But 30 seconds separation has similar size range of particles compared to both 20 seconds and 10 seconds treatment. These results indicate that 30 seconds magnate separation would be more optimum to separate large unbound particles and make homogenous population of particles.

After primary screening of separating unbound and larger particles, the supernatant was discarded, and remaining NPs were resuspended in water. Then magnetic separation was again performed 3 times for 2 minutes each for removing remaining unbound polymer particles.

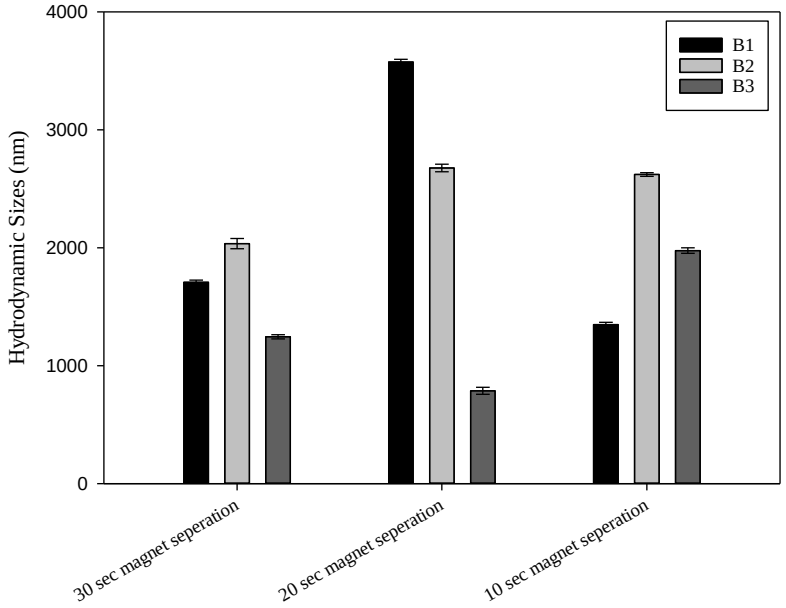

Figure 36: Graph represents the hydrodynamic size of chitosan coated IONPs at different magnetic separation times

3.5.4 Design of Experiment using JMP

Screening design was made in JMP software, in order to study the effect of IONPs concentration, polymer concentration, volume of non-solvent and flow rate of solvent phase on the size of chitosan coated IONPs. The design of experiments is attached in appendix H. In this design, the polymer used was chitosan B, with molecular weight of 198kDa. The IONPs concentration was

fixed at 2.5 and 5 mg/ml, the polymer concentration was set to 0.5 and 2, the flow rate of solvent phase was maintained at 29.05, 58.06 and 116.1 ml/h and non-solvent volume was fixed at 5 and 10 ml. The goal of this study was to synthesize small NPs for biomedical application. The optimum size range of a nanoparticle is between 150-800 nm for biomedical application [91]. In some of the studies it was observed that after administration of NPs into the living system, small sizes (10-30 nm) are eliminated by renal excretion [92] and larger particles will be engulfed by mononuclear phagocytes [91].

12 experiments were conducted and the purpose of this study was to identify which parameters would give relatively small NP sizes. After completion of this design, it was found that the R^2 for this experimental design was obtained to be 0.22. The design does not fit well and from this study it was difficult to choose which variables have higher or lower significant values. This JMP study could not figure out which parameters had the largest and least effect on the data set could be because there was just no specific correlation between the parameters varied and the sizes measured. There were challenges in separating the chitosan coated IONPs by magnet which could also influence the results. Experimental errors in DLS sample preparation might also mislead the experiment results.

Table 8 displayed the model parameter estimates and provided a t test for the hypothesis that it equals zero for each parameter. The p values from the parameters suggested that the model was not fitted and the parameters have no real influence on the hydrodynamic sizes.

Table 8. Summary of parameter estimates for screening design.

Parameters Estimates	
Term	**Prob > t**
Intercept	0.0158
Flowrate (ml/h) (29.05, 116.1)	0.7104
IONPs concentration (mg/ml) (2.5, 5)	0.611
Chitosan concentration (mg/ml) (0.5, 2)	0.3922
Methanol Volume (ml) (5,10)	0.4399

After conducting those 12 experiments, the lowest hydrodynamic sizes of the NPs were obtained from experiment 3 and 4 (table H1). It was observed that experiment 3 and 4 have lowest flow rates (29.05 ml/h) and similarly in bare chitosan NP synthesis there was also an observation that low flowrate gave smaller NP sizes (section 3.2.1.5). Then the parameters of these two experiments were more focused to continue size optimization studies which will be discussed in the following section.

Table 9. Synthesis parameters of experiment 3 and 4 from screening study

Experiments	Flow rate (ml/h)	IONPs concentration (mg/ml)	Polymer concentration (mg/ml)	Methanol volume (ml)
3	29.05	5	0.5	10
4	29.05	5	2	5

3.3.5 Continued size optimization study of chitosan coated IONPs

The statistical screening design did not give a good fit to the parameters. But from the large data set of the screening design, the smallest sizes were obtained from two experiment parameters (table 9). So, the aim of these studies was to narrow down to the parameters which can give even smaller sizes. Study on non-solvent volume, concentration of IONPs and concentration of surfactants were chosen to see the effects on the sizes. In this continued study, the non-solvent volume was fixed at 5, 10, 20, 40 and 60 ml, IONPs concentration was fixed at 2.5, 5 and 7.5 mg/ml, the concentration of the tween 80 was determined at 0.05% to 0.2%.

The volume of non-solvent varied in 20 ml, 40 ml and 60 ml to see the changing hydrodynamic sizes. Studies from (Luque-Alcaraz et. al, 2016) suggest that keeping the solvent phase constant and increasing the non-solvent phase has no effect on hydrodynamic sizes in nanoprecipitation method. Another researcher suggests that increase in proportion of non-solvent with respect to solvent generally produces smaller nanoparticles [60]. By observing the data from table 10 and 11, there was a trend of increasing the sizes when non-solvent volume was increasing in batches might be because of nonhomogeneous mixing of the NPs (Table 11). But the size of the NPs from (Table 10) were in the similar range from 1000-1400 nm apart from one sample (sample 2 -2700 nm). The large sizes indicate a possible increased super saturation during nanoprecipitation. But it should be noted that for experiment 3 and experiment 4 the chitosan concentration was not same. Batches from experiment 3 have lower chitosan concentration (0.5 mg/ml) than experiment 4

(2mg/ml). So, lower concentration of polymer will produce smaller sizes because of less polymer chain present in non-solvent phase and increasing the non-solvent volume decreases the NP sizes because of decreasing in viscosity of the organic phase as it was discussed earlier in section 3.2.1.3. The PDI range was between 0.3 -0.36 suggested single population in the samples for batches in table 10.

To ensure the reproducibility of the smaller hydrodynamic sizes experiments were conducted 3 times. For the next screening study, parameters from experiment 3 were chosen to see the effects on sizes.

Table 10. Hydrodynamic size, PDI and zeta potential of Chitosan coated IONPs for experiment 3 parameter

Sample	Chitosan concentration (mg/ml)	Methanol volume (ml)	Hydrodynamic size (nm)	PDI	Zeta Potential (mv)
1	0.5	10	1448	0.303	16
2	0.5	20	2700	0.368	20
3	0.5	40	1061	0.32	27
4	0.5	60	1151	0.323	24

Table 11. Hydrodynamic size, PDI and zeta potential of Chitosan coated IONPs for experiment 4 parameter

Sample	Chitosan concentration (mg/ml)	Methanol volume (ml)	Hydrodynamic size (nm)	PDI	Zeta Potential (mv)
1	2	5	1630	0.28	14
2	2	20	9475	0.27	24
3	2	40	13349	0.31	29.2
4	2	60	96789	0.52	13

Three different IONPs (2.5 mg/ml, 5 mg/ml and 7.5 mg/ml) concentration were used to see the effect in hydrodynamic sizes. The sizes decreased when the IONPs concentration increased from 2.5 to 5 mg/ml, but the sizes increase when the concentration increased from 5 to 7.5 mg/ml. The reason could be that at 5mg/ml concentration IONPs, the polymer might coat a thinner layer around the IONPs than at 2.5 and7.5 mg/ml concentrated samples. Another reason could be since IONPs surface is not functionalized, the interaction between negatively charged IONPs and positively

charged CS-IONPs which could cause aggregation. 5 mg/ml concentrated samples could have better mixing with during nucleation growth with could cause smaller sizes than other two samples.

Table 12. DLS size, PDI zeta potential of Chitosan coated IONPs for different IONP concentration.

Sample	Hydrodynamic size (nm)	PDI	Zeta potential (mV)
2.5 mg/ml conc IONPs	1584	0.35	27
5 mg/ml conc IONPs	1384	0.27	23
7.5 mg/ml conc IONPs	4284	0.32	21

The surfactant concentration was also varied to observed effects on hydrodynamic sizes. Concentration of surfactant in non-solvent is known to influence size of the nanoparticles formed. Generally, a concentration range between 0.1-1% surfactant is found sufficient to stabilize the nanoparticles, however, sometimes concentrations as high as 7% w/v are required depending upon type of stabilizer and dispersion medium [93]. 0.05 % tween concentration in non-solvent solution produced lowest hydrodynamic sizes for polymer coated IONPs. The hydrodynamic sizes of the NPs were bigger in both cases (tween absent and 0.2%) which might indicate that 0.05% concentration tween80 is sufficient to stabilize the chitosan coated IONPs

Table 13. Hydrodynamic size, PDI and zeta potential of Chitosan coated IONPs for different concentrations of tween80.

Sample	Hydrodynamic size (nm)	PDI	Zeta Potential (mV)
No Tween	1655	0.26	21
0.05 % Tween	1384	0.27	23
0.2 % Tween	1752	0.27	26

So, after these screening designs the optimum parameters for obtaining smallest sizes of chitosan coated IONPs are narrowed down to this table below.

Table 14. The input parameters for chitosan coated IONPs

Sample: Chitosan coated IONPs	
Flowrate (ml/h)	29.05
IONPs concentration (mg/ml)	5
Chitosan concentration (mg/ml)	0.5
Non-solvent volume (ml)	40
Surfactant concentration (%)	0.05%

4. Conclusion

The aim of this project was to synthesize, optimize and characterize the chitosan coated IONPs for biomedical applications. The project was divided into three phases. First to synthesize and characterize bare chitosan NPs, second is bare IONPs synthesis and characterization and third to synthesize and characterize chitosan coated IONPs.

But before that, the process of obtaining polymer NPs through nanoprecipitation was observed by conducting the preliminary study of PLGA NP and PLGA-IONPs. The effects of concentration and flow rates were studied. The hydrodynamic sizes of the NPs got bigger when the polymer concentration as well as flow rates increased.

Chitosan NP was synthesized by nanoprecipitation method. For bare chitosan NP synthesis, two types of chitosan were used: Chitosan A and Chitosan B. The amino group of the Chitosan A was not charged which makes it insoluble in water and the presence of Cl^- counter ion makes Chitosan B soluble in water. Different techniques such as centrifugation and rotary evaporator were tried to remove methanol from the chitosan NPs solution. The hydrodynamic sizes ranged between 100-350 nm and zeta potentials were negative ranged from -18 to -40 (after centrifugation) and 25-35 (after rotary evaporator). The effect of polymer concentration, flow rates, molecular weight, stirring time were observed. Hydrodynamic sizes of the NPs were increased when polymer concentration and flow rates increased but different molecular weight chitosan produce same size range of NPs. Different stirring time gave different sizes of NPs (1h> 3h <5h). STEM images of chitosan A NPs showed polydispersity populations.

The polymer NP sample contains a low number of NPs in the solution so it might affect the DLS measurement if they are diluted even further. So, DLS measurement of chitosan A NPs was also optimized. The hydrodynamic sizes of Diluted samples (100µl sample in 1.9 ml of water) and direct samples were compared. The sizes of the diluted samples and direct samples were between 150-300 nm and 500-2000 nm according to different concentrations (0.5 and 2 mg/ml) which are in similar ranges according to (Alcaraz et. al, 2016). After this study, DLS measurements were continued using direct samples without dilution in the DLS cells.

Chitosan B NPs were synthesized and measured hydrodynamic sizes between 500-600 nm and 900-1200 nm range for two different concentrated chitosan B solution (0.5 and 2 mg/ml). The size

distribution was analyzed by lumisizer and the mean average sizes were 1271 nm for 2 mg/ml concentrated chitosan solution. FT-IR was conducted on one sample of chitosan B NPs to observe the spectrum. According to other researchers, the peaks could indicate – OH stretching vibrations of water, hydroxyls and NH2 stretching vibrations of free amino groups and a C=O bond of ester and this could confirm the presence of chitosan NPs in the solution and tween80 coating on the surface of the chitosan NPs.

IONPs were synthesized by co-precipitation method and the hydrodynamic sizes and zeta potentials of the IONPs were 176 ± 4 nm and -32 ± 0.3 mV accordingly. The lumisizer analyzed the size distribution of the IONPs. The smallest, largest and mean population of IONPs were 24, 39 and 30 nm. The average size was estimated to be 10 ± 3 nm on TEM. The magnetic characterization was also conducted by VSM and showed no hysteresis loop which suggested the superparamagnetism properties of IONPs. The magnetic moment was calculated 56.7 emu/g. The FT-IR data gave a characteristic metal-oxygen peak.

Comparison studies were done for nanoprecipitation and mixing IONP with chitosan. Both samples were characterized by STEM. The samples obtained from nanoprecipitation were more spherical in size and chitosan particles were also detected around the IONPs. Sizes were between 100-250 nm. The samples from mixing process were given bigger sizes from 1-5 µm and irregular shapes. This could suggest chitosan coated IONPs can be synthesized by nanoprecipitation method.

The hydrodynamic sizes of the coated IONPs were between 900-1500 nm and zeta potential were between 25-30 mV. The size distribution of the chitosan coated IONPs were analyzed by lumisizer. Mean hydrodynamic sizes were 91 nm and largest population was 261 nm.

Surface characterization of the chitosan coated IONPs were observed by the effect of pH on zeta potential and FT-IR characterization. The zeta potential changed from positive to negative when the pH increased. The FT-IR spectrum gave characteristic FeO^- bond and-NH_2 bond which might be because of chitosan particle in the surface.

The washing steps of the chitosan coated IONPs were followed first according to preliminary studies of PLGA-IONPs particles. In PLGA-IONPs, the coated particles were separated after 30 seconds magnet separation and they were found in the supernatant. Then they were further washed

3 times to get rid of bare PLGA NPs, free surfactant and DMSO. The IONPs were separated after 30 seconds magnet separation and less than 5% of the IONPs containing particles were in the supernatant which suggested polymer coated IONPs might be among those IONPs population. The IONPs were in vial 1 and supernatant were transferred in vial 2. The hydrodynamic sizes of the NPs from solution in vial 1 and vial 2 were measured. The NP sizes were bigger in both particles, but NPs separated in vial 1 have most of the IONPs, so it could be possible that polymer coated IONPs would most likely be in that vial and decided to discard supernatant. Then solution in vial 1 was washed 3 times to purify the NPs and remove non-magnetic particles (chitosan, surfactant).

Screening design was conducted using JMP to observe the hydrodynamic sizes effects on different synthesis parameters such as concentration of IONPs, concentration of polymer, flow rate and methanol volume. The aim of the screening design was to differentiate which sets of parameters would give small sizes of polymer coated IONPs around 150-800 nm for biomedical application. The statistical design did not give any satisfactory results for the variation of different parameters that affect the size. The possible reason might be those parameters (polymer concentration, IONPs concentration, flow rate and volume of methanol) have any correlation between the sizes. 12 experiments were conducted for this study. The smallest of the sizes among these experiments were chosen to do further size optimization study and the goal was to identify which parameters would give smallest hydrodynamic sizes of NPs for biomedical application.

Future Prospects

Synthesis of chitosan coated IONPs with nanoprecipitation, surface characterization by pH and FT-IR, effect of sizes on different synthesis parameters were shown within the scope of this study. The statistical screening design was not a good fit on the synthesis experiments so it would be good to do another screening design using different experiment conditions such as use of different organic compounds (acetone, isopropanol) as non-solvent than methanol, different grades of chitosan (Mw and DA), different temperature.

In future, it would be interesting to study the loading of drugs and magneto-responsive drug releases under dynamic conditions using Magnetherm and drug loading efficiency using Ultraviolet Visible Spectroscopy (UV-Vis) of the chitosan coated IONPs using different drugs (hydrophobic and/or hydrophilic) to see the interaction between the drug molecule and the NPs. If the polymer coated IONPs could not reach in a certain size range for drug delivery, it would be interesting to use those particles in different applications such as wastewater treatment or tissue engineering etc [94].

Appendices

Appendix A

Table A 1. Hydrodynamic sizes, zeta potentials and PDI of chitosan NPs from Chitosan A

Number of Experiments	Molecular weight of chitosan A (kDa)	Flowrate (ml/h)	Chitosan conc (mg/ml)	Stirring time (h)	Hydrodynamic Size (nm)	Zeta Potential (mV)	Polydispersity Index (PDI)
1	198	29.05	0.5	5h	139	-18	0.346
2	198	58.06	0.5	1h	271	-40	0.422
3	198	58.06	0.5	1h	186	-34	0.347
4	198	58.06	0.5	3h	152	-30	0.43
5	198	58.06	0.5	3h	151	-29	0.424
6	198	58.06	0.5	3h	193	-35	0.345
7	198	58.06	0.5	3h	273	-29	0.384
8	198	58.06	0.5	3h	170	-33	0.285
9	198	58.06	0.5	5h	241	-23	0.442
10	198	58.06	0.5	5h	232	-38	0.417
11	198	58.06	2	5h	273	-26	0.304
12	198	58.06	2	5h	333	-32	0.297
13	198	58.06	2	5h	293	-10	0.448
14	198	116.1	0.5	5h	326	-34	0.376
15	307	58.06	0.5	5h	245	-28	0.394
16	604	58.06	0.5	5h	232	-34	0.376
17	604	58.06	0.5	5h	300	-35	0.376
18	604	58.06	2	5h	273	-28	0.463
19	604	58.06	2	5h	167	-40	0.245
20	604	58.06	2	5h	186	-26	0.328

Weight tracing of chitosan NPs

The weight of the chitosan NPs solutions was measured to see if there were any solution present after extracting the methanol in rotary evaporation and running DLS on that sample. The solution + NPs weight of all samples are between 8.5-8.6 g of 11 ml of chitosan NPs in methanol solution (1ml chitosan solution + 10 ml methanol) (table A3). After rotavapor was finished the solution weight decreased to 0.5-0.65 g and boiling point of methanol in 64.7°C is much higher than water (100°C) which means methanol will evaporate first. This can confirm that methanol was extracted from the sample and chitosan NPs was only present in the flask.

Table A 2. Weight of the chitosan NPs before and after rotavapor

Chitosan A_198 kDa					
Sample	**Empty Flask weight (g)**	**Flask + solution weight before rotavapor (g)**	**Solution + NPs weight (g)**	**Flask + solution weight after rotavapor (g)**	**Solution weight after rotavapor (g)**
1	48.89	57.49	8.6	49.42	0.53
2	48.9	57.59	8.69	49.49	0.49
3	48.91	57.52	8.61	49.45	0.54
Chitosan A_604 kDa					
1	48.85	57.5	8.65	49.5	0.65
2	49.13	57.76	8.63	49.65	0.52
3	49.14	57.67	8.53	49.78	0.64

Further Studies on DLS

In the DLS machine, the measurement angle from back scattering 175° to side scattering 90° was changed to see effect on the hydrodynamic sizes of chitosan NPs. This study was done on chitosan B NPs at 0.5 mg/ml concentration. The sample of chitosan NPs contains different populations of particles (STEM pics). One assumption was made by Anton Paar, if a photon is scattered by multiple particles, the sensor will not be able to efficiently correlate the degree of the pattern change with the particle size. Back scattering is used to detect particles in a concentrated solution because the photon has less sample volume to travel through and which makes it less likely for it to contact many particles and experience several scattering events. But it is the opposite for low concentrated solution. So, side scattering is optimum for this kind of detection. Another possible reason is smaller particles produce weak scattering light of photon which can be detected and analyzed in a "side scattering" mode efficiently. Such samples may be challenging to evaluate from the back angle because the scattering signal of the sample is muffled out by the flare that results from the impact of the laser with the cuvette wall. Side angle measurements effectively avoid these problems and provide signal-to-noise ratios that are better (Anton Par 500 manual).

The hydrodynamic sizes were found to be smaller when the NPs were measured using side scattering angle than back scattering.

Table A 3. DLS results of sizes and PDI of chitosan nanoparticles at 90° side scattering angle

Sample	Size (nm)	PDI
1	492	0.28
2	253	0.31
3	554	0.28

Appendix B

Table B 1. Lumisizer sample analyzer profile

Separation Type: Sedimentation
Distribution Type: Volume Weighted Particle Size Distribution
Analysis mode: Constant position
Sample Cell: LUM 2mm, PA, Rect. Synthetic Cell (110-134xx)

Table B 2. Lumisizer SOP for Chitosan NPs, IONPs and chitosan coated IONPs size distribution

Number	Profiles	Intervals	Speed	Light Factor	Temperature
1	10	10s	250 RPM	1.00	25.0°C
2	10	10s	500 RPM	1.00	25.0°C
3	10	10s	750 RPM	1.00	25.0°C
4	10	10s	1000 RPM	1.00	25.0°C
5	10	10s	1250 RPM	1.00	25.0°C
6	10	10s	1500 RPM	1.00	25.0°C
7	10	10s	1750 RPM	1.00	25.0°C
8	10	10s	2000 RPM	1.00	25.0°C
9	10	10s	2500 RPM	1.00	25.0°C
10	10	10s	3000 RPM	1.00	25.0°C
11	10	10s	4000 RPM	1.00	25.0°C
12	10	10s	4000 RPM	1.00	25.0°C

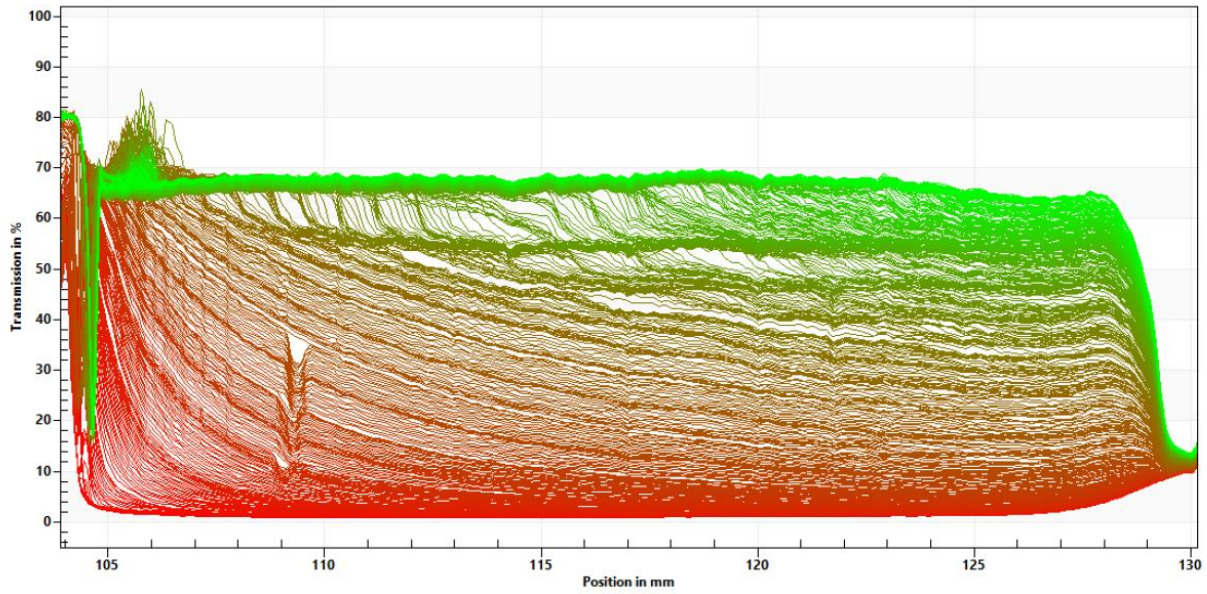

Figure B 1: Time lapse of sedimentation graph of Chitosan coated IONPs (Lumisizer)

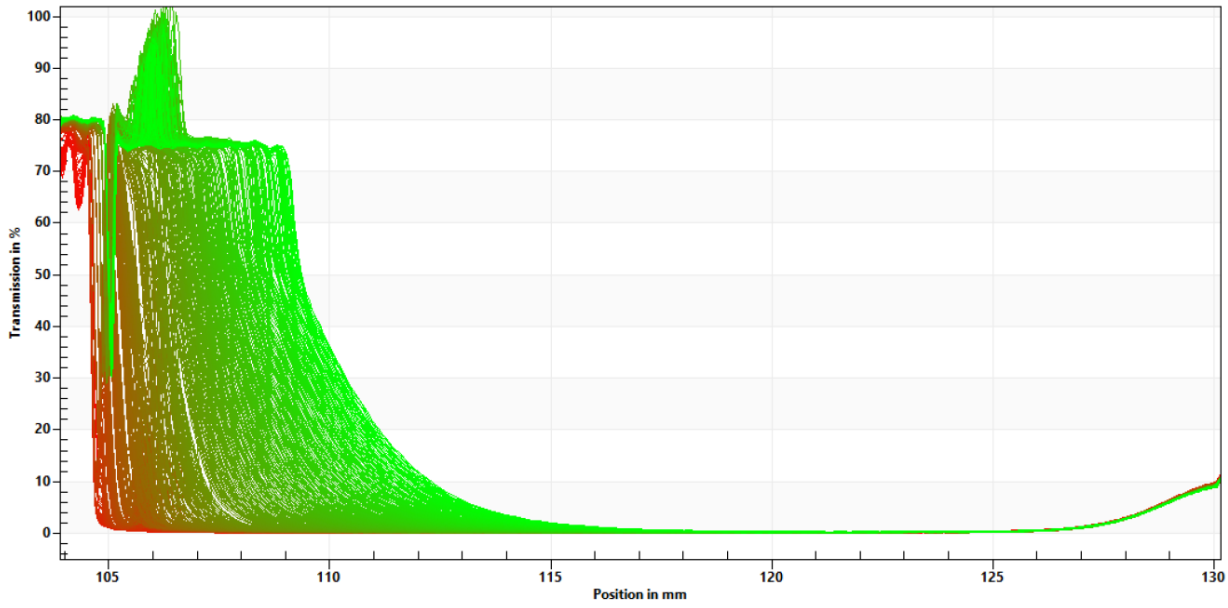

Figure B 2: Time lapse of sedimentation graph of IONPs (Lumisizer)

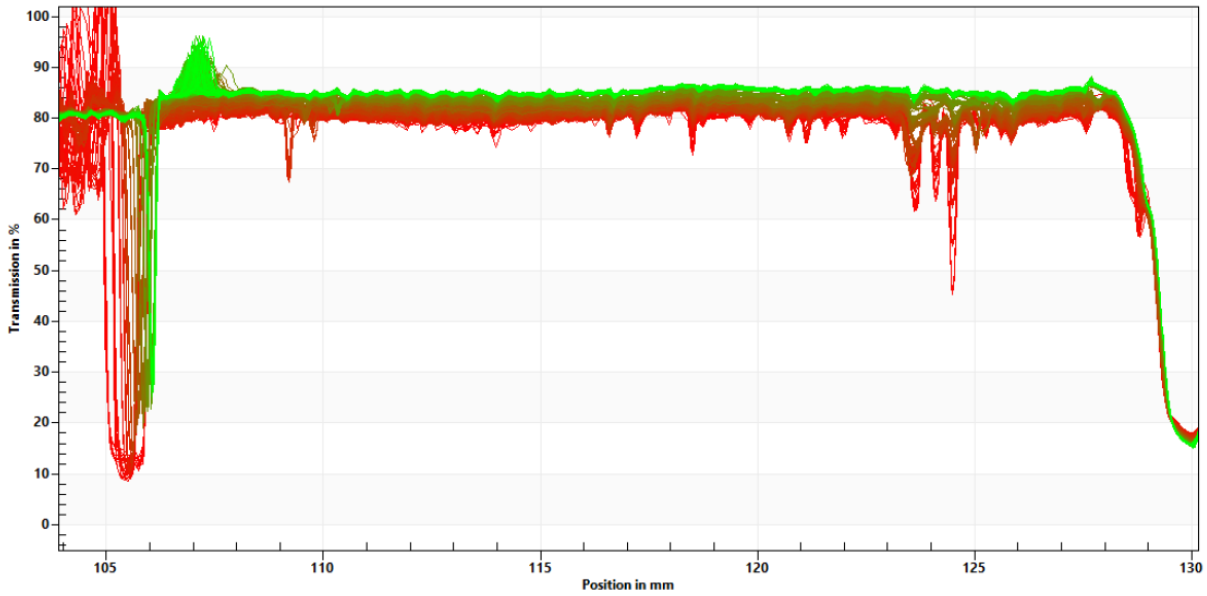

Figure B 3: Time lapse of sedimentation graph of chitosan NPs from chitosan B (Lumisizer)

Appendix C

Table C 1. pH range of chemical compounds used in this study

Chemical Compound	pH range
Methanol	7-8.5
Tween 20	6-8
Tween 80	5-7

Appendix D

Table D 1. DLS results of chitosan coated IONPs in different duration of magnet separation

30 secs separation		
Sample	**Hydrodynamic Size (nm)**	**Zeta Potential (mV)**
1	1708	23
2	2036	26
3	1246	32
20 secs separation		
Sample	**Hydrodynamic Size (nm)**	**Zeta Potential (mV)**
1	3575	37
2	2677	38
3	787	34
10 secs separation		

Sample	Hydrodynamic Size (nm)	Zeta Potential (mV)
1	1349	33
2	2622	24
3	1977	26

Appendix E

Different DLS SOP comparison on chitosan coated IONPs samples

The refractive index (R.I) of the sample solvent is a required input parameter for measuring hydrodynamic sizes in DLS. The DLS system has different built-in refractive index categories, but no refractive index of coated polymer sample is present. According to the Mironenko et al, the refractive index of chitosan coated silver NPs were (1.53-1.69) range [95]. The polystyrene latex has a similar R.I of 1.5850. If the measured particles do not match any R.I from the DLS machine, there is an option for unknown material to select and it will give a R.I of 1.3303. Both unknown material and polystyrene R.I were selected for 3 triplicates samples and measured to compare the hydrodynamic sizes. The concentration of IONPs was 5 mg/ml and concentration of chitosan was 2 mg/ml. According to table E1, sample 1 and 2 have bigger hydrodynamic sizes in unknown material than polystyrene latex. Sample 3 has bigger sizes for polystyrene latex R.I than unknown material. The reason might be the presence of aggregated large NPs.

Table E 1. DLS size and zeta potential of Chitosan coated IONPs in two different SOP

	Sample	Size (nm)		Sample	Size (nm)
Unknown material	1	3742	**Polystyrene latex**	1	3053
	2	1911		2	1597
	3	7937		3	16095

Appendix F

Different measurment angle for DLS

The Anton Paar DLS machine has three measurement angles (15°, 90° and 175°). So, all measurement angles were used on the same sample to see size differences. Sample 1 from (table F1) was used for three angles. The sample size range was almost similar in range.

Table F 1. DLS size and zeta potential of Chitosan coated IONPs

CS+ IONPs (5 mg/ml)			
Angle	**Size (nm)**	**PDI**	**Zeta**
Forward scattering 15°	744	28.90%	28
Back Scattering 175°	667	28.70%	
Side scattering 90°	715	8.40%	

Appendix G

Table G 1. Zeta potential of the polymer, IONPs and polymer coated IONPs at different pH

Chitosan coated IONPs with surfactant			**Chitosan coated IONPs without surfactant**			**Bare Chitosan with surfactant**			**Bare Chitosan without surfactant**			**Bare IONPs**		
pH		**zeta potential (mV)**	**pH**		**zeta potential (mV)**	**pH**		**zeta potential (mV)**	**pH**		**zeta potential (mV)**	**pH**		**zeta potential (mV)**
Initial pH	**Final pH**		**Initial pH**	**Final pH**		**Initial pH**	**Final pH**		**Initial pH**	**Final pH**		**Initial pH**	**Final pH**	
3.9	3.2	45.1	4.4	3.1	44.3	4.5	3.6	49.9	4.4	3.3	46.7	4.6	3.1	29.7
5.6	3.9	44.9	5.3	4.4	45	5.6	4.5	44.4	5.6	4.4	39.3	5.6	4.6	-6.7
6.9	5.6	39	6.8	5.3	38	Starting point pH	5.6	43.8	Starting point pH	5.6	41.2	6.5	5.6	-26
Starting point pH	6.9	31	Starting point pH	6.8	29.4	5.6	6.4	27.4	5.6	6.3	28.4	7.3	6.5	-33
6.9	7.6	16.7	6.8	7.4	19	6.5	7.5	12.6	6.3	7.4	14.1	8.3	7.4	-34
7.6	8.4	4.4	7.4	8.2	5.3	7.5	8.2	2.1	7.4	8.3	1.9	9.4	8.3	-31.5
8.4	9.4	-22.2	8.2	9.3	-18.9	8.2	9.2	-2.9	8.3	9.4	-3.3	Starting point pH	9.4	-34.5

Appendix H

Table H 1. Experimental design for JMP study of chitosan coated IONPs

Exp No	Flowrate (ml/h)	IONPs concentration (mg/ml)	Chitosan concentration (mg/ml)	Methanol volume (ml)	Hydrodynamic Sizes (nm)
1	29.05	2.5	0.5	10	14031
2	29.05	2.5	2	5	2256
3	29.05	5	0.5	10	1448
4	29.05	5	2	5	1630
5	58.06	2.5	0.5	5	1914
6	58.06	2.5	2	10	2196
7	58.06	5	0.5	5	2400
8	58.06	5	2	10	3723
9	116.12	2.5	0.5	10	2363
10	116.12	2.5	2	5	2426
11	116.12	5	0.5	5	5558
12	116.12	5	2	10	3334

References

[1] A. D. McNaught and A. Wilkinson, *Compendium of Chemical Terminology*, 2nd ed. Oxford: Blackwell Science, 1997.

[2] M. Mohiuddin, B. Kumar, and S. Haque, *Biopolymer Composites in Photovoltaics and Photodetectors*. Elsevier Inc., 2017.

[3] S. Bin Park, E. Lih, K. S. Park, Y. K. Joung, and D. K. Han, "Biopolymer-based functional composites for medical applications," *Prog. Polym. Sci.*, vol. 68, pp. 77–105, May 2017, doi: 10.1016/J.PROGPOLYMSCI.2016.12.003.

[4] L. Lacerda, A. L. Parize, V. Fávere, M. C. M. Laranjeira, and H. K. Stulzer, "Development and evaluation of pH-sensitive sodium alginate/chitosan microparticles containing the antituberculosis drug rifampicin," *Mater. Sci. Eng. C*, vol. 39, no. 1, pp. 161–167, Jun. 2014, doi: 10.1016/J.MSEC.2014.01.054.

[5] D. Nagaonkar, S. Gaikwad, and M. Rai, "Catharanthus roseus leaf extract-synthesized chitosan nanoparticles for controlled in vitro release of chloramphenicol and ketoconazole," doi: 10.1007/s00396-015-3538-3.

[6] E. A. El-Alfy, M. K. El-Bisi, G. M. Taha, and H. M. Ibrahim, "Preparation of biocompatible chitosan nanoparticles loaded by tetracycline, gentamycin and ciprofloxacin as novel drug delivery system for improvement the antibacterial properties of cellulose based fabrics," *Int. J. Biol. Macromol.*, vol. 161, pp. 1247–1260, Oct. 2020, doi: 10.1016/J.IJBIOMAC.2020.06.118.

[7] D. J. H. and D. L. Kaplan, "Poly(lactic-co-glycolic) Acid−Controlled-Release Systems: Experimental and Modeling Insights," in *Critical Reviews™ in Therapeutic Drug Carrier Systems*, .

[8] S. M. El-Sawy, Y. M. Abu-Ayana, and F. A. Abdel-Mohdy, "Some chitin/chitosan derivatives for corrosion protection and waste water treatments," *Anti-Corrosion Methods Mater.*, vol. 48, no. 4, pp. 227–234, 2001, doi: 10.1108/EUM0000000005630.

[9] P. Agrawal, G. J. Strijkers, and K. Nicolay, "Chitosan-based systems for molecular imaging," *Adv. Drug Deliv. Rev.*, vol. 62, no. 1, pp. 42–58, Jan. 2010, doi: 10.1016/J.ADDR.2009.09.007.

[10] R. A. A. MUZZARELLI, *Chitin Chemistry*. 1977.

[11] B. A. Dmitriev, Y. A. Knirel, and N. K. Kochetkov, "Selective cleavage of glycosidic linkages: Studies with the O-specific polysaccharide from Shigella dysenteriae type 3," *Carbohydr. Res.*, vol. 40, no. 2, pp. 365–372, Apr. 1975, doi: 10.1016/S0008-6215(00)82617-8.

[12] H. Yi *et al.*, "Reviews Biofabrication with Chitosan," 2005, doi: 10.1021/bm050410l.

[13] J. K. Francis Suh and H. W. T. Matthew, "Application of chitosan-based polysaccharide biomaterials in cartilage tissue engineering: a review," *Biomaterials*, vol. 21, no. 24, pp. 2589–2598, Dec. 2000, doi: 10.1016/S0142-9612(00)00126-5.

[14] V. K. Mourya, N. N. Inamdar, and Y. M. Choudhari, "Chitooligosaccharides: Synthesis, characterization and applications," *Polym. Sci. - Ser. A*, vol. 53, no. 7, pp. 583–612, 2011, doi: 10.1134/S0965545X11070066.

[15] J. Santoso, K. C. Adiputra, L. C. Soerdirga, and K. Tarman, "Effect of acetic acid hydrolysis on the characteristics of water soluble chitosan," *IOP Conf. Ser. Earth Environ. Sci.*, vol. 414, no. 1, p. 012021, Jan. 2020, doi: 10.1088/1755-1315/414/1/012021.

[16] M. Huang, E. Khor, and L.-Y. Lim, "Uptake and Cytotoxicity of Chitosan Molecules and Nanoparticles: Effects of Molecular Weight and Degree of Deacetylation," 2004.

[17] H. M. I. and E. M. R. E.- Zairy, “Chitosan as a Biomaterial — Structure, Properties, and Electrospun Nanofibers,” in *Concepts, Compounds and the Alternatives of Antibacterials*, V. Bobbarala, Ed. .
[18] J. D. Funkhouser and N. N. Aronson, “Chitinase family GH18: Evolutionary insights from the genomic history of a diverse protein family,” *BMC Evol. Biol.*, vol. 7, pp. 1–16, 2007, doi: 10.1186/1471-2148-7-96.
[19] S. H. Pangburn, P. V. Trescony, and J. Heller, “Lysozyme degradation of partially deacetylated chitin, its films and hydrogels,” *Biomaterials*, vol. 3, no. 2, pp. 105–108, 1982, doi: 10.1016/0142-9612(82)90043-6.
[20] K. Tomihata and Y. Ikada, “In vitro and in vivo degradation of films of chitin and its deacetylated derivatives,” *Biomaterials*, vol. 18, no. 7, pp. 567–575, 1997, doi: 10.1016/S0142-9612(96)00167-6.
[21] F. Croisier and C. Jérôme, “Chitosan-based biomaterials for tissue engineering,” *Eur. Polym. J.*, vol. 49, no. 4, pp. 780–792, 2013, doi: 10.1016/j.eurpolymj.2012.12.009.
[22] W. L. Teng, E. Khor, T. K. Tan, L. Y. Lim, and S. C. Tan, “Concurrent production of chitin from shrimp shells and fungi,” *Carbohydr. Res.*, vol. 332, no. 3, pp. 305–316, 2001, doi: 10.1016/S0008-6215(01)00084-2.
[23] M. Seenuvasan, G. Vinodhini, C. Geor Malar, N. Balaji, and K. Sathish Kumar, “Magnetic nanoparticles: a versatile carrier for enzymes in bio-processing sectors,” 2017, doi: 10.1049/iet-nbt.2017.0041.
[24] M. Z. Albanna, T. H. Bou-Akl, O. Blowytsky, H. L. Walters, and H. W. T. Matthew, “Chitosan fibers with improved biological and mechanical properties for tissue engineering applications,” *J. Mech. Behav. Biomed. Mater.*, vol. 20, pp. 217–226, 2013, doi: 10.1016/j.jmbbm.2012.09.012.
[25] L. Cui *et al.*, “Preparation and characterization of chitosan membranes,” 2018, doi: 10.1039/c8ra05526b.
[26] Y. Ohya, M. Shiratani, H. Kobayashi, and T. Ouchi, “Release Behavior of 5-Fluorouracil from Chitosan-Gel Nanospheres Immobilizing 5-Fluorouracil Coated with Polysaccharides and Their Cell Specific Cytotoxicity,” 2008, doi: 10.1080/10601329409349743.
[27] A. Grenha, “Chitosan nanoparticles: a survey of preparation methods,” *J. Drug Target.*, vol. 20, no. 4, pp. 291–300, 2012, doi: 10.3109/1061186X.2011.654121.
[28] Z. Songjiang and W. Lixiang, “Amyloid-Beta Associated with Chitosan Nano-Carrier has Favorable Immunogenicity and Permeates the BBB,” doi: 10.1208/s12249-009-9279-1.
[29] M. H. El-Shabouri, “Positively charged nanoparticles for improving the oral bioavailability of cyclosporin-A,” *Int. J. Pharm.*, vol. 249, no. 1–2, pp. 101–108, Dec. 2002, doi: 10.1016/S0378-5173(02)00461-1.
[30] S. Mitra, U. Gaur, P. C. Ghosh, and A. N. Maitra, “Tumour targeted delivery of encapsulated dextran–doxorubicin conjugate using chitosan nanoparticles as carrier,” *J. Control. Release*, vol. 74, no. 1–3, pp. 317–323, Jul. 2001, doi: 10.1016/S0168-3659(01)00342-X.
[31] W. Fan, W. Yan, Z. Xu, and H. Ni, “Formation mechanism of monodisperse, low molecular weight chitosan nanoparticles by ionic gelation technique,” *Colloids Surfaces B Biointerfaces*, vol. 90, no. 1, pp. 21–27, Feb. 2012, doi: 10.1016/J.COLSURFB.2011.09.042.
[32] U. S. & R. . Cornell, *Iron oxides in the laboratory: preparation and characterization*, 2nd ed. Wiley-VCH, 2008.

[33] G. V Kurlyandskaya *et al.*, “Water-Based Suspensions of Iron Oxide Nanoparticles with Electrostatic or Steric Stabilization by Chitosan: Fabrication, Characterization and Biocompatibility,” *Sensors*, vol. 17, 2017, doi: 10.3390/s17112605.
[34] S. I. C. J. Palma, M. Marciello, A. Carvalho, S. Veintemillas-Verdaguer, M. del P. Morales, and A. C. A. Roque, “Effects of phase transfer ligands on monodisperse iron oxide magnetic nanoparticles,” *J. Colloid Interface Sci.*, vol. 437, pp. 147–155, Jan. 2015, doi: 10.1016/J.JCIS.2014.09.019.
[35] Y. Wang, J. F. Wong, X. Teng, X. Z. Lin, and H. Yang, “‘Pulling’ Nanoparticles into Water: Phase Transfer of Oleic Acid Stabilized Monodisperse Nanoparticles into Aqueous Solutions of r-Cyclodextrin,” 2003, doi: 10.1021/nl034731j.
[36] M. Anbarasu, M. Anandan, E. Chinnasamy, V. Gopinath, and K. Balamurugan, “Synthesis and characterization of polyethylene glycol (PEG) coated Fe3O4 nanoparticles by chemical co-precipitation method for biomedical applications,” *Spectrochim. Acta Part A Mol. Biomol. Spectrosc.*, vol. 135, pp. 536–539, Jan. 2015, doi: 10.1016/J.SAA.2014.07.059.
[37] A. Bin Ashar, “Magnetic Polymeric Nanoparticles for Biomedical Applications,” no. February, 2021.
[38] I. Kikic and F. Vecchione, “Supercritical impregnation of polymers,” *Curr. Opin. Solid State Mater. Sci.*, vol. 7, no. 4–5, pp. 399–405, Aug. 2003, doi: 10.1016/J.COSSMS.2003.09.001.
[39] C. Pinto Reis, R. J. Neufeld, A. J. Ribeiro, and F. Veiga, “Nanoencapsulation I. Methods for preparation of drug-loaded polymeric nanoparticles,” *Nanomedicine Nanotechnology, Biol. Med.*, vol. 2, no. 1, pp. 8–21, Mar. 2006, doi: 10.1016/J.NANO.2005.12.003.
[40] C. Wischke and S. P. Schwendeman, “Principles of encapsulating hydrophobic drugs in PLA/PLGA microparticles,” *Int. J. Pharm.*, vol. 364, no. 2, pp. 298–327, Dec. 2008, doi: 10.1016/J.IJPHARM.2008.04.042.
[41] A. R. C. Duarte, J. F. Mano, and R. L. Reis, “Preparation of chitosan scaffolds loaded with dexamethasone for tissue engineering applications using supercritical fluid technology,” *Eur. Polym. J.*, vol. 45, no. 1, pp. 141–148, 2009, doi: 10.1016/j.eurpolymj.2008.10.004.
[42] G. M. Demir and I. T. Degim, “Preparation of chitosan nanoparticles by nano spray drying technology,” *Fabad J. Pharm. Sci.*, vol. 38, no. 3, pp. 127–133, 2013.
[43] M. Zhang *et al.*, “Impact of Freeze-and Spray-Drying Microencapsulation Techniques on β-Glucan Powder Biological Activity: A Comparative Study,” 2022, doi: 10.3390/foods11152267.
[44] X. Li, N. Anton, C. Arpagaus, F. Belleteix, and T. F. Vandamme, “Nanoparticles by spray drying using innovative new technology: The Büchi Nano Spray Dryer B-90,” *J. Control. Release*, vol. 147, no. 2, pp. 304–310, Oct. 2010, doi: 10.1016/J.JCONREL.2010.07.113.
[45] H. Wang *et al.*, “A rapid pathway toward a superb gene delivery system: Programming structural and functional diversity into a supramolecular nanoparticle library,” *ACS Nano*, vol. 4, no. 10, pp. 6235–6243, 2010, doi: 10.1021/nn101908e.
[46] L. Shui, J. C. T. Eijkel, and A. van den Berg, “Multiphase flow in microfluidic systems - Control and applications of droplets and interfaces,” *Adv. Colloid Interface Sci.*, vol. 133, no. 1, pp. 35–49, 2007, doi: 10.1016/j.cis.2007.03.001.
[47] M. James, R. A. Revia, Z. Stephen, and M. Zhang, “Microfluidic synthesis of iron oxide nanoparticles,” *Nanomaterials*, vol. 10, no. 11, pp. 1–19, 2020, doi: 10.3390/nano10112113.
[48] F. Moradikhah, M. Doosti-Telgerd, I. Shabani, S. Soheili, B. Dolatyar, and E. Seyedjafari,

"Microfluidic fabrication of alendronate-loaded chitosan nanoparticles for enhanced osteogenic differentiation of stem cells," *Life Sci.*, vol. 254, no. May, p. 117768, 2020, doi: 10.1016/j.lfs.2020.117768.

[49] H. Fessi, F. Puisieux, J. P. Devissaguet, N. Ammoury, and S. Benita, "Nanocapsule formation by interfacial polymer deposition following solvent displacement," *Int. J. Pharm.*, vol. 55, no. 1, pp. 1–4, 1989, doi: 10.1016/0378-5173(89)90281-0.

[50] M. Jelvehgari *et al.*, "Development of a nanoprecipitation method for the entrapment of a very water soluble drug into Eudragit RL nanoparticles," 2017.

[51] C. E. Mora-Huertas, H. Fessi, and A. Elaissari, "Influence of process and formulation parameters on the formation of submicron particles by solvent displacement and emulsification–diffusion methods: Critical comparison," *Adv. Colloid Interface Sci.*, vol. 163, no. 2, pp. 90–122, Apr. 2011, doi: 10.1016/J.CIS.2011.02.005.

[52] M. V. Ostrovsky and R. M. Ostrovsky, "Dynamic interfacial tension in binary systems and spontaneous pulsation of individual drops by their dissolution," *J. Colloid Interface Sci.*, vol. 93, no. 2, pp. 392–401, Jun. 1983, doi: 10.1016/0021-9797(83)90422-8.

[53] I. J. Joye and D. J. McClements, "Production of nanoparticles by anti-solvent precipitation for use in food systems," *Trends Food Sci. Technol.*, vol. 34, no. 2, pp. 109–123, Dec. 2013, doi: 10.1016/J.TIFS.2013.10.002.

[54] T. Sugimoto, "Preparation of monodispersed colloidal particles," *Adv. Colloid Interface Sci.*, vol. 28, no. C, pp. 65–108, Jan. 1987, doi: 10.1016/0001-8686(87)80009-X.

[55] D. N. R. Shikida, L. F. Dalmolin, F. Fumagalli, F. da Silva Emery, and R. F. V. Lopez, "Arginine-conjugated chitosan nanoparticles for topical arginine release in wounds," *J. Drug Deliv. Sci. Technol.*, vol. 61, p. 102115, Feb. 2021, doi: 10.1016/J.JDDST.2020.102115.

[56] N. Lammari, O. Louaer, A. H. Meniai, and A. Elaissari, "Encapsulation of essential oils via nanoprecipitation process: Overview, progress, challenges and prospects," *Pharmaceutics*, vol. 12, no. 5, pp. 1–21, 2020, doi: 10.3390/pharmaceutics12050431.

[57] C. M. Belda-Galbis, M. C. Pina-Pérez, A. Leufvén, A. Martínez, and D. Rodrigo, "Impact assessment of carvacrol and citral effect on Escherichia coli K12 and Listeria innocua growth," *Food Control*, vol. 33, no. 2, pp. 536–544, Oct. 2013, doi: 10.1016/J.FOODCONT.2013.03.038.

[58] A. G. Luque-Alcaraz, J. Lizardi-Mendoza, F. M. Goycoolea, I. Higuera-Ciapara, and W. Argüelles-Monal, "Preparation of chitosan nanoparticles by nanoprecipitation and their ability as a drug nanocarrier," *RSC Adv.*, vol. 6, no. 64, pp. 59250–59256, 2016, doi: 10.1039/c6ra06563e.

[59] K. Yesenia *et al.*, "PLGA nanoparticle preparations by emulsification and nanoprecipitation techniques: effects of formulation parameters," 2020, doi: 10.1039/c9ra10857b.

[60] J. Y. Zhang *et al.*, "Preparation of amorphous cefuroxime axetil nanoparticles by controlled nanoprecipitation method without surfactants," *Int. J. Pharm.*, vol. 323, no. 1–2, pp. 153–160, Oct. 2006, doi: 10.1016/J.IJPHARM.2006.05.048.

[61] M. Khosravani, M. Adabi, F. Madani, S. S. Esnaashari, B. Mujokoro, and F. Dorkoosh, "Investigation of Effective Parameters on Size of Paclitaxel Loaded PLGA Nanoparticles," *Tabriz Univ. Med. Sci.*, vol. 8, no. 1, pp. 77–84, 2018, doi: 10.15171/apb.2018.010.

[62] M. Beck-Broichsitter, "Solvent impact on polymer nanoparticles prepared nanoprecipitation," *Colloids Surfaces A Physicochem. Eng. Asp.*, vol. 625, p. 126928, Sep. 2021, doi: 10.1016/J.COLSURFA.2021.126928.

[63] A. A. Öztürk, E. Yenilmez, and M. Güçlü Özarda, "Clarithromycin-Loaded Poly (Lactic-co-glycolic Acid) (PLGA) Nanoparticles for Oral Administration: Effect of Polymer Molecular Weight and Surface Modification with Chitosan on Formulation, Nanoparticle Characterization and Antibacterial Effects," doi: 10.3390/polym11101632.
[64] L. Martín-Banderas *et al.*, "Cannabinoid derivate-loaded PLGA nanocarriers for oral administration: formulation, characterization, and cytotoxicity studies," *Int. J. Nanomedicine*, vol. 7, pp. 5793–5806, 2012, doi: 10.2147/IJN.S34633.
[65] A. V. Delgado, F. González-Caballero, R. J. Hunter, L. K. Koopal, and J. Lyklema, "Measurement and interpretation of electrokinetic phenomena," *J. Colloid Interface Sci.*, vol. 309, no. 2, pp. 194–224, May 2007, doi: 10.1016/J.JCIS.2006.12.075.
[66] R. Xu, "Progress in nanoparticles characterization: Sizing and zeta potential measurement," *Particuology*, vol. 6, no. 2, pp. 112–115, 2008, doi: 10.1016/j.partic.2007.12.002.
[67] R. Tantra, P. Schulze, and P. Quincey, "Effect of nanoparticle concentration on zeta-potential measurement results and reproducibility," *Particuology*, vol. 8, no. 3, pp. 279–285, 2010, doi: 10.1016/j.partic.2010.01.003.
[68] B. A. Bhanvase, *stability to make stable nanofluids*. INC, 2020.
[69] M. Li, Q. Huang, and Y. Wu, "A novel chitosan-poly(lactide) copolymer and its submicron particles as imidacloprid carriers," doi: 10.1002/ps.2120.
[70] S. Skylab Rajan, A. Pandian, and T. Palaniappan, "Curcumin loaded in bovine serum albumin-chitosan derived nanoparticles for targeted drug delivery," *Bull. Mater. Sci*, vol. 39, no. 3, pp. 811–817, 2016, doi: 10.1007/s12034-016-1213-z.
[71] E. Bilensoy *et al.*, "Intravesical cationic nanoparticles of chitosan and polycaprolactone for the delivery of Mitomycin C to bladder tumors," *Int. J. Pharm.*, vol. 371, no. 1–2, pp. 170–176, 2009, doi: 10.1016/j.ijpharm.2008.12.015.
[72] A. G. Luque-Alcaraz *et al.*, "Characterization and antiproliferative activity of nobiletin-loaded chitosan nanoparticles," *J. Nanomater.*, vol. 2012, 2012, doi: 10.1155/2012/265161.
[73] Z. N. Correa-Pacheco, S. Bautista-Baños, M. de L. Ramos-García, M. del C. Martínez-González, and J. Hernández-Romano, "Physicochemical characterization and antimicrobial activity of edible propolis-chitosan nanoparticle films," *Prog. Org. Coatings*, vol. 137, p. 105326, Dec. 2019, doi: 10.1016/J.PORGCOAT.2019.105326.
[74] A. Gómez Pérez *et al.*, "Chitosan-coated magnetic iron oxide nanoparticles for DNA and rhEGF separation," *Colloids Surfaces A Physicochem. Eng. Asp.*, vol. 591, p. 124500, Apr. 2020, doi: 10.1016/J.COLSURFA.2020.124500.
[75] H. C. Araujo *et al.*, "Antimicrobial, antibiofilm and cytotoxic effects of a colloidal nanocarrier composed by chitosan-coated iron oxide nanoparticles loaded with chlorhexidine," *J. Dent.*, vol. 101, p. 103453, Oct. 2020, doi: 10.1016/J.JDENT.2020.103453.
[76] F. Editors *et al.*, *Nucleation Theory*. 2013.
[77] F. Lince, D. L. Marchisio, and A. A. Barresi, "Strategies to control the particle size distribution of poly-ε-caprolactone nanoparticles for pharmaceutical applications," *J. Colloid Interface Sci.*, vol. 322, no. 2, pp. 505–515, Jun. 2008, doi: 10.1016/J.JCIS.2008.03.033.
[78] J. D. Clogston and A. K. Patri, "Zeta potential measurement.," *Methods Mol. Biol.*, vol. 697, pp. 63–70, 2011, doi: 10.1007/978-1-60327-198-1_6.
[79] M. Kosmulski and E. Matijević, "Zeta potential of anatase (TiO2) in mixed solvents," *Colloids and Surfaces*, vol. 64, no. 1, pp. 57–65, May 1992, doi: 10.1016/0166-

6622(92)80162-U.
[80] D. Quintanar-Guerrero, E. Allémann, H. Fessi, E. Doelker, D. Qu, and A. Iem an, “Hatem Fessi & Eric Doelker (1998) Preparation Techniques and Mechanisms of Formation of Biodegradable Nanoparticles from Preformed Polymers,” *Drug Dev. Ind. Pharm.*, vol. 24, pp. 1113–1128, 2008, doi: 10.3109/03639049809108571.
[81] P. Renz, M. Kokkinopoulou, K. Landfester, and I. Lieberwirth, “Trend Imaging of Polymeric Nanoparticles: Hard Challenge for Soft Objects,” 2016, doi: 10.1002/macp.201600246.
[82] M. Elsayed Abdelfattah Ali, M. Mohamed Saeid Aboelfadl, A. Mahmoud Selim, H. Fathy Khalil, and G. Mohamed Elkady, “Separation Science and Technology Chitosan nanoparticles extracted from shrimp shells, application for removal of Fe(II) and Mn(II) from aqueous phases) Chitosan nanoparticles extracted from shrimp shells, application for removal of Fe(II) and Mn(II) from aqueous phases Chitosan nanoparticles extracted from shrimp shells, application for removal of Fe(II) and Mn(II) from aqueous phases,” *Sep. Sci. Technol.*, vol. 53, pp. 2870–2881, 2018, doi: 10.1080/01496395.2018.1489845.
[83] K. Pramod, C. V. Suneesh, S. Shanavas, S. H. Ansari, and J. Ali, “Unveiling the compatibility of eugenol with formulation excipients by systematic drug-excipient compatibility studies,” *J. Anal. Sci. Technol.*, vol. 6, no. 1, 2015, doi: 10.1186/s40543-015-0073-2.
[84] E. Cheraghipour, S. Javadpour, and A. R. Mehdizadeh, “Citrate capped superparamagnetic iron oxide nanoparticles used for hyperthermia therapy,” *J. Biomed. Sci. Eng.*, vol. 05, no. 12, pp. 715–719, 2012, doi: 10.4236/jbise.2012.512089.
[85] S. L. Easo and P. V. Mohanan, “Dextran stabilized iron oxide nanoparticles: Synthesis, characterization and in vitro studies,” *Carbohydr. Polym.*, vol. 92, no. 1, pp. 726–732, Jan. 2013, doi: 10.1016/J.CARBPOL.2012.09.098.
[86] P. N. Dave and L. V Chopda, “Application of Iron Oxide Nanomaterials for the Removal of Heavy Metals,” 2014, doi: 10.1155/2014/398569.
[87] N. Basavegowda, K. Mishra, and Y. R. Lee, “Sonochemically synthesized ferromagnetic Fe 3 O 4 nanoparticles as a recyclable catalyst for the preparation of pyrrolo[3,4-c]quinoline-1,3-dione derivatives,” 2014, doi: 10.1039/c4ra11623b.
[88] A. Mishra, R. Ahmad, M. Perwez, and M. Sardar, “Reusable Green Synthesized Biomimetic Magnetic Nanoparticles for Glucose and H 2 O 2 Detection,” 2016, doi: 10.1007/s12668-016-0197-x.
[89] B. Herranz-Blanco *et al.*, “pH-Switch Nanoprecipitation of Polymeric Nanoparticles for Multimodal Cancer Targeting and Intracellular Triggered Delivery of Doxorubicin,” 2016, doi: 10.1002/adhm.201600160.
[90] B. Stephen Inbaraj, T. Y. Tsai, and B. H. Chen, “Synthesis, characterization and antibacterial activity of superparamagnetic nanoparticles modified with glycol chitosan,” *Sci. Technol. Adv. Mater.*, vol. 13, no. 1, 2012, doi: 10.1088/1468-6996/13/1/015002.
[91] M. Gaumet, A. Vargas, R. Gurny, and F. Delie, “Nanoparticles for drug delivery: The need for precision in reporting particle size parameters,” *Eur. J. Pharm. Biopharm.*, vol. 69, no. 1, pp. 1–9, 2008, doi: 10.1016/j.ejpb.2007.08.001.
[92] R. Nakaoka, Y. Tabata, T. Yamaoka, and Y. Ikada, “Prolongation of the serum half-life period of superoxide dismutase by poly(ethylene glycol) modification,” *J. Control. Release*, vol. 46, no. 3, pp. 253–261, Jun. 1997, doi: 10.1016/S0168-3659(96)01605-7.
[93] S. A. Khan and M. Schneider, “Improvement of Nanoprecipitation Technique for

Preparation of Gelatin Nanoparticles and Potential Macromolecular Drug Loading," doi: 10.1002/mabi.201200382.
[94] D. Zhao, S. Yu, B. Sun, S. Gao, S. Guo, and K. Zhao, "polymers Biomedical Applications of Chitosan and Its Derivative Nanoparticles," doi: 10.3390/polym10040462.
[95] A. Mironenko, E. Modin, A. Sergeev, S. Voznesenskiy, and S. Bratskaya, "Fabrication and optical properties of chitosan/Ag nanoparticles thin film composites," *Chem. Eng. J.*, vol. 244, pp. 457–463, May 2014, doi: 10.1016/J.CEJ.2014.01.094.